University of Nottingham

School of Mathematical Sciences

Advances in quantum information and thermodynamics with continuous variable systems

Buqing Xu

A thesis submitted to the University of Nottingham for the degree of

Doctor of Philosophy

January 2023

Acknowledgements

I would first like to thank my supervisor, Prof. Gerardo Adesso. He has given me support both in my studies over the last several years and personal matters and for this I am extremely grateful. I would also like to thank the Quantum Correlations group at the University of Nottingham. They are Dr. Tommaso Tufarelli, Dr Rosanna Nichols, Dr. Luis Correa, Dr. Javier Onam Gonzalez, Dr. Ladislav Mišta, Jr., Dr. Paul Knott, Dr. Ben Morris, Giorgio Nocerino, Dr. Carmine Napoli, Dr. Bartosz Regula, Dr. Gokhan Torun, Dr. Giannis Kogias, Dr. Antony Lee, Dr. Yu Xiang, Dr. Ludovico Lami, Dr. Pietro Liuzzo Scorpo, Prof. Soojoon Lee. Finally, I would like to thank my parents and friends for their support and encouragement.

Abstract

This thesis focuses on fundamental resources in quantum information theory with continuous variables and their applications to quantum optics and quantum thermodynamics. Our analysis mainly considers Gaussian states of continuous variable systems formed by two, three, or more modes, and adopts a variety of techniques to study their static and dynamical properties. Our original results include three main case studies: (i) quantifying genuine multipartite Bell nonlocality in permutationally invariant Gaussian states; (ii) characterising bipartite Einstein-Podolsky-Rosen (EPR) steering with non-Gaussian measurements; and (iii) benchmarking the reaction-coordinate mapping in non-equilibrium quantum harmonic chains.

In project (i), we investigate genuine multipartite nonlocality of multimode Gaussian states, as detected by the violation of Svetlichny inequality. We consider both displaced parity and pseudospin measurements and identify the largest violation of the inequality on permutationally invariant states. In the pseudospin case, we show that the maximum violation of Svetlichny inequality allowed by quantum mechanics can be approached for asymptotically large squeezing.

In project (ii) we study the detection of EPR steering (an asymmetric quantum correlation intermediate between entanglement and Bell nonlocality) in bipartite Gaussian states by pseudospin measurements. Our analysis reveals previously unexplored regimes where non-Gaussian measurements are more effective than Gaussian ones to witness steering of Gaussian states in the presence of local noise.

Finally, in project (iii) we analyze the validity of the reaction-coordinate mapping to characterise heat transport in an exactly solvable model: a two-node linear "quantum wire" connecting two baths at different temperatures. We find surprisingly that the stationary state of the original problem can be reproduced accurately by a weak-coupling treatment even in the regime of very strong residual dissipation.

CONTENTS

1 INTRODUCTION 1

1.1 Continuous variable systems and Gaussian states 3

1.2 Non-Gaussian measurements 4

1.2.1 Displaced parity measurements 4

1.2.2 Pseudospin measurements 5

2 GENUINE MULTIPARTITE NONLOCALITY 7

2.1 Overview 7

2.2 Preliminaries 9

2.2.1 Permutationally invariant Gaussian states 9

2.2.2 Svetlichny inequality 10

2.3 Violation of Svetlichny inequality for Gaussian states 13

2.3.1 Displaced parity measurements: Multipartite nonlocality . . 13

2.3.2 Pseudospin measurements: Maximum tripartite nonlocality . 18

2.4 Discussion 24

3 QUANTUM STEERING 26

3.1 Overview 26

3.2 Preliminaries 28

3.2.1 Two-mode Gaussian states 28

3.2.2 Steering criteria 29

3.3 Fock representation of two-mode squeezed thermal states 31

3.4 Steering of two-mode Gaussian states: Gaussian versus non-Gaussian measurements 35

3.4.1 Expectation values of pseudospin measurements 36

3.4.2 Steering analysis, examples and discussion 38

3.5 Steering of continuous variable non-Gaussian Werner states 44
3.6 Discussion 48

4 REACTION-COORDINATE MAPPING 50
4.1 Overview 50
4.2 The model and its solution 54
4.2.1 A two-node non-equilibrium quantum wire 54
4.2.2 Markovian master equation and its stationary solution 58
4.2.3 Exact stationary solution 64
4.3 Discussion 67
4.3.1 Steady state and stationary heat currents 67
4.3.2 Dynamics 71
4.4 Discussion 75

5 CONCLUSIONS 78

A APPENDIX 81
A.1 Compact expression for multidimensional Hermite polynomials . . . 81
A.2 Pseudospin operators and the "Quantum Phase" 83
A.3 Lie algebra sl_2 and its representation 86

BIBLIOGRAPHY 89

1

INTRODUCTION

The development of quantum technologies is being vigorously pursued thanks to substantial international investments. Broadly speaking, quantum technologies are expected to revolutionise the sectors of information and communication, computation, cooling, sensing and metrology, by exploiting quantum phenomena such as entanglement, superposition, squeezing and other forms of nonclassicality as resources to overcome limitations of current devices [1]. The development of quantum technologies is therefore strictly tied to advances in the characterisation of fundamental quantum resources using the language of quantum information theory.

Traditionally, much of the focus of quantum information science and technology has been on discrete variable systems; i.e., qubits, realised by dichotomic degrees of freedom such as the polarisation of a photon or the nuclear spin of an atom. However, an alternative approach (that may be referred to as "analog" as opposed to "digital") relies on the use of continuous variable systems; i.e., harmonic oscillators, in which quantum superposition and entanglement arise between degrees of freedom with a continuous spectrum, such as quadratures of light beams, collective spin components of atomic ensembles, or vibrational modes of nanoscale oscillators [2].

This thesis focuses on the investigation of fundamental resources and methods in continuous variable quantum systems and their applications in quantum optics and quantum thermodynamics. Our analysis mainly considers Gaussian states of continuous variable systems formed by two, three, or more modes, and adopts a variety of techniques to study their static and dynamical properties. After presenting the main definitions in this Chapter, our original results revolve around three main

case studies: (i) quantifying genuine multipartite Bell nonlocality in permutationally invariant Gaussian states [3]; (ii) characterising bipartite Einstein-Podolsky-Rosen (EPR) steering with non-Gaussian measurements [4]; and (iii) benchmarking the reaction-coordinate mapping in non-equilibrium quantum harmonic chains [5].

More specifically, in Chapter 2 we investigate genuine multipartite nonlocality of pure permutationally invariant multimode Gaussian states of continuous variable systems, as detected by the violation of Svetlichny inequality. We identify the phase space settings leading to the largest violation of the inequality when using displaced parity measurements, distinguishing our results between the cases of even and odd total number of modes. We further consider pseudospin measurements and show that, for three-mode states with asymptotically large squeezing degree, particular settings of these measurements allow one to approach the maximum violation of Svetlichny inequality allowed by quantum mechanics. This indicates that the strongest manifestation of genuine multipartite quantum nonlocality is in principle verifiable on Gaussian states.

In Chapter 3 we perform a systematic investigation of EPR steering (an asymmetric form of quantum correlations intermediate between plain entanglement and Bell nonlocality) in bipartite Gaussian states by pseudospin measurements, as detected by a nonlinear criterion based on second moments of the pseudospin correlation matrix. This analysis reveals previously unexplored regimes where non-Gaussian measurements are more effective than Gaussian ones to witness steering of Gaussian states in the presence of local noise. We also investigate continuous variable Werner states, which are non-Gaussian mixtures of Gaussian states, and find that pseudospin measurements are always more effective than Gaussian ones to reveal their steerability. These results provide useful insights on the role of non-Gaussian measurements in characterising quantum correlations of Gaussian and non-Gaussian states.

Finally, in Chapter 4 we consider heat transport in an exactly solvable model: a two-node linear "quantum wire" connecting two baths at different temperatures. We investigate the validity of the reaction-coordinate mapping for the considered model; this technique aims to mimic the original problem by means of an augmented system, which includes a suitably chosen collective environmental coordi-

nate (reaction-coordinate), coupled to a simpler effective reservoir. We allow for a structured spectral density at the interface with one of the reservoirs and perform the reaction-coordinate mapping, writing a perturbative master equation for the augmented system. We find that, strikingly, the stationary state of the original problem can be reproduced accurately by a weak-coupling treatment even when the residual dissipation on the augmented system is very strong, and the agreement holds throughout the entire dynamics under large residual dissipation in the overdamped regime. These observations can be crucial when using the reaction-coordinate mapping to study the largely unexplored strong-coupling regime in quantum thermodynamics.

1.1 CONTINUOUS VARIABLE SYSTEMS AND GAUSSIAN STATES

The object of our study is a continuous variable (CV) quantum system, composed in general of n bosonic modes, and described by an infinite-dimensional Hilbert space constructed as a tensor product of the Fock spaces of each individual mode. The quadrature operators for a mode j can be defined as $\hat{q}_j = (\hat{a}_j + \hat{a}_j^\dagger)/\sqrt{2}$, $\hat{p}_j = -i(\hat{a}_j - \hat{a}_j^\dagger)/\sqrt{2}$, where $\hat{a}_j, \hat{a}_j^\dagger$ are the ladder operator satisfying $[\hat{a}_j, \hat{a}_j^\dagger] = 1$, and $\hat{n}_j = \hat{a}_j^\dagger \hat{a}_j$ is the number operator, whose eigenvectors define the Fock basis, $\hat{n}_j|n\rangle_j = n_j|n\rangle_j$. Collecting the quadrature operators for all the modes into a vector $\hat{\boldsymbol{R}} = (\hat{q}_1, \hat{p}_1, \hat{q}_2, \hat{p}_2, \ldots, \hat{q}_N, \hat{p}_N)^T$, the canonical commutation relations can be expressed as $[\hat{R}_j, \hat{R}_k] = i\,(\boldsymbol{\omega}^{\oplus n})_{j,k}$ with $\boldsymbol{\omega} = \left(\begin{smallmatrix} 0 & 1 \\ -1 & 0 \end{smallmatrix}\right)$ being the symplectic form.

We will mainly focus our attention on Gaussian states [2, 6–8], defined as those CV states whose Wigner phase space distribution is a multivariate Gaussian function of the form

$$W_\rho(\boldsymbol{\xi}) = \frac{1}{\pi^n \sqrt{\det \boldsymbol{\sigma}}} \exp\Big[-(\boldsymbol{\xi} - \boldsymbol{\delta})^T \boldsymbol{\sigma}^{-1} (\boldsymbol{\xi} - \boldsymbol{\delta}) \Big], \tag{1}$$

where $\boldsymbol{\xi} \in R^{2n}$ denotes a phase space coordinate vector, $\boldsymbol{\delta} = \langle \hat{\boldsymbol{R}} \rangle$ is the displacement vector, and $\boldsymbol{\sigma}$ is the covariance matrix collecting the second moments of the canonical operators,

$$\sigma_{j,k} = \langle \{ \hat{R}_j - \delta_j, \hat{R}_k - \delta_k \}_+ \rangle\,, \tag{2}$$

with $\{\cdot,\cdot\}_+$ standing for the anticommutator, and $\langle\cdot\rangle = \mathrm{tr}\left[\hat{\rho}\,\cdot\right]$ denoting the expectation value.

Since we are interested in correlations between the modes, we can assume without any loss of generality that the states have vanishing first moments, $\delta = \mathbf{0}$, as the latter can be adjusted by local displacements which have no effect on the correlations. The covariance matrix σ contains all the relevant information of a Gaussian state, and needs to obey the *bona fide* condition [9]

$$\sigma + i\omega^{\oplus n} \geq 0\,, \tag{3}$$

in order to correspond to a physical density matrix $\hat{\rho}$ in the Hilbert space. In passing, note how Eq. (3) may be seen as a generalisation of the Robertson-Schrödinger uncertainty principle.

The purity of a Gaussian state $\hat{\rho}$ is given simply by $\mu(\hat{\rho}) = \mathrm{tr}\,\hat{\rho}^2 = (\det\sigma)^{-\frac{1}{2}}$, so that a pure Gaussian state $\hat{\rho} = |\psi\rangle\langle\psi|$ has a covariance matrix σ with $\det\sigma = 1$, saturating the above matrix inequality (3).

Gaussian measurements can be generally implemented via symplectic transformations followed by balanced homodyne detection.

1.2 NON-GAUSSIAN MEASUREMENTS

To investigate correlations beyond quadrature operators, we will consider also some types of non-Gaussian measurements.

1.2.1 *Displaced parity measurements*

For a n-mode continuous variable optical system, the *displaced parity observable* $\hat{P}^j$ on mode j can be measured by photon counting, preceded by a phase space displacement, the latter implemented e.g. by beamsplitting the input mode with a tunable coherent field [10, 11]. In formula,

$$\hat{P}^j(\xi^j_{x_j}) = \sum_{n=0}^{\infty}(-1)^n|\xi^j_{x_j}, n\rangle\langle\xi^j_{x_j}, n|\,, \tag{4}$$

where $|\xi^j_{x_j}, n\rangle$ is the n^{th} Fock state of mode j, displaced by a phase space vector $\xi^j_{x_j} \equiv (q^j_{x_j}, p^j_{x_j})$; notice that we are keeping a binary tag $x_j \in \{0,1\}$ to allow for the choice of two different phase space settings on each mode j. These measurements have been implemented in recent Bell-type experiments with optical vortex beams [12].

1.2.2 *Pseudospin measurements*

In this thesis we consider two different sets of pseudospin measurements for CV systems. Pseudospin operators of the first type were originally defined in [13] in order to investigate Bell nonlocality of EPR states, they can be expressed as follows with respect to the Fock basis $\{|n\rangle\}$,

$$\begin{aligned} \hat{S}^x &= \sum_{n=0}^{\infty} \left[|2n\rangle\langle 2n+1| + |2n+1\rangle\langle 2n| \right], \\ \hat{S}^y &= \sum_{n=0}^{\infty} i\left[|2n\rangle\langle 2n+1| - |2n+1\rangle\langle 2n| \right], \\ \hat{S}^z &= \sum_{n=0}^{\infty} \left[|2n+1\rangle\langle 2n+1| - |2n\rangle\langle 2n| \right] = -\hat{P}, \end{aligned} \tag{5}$$

where $\hat{P} = (-1)^{\hat{n}}$ is the parity operator. One can easily check that the operators $\{\hat{S}^j\}$ obey the standard SU(2) algebra just like the Pauli operators $\{\sigma^j\}$, hence they can be regarded as infinite-dimensional analogues of the conventional spin observables, which motivates their denomination as pseudospin. Further details on the pseudospin operators are presented in Appendix A.2. Pseudospin operators as defined by Eq. (5) have proven useful to analyze theoretically bipartite and multipartite Bell nonlocality of Gaussian and non-Gaussian states [3, 13–16] (as presented in Chapter 2). However, evaluating expectation values of these operators requires handling the density matrix $\hat{\rho}$ expressed in the Fock basis, which may be quite nontrivial in general, as further discussed in detail in Sec. 3.3.

To sidestep this difficulty, an alternative set of pseudospin operators was introduced in [17]. For a single mode, they can be expressed as follows in terms of even and odd superpositions of the eigenstates $|q\rangle$ of the position operator $\hat{q}$,

$$\begin{aligned}
\hat{\Pi}^x &= \int_0^\infty [|\chi^+\rangle\langle\chi^-| + |\chi^-\rangle\langle\chi^+|]dq\,, \\
\hat{\Pi}^y &= \int_0^\infty i[|\chi^-\rangle\langle\chi^+| - |\chi^+\rangle\langle\chi^-|]dq\,, \\
\hat{\Pi}^z &= \int_0^\infty [|\chi^+\rangle\langle\chi^+| - |\chi^-\rangle\langle\chi^-|]dq = \hat{P}\,,
\end{aligned} \tag{6}$$

where $|\chi^\pm\rangle = (|q\rangle \pm |-q\rangle)/\sqrt{2}$. The operators $\{\hat{\Pi}^j\}$ also satisfy the standard SU(2) algebra, and will be referred to as pseudospin operators of the second type (or type-ii in short) in this thesis, to distinguish them from the type-i ones of Eq. (5). The type-ii pseudospin operators of Eq. (6) admit a compact Wigner representation, given by [18]

$$\begin{aligned}
W_{\Pi^x}(q,p) &= \mathrm{sgn}(q)\,, \\
W_{\Pi^y}(q,p) &= -\delta(q)\ \wp\frac{1}{p}\,, \\
W_{\Pi^z}(q,p) &= -\pi\,\delta(q)\,\delta(p),
\end{aligned} \tag{7}$$

where $\wp$ denotes the principal value. This allows one to evaluate expectation values of type-ii pseudospin operators directly from their Wigner function representation, with no need to resort to the Fock basis. Explicitly, for a two-mode state $\hat{\rho}$, we have [18]

$$\langle \hat{\Pi}_A^j \otimes \hat{\Pi}_B^k \rangle = \frac{1}{(2\pi)^2} \int d^4\boldsymbol{\xi}\ W_\rho(\boldsymbol{\xi})\ W_{\Pi_A^j}(q_A,p_A)\ W_{\Pi_B^k}(q_B,p_B)\,, \tag{8}$$

with $\boldsymbol{\xi} = (q_A, p_A, q_B, p_B)^T$. The type-ii pseudospin operators have also been employed for studies of bipartite and tripartite Bell nonlocality [17–19].

A comparison between the performance of the two types of pseudospin operators for verifying the quantumness of correlations in a model of the early universe was also recently reported [20]. However, both type-i and type-ii pseudospin measurements remain challenging to implement experimentally with current technology.

2

GENUINE MULTIPARTITE NONLOCALITY

2.1 OVERVIEW

Quantum mechanical systems can be correlated in ways stronger than classical ones. The characterisation and exploitation of such correlations is enabling the development of a wealth of quantum technologies, set to revolutionize information and communication and other industrial sectors. Bell nonlocality is the strongest form of quantum correlations [21]. It manifests itself when two or more subsystems are in an entangled state [22] and additionally fulfill the more stringent condition that the outcomes of local measurements on each subsystem cannot be explained by using a local hidden variable model [23, 24]. This entails that the entanglement distributed among the subsystems, which may be located in different laboratories, can be verified without any need for characterising, or trusting, the measurement apparatuses available in each laboratory [21]. In turn, this ensures that the states exhibiting Bell nonlocality can be useful as resources for fully device-independent quantum communication, including in particular unconditionally secure quantum key distribution [25].

Nonlocal correlations can be detected by the violation of Bell-type inequalities [24]. While a great deal of attention has been devoted to the study of Bell inequalities in bipartite systems [21, 23, 24, 26, 27], including most recently the first loophole-free experimental demonstrations [28–30], a few criteria have been formulated for the verification of Bell nonlocality in multipartite systems as well [21, 31–45]. However, the concept of *genuine* multipartite nonlocality has been formalised only re-

cently from an operational point of view [44, 45] and its full exploration remains challenging both theoretically and experimentally.

In this Chapter, based on original results published in [3], we present a theoretical study of genuine multipartite nonlocality in multimode Gaussian states of infinite-dimensional systems. As introduced in the previous Chapter, these states, which include squeezed and thermal states of quantised electromagnetic fields, are the theoretical pillars and the resources of choice for a number of applications in quantum information with continuous variables [2, 7, 8, 46, 47]. Their nonlocal properties have been explored in a few papers [10, 13, 48–60], albeit mostly limited to two or three modes. We investigate genuine multipartite nonlocality as revealed by the violation of an inequality first proposed for tripartite states by Svetlichny [33]. Such an inequality can be violated e.g. by both Greenberger-Horne-Zeilinger (GHZ) and W classes of states for three qubits [36–39], and it stands as the conventional witness of genuine nonlocality when all three parties perform two measurements with two outcomes each [45], even though a large number of weaker inequalities revealing genuine nonlocality in more general settings have been constructed more recently [44, 45]. While originally formulated for dichotomic observables, Bell-type inequalities such as the Svetlichny one can be tested for continuous variable systems either by binning outcomes of observables with continuous spectrum (typically Gaussianity-preserving measurements such as homodyne detection) [48–52], or by considering directly operators with a discrete spectrum [10, 13]. The first kind of approach is of no use with Gaussian states, since their defining property of admitting a phase space description in terms of Gaussian (i.e., classical-like) Wigner distributions entails that all the results of homodyne detections can be fully explained by a local hidden variable model, even for entangled states. However, Gaussian states do exhibit trademark nonclassical and nonlocal features, as revealed by violations of Bell-type inequalities using observables of the second kind (which do not preserve Gaussianity), including most importantly displaced parity [10] and pseudospin [13].

Here we investigate the maximum violation of the Svetlichny inequality in pure permutationally invariant multimode Gaussian states, which can be seen as continuous variable analogs of multiqubit GHZ states [61–65], by considering these two

types of measurements. For displaced parity measurements (Sec. 1.2.1), we extend the results of [60] from three to an arbitrary number of modes, providing a prescription to identify the phase space settings leading to the largest violations. However, we show that (as in the case of two and three modes) these violations do not reach the absolute maximum allowed by quantum mechanics, that is the multipartite analogue of the Tsirelson bound [21]. On the contrary, we provide substantial evidence that by using pseudospin operators one can approach such a maximum violation asymptotically in pure permutationally invariant three-mode Gaussian states (Sec. 2.3.2). This result, which mirrors the case of bipartite nonlocality in two-mode squeezed Gaussian states [13], demonstrates theoretically that maximum genuine multipartite quantum nonlocality is in fact attainable in continuous variable Gaussian states, provided arbitrarily large squeezing is available. Extensions of the latter analysis to an arbitrary number of modes are certainly possible but cumbersome, since our treatment of pseudospin measurements relies on the explicit expansion of Gaussian states in the Fock basis. Such generalisations are thus left for future work.

2.2 PRELIMINARIES

2.2.1 *Permutationally invariant Gaussian states*

Continuous variable quantum systems and Gaussian states have been introduced in Section 1.1, to which the reader is referred for definitions and notations.

Here we will focus our analysis on pure permutationally invariant n-mode Gaussian states [64], which are known as the continuous variable counterparts of both GHZ and W states of n qubits, as they maximize both the genuine n-partite entanglement and the residual bipartite entanglement between any pair of modes, within the set of Gaussian states [66–71]. These states, often referred to as continuous variable GHZ-like states [62, 63, 65], have been investigated theoretically and experimentally as useful resources for multipartite teleportation networks [61, 72, 73], error correcting codes [74], and cryptographic protocols such as quantum secret sharing [75–77] and Byzantine agreement [78]. In the following we will show that they are very

good candidates to reveal strong manifestations of genuine multipartite nonlocality by means of suitable measurements.

Up to local unitaries, the covariance matrix of these Gaussian states can be written in the following normal form in terms of 2×2 subblocks [64],

$$\sigma = \begin{pmatrix} \boldsymbol{\alpha} & \boldsymbol{\gamma} & \boldsymbol{\gamma} & \cdots & \boldsymbol{\gamma} \\ \boldsymbol{\gamma} & \boldsymbol{\alpha} & \boldsymbol{\gamma} & \cdots & \boldsymbol{\gamma} \\ \boldsymbol{\gamma} & \boldsymbol{\gamma} & \ddots & \cdots & \boldsymbol{\gamma} \\ \vdots & \vdots & \vdots & \ddots & \boldsymbol{\gamma} \\ \boldsymbol{\gamma} & \boldsymbol{\gamma} & \boldsymbol{\gamma} & \boldsymbol{\gamma} & \boldsymbol{\alpha} \end{pmatrix} \tag{9}$$

where $\boldsymbol{\alpha} = \mathrm{diag}(a,\, a)$ and $\boldsymbol{\gamma} = \mathrm{diag}(z_n^+,\, z_n^-)$, with $a \geq 1$ and

$$z_n^{\pm} = \frac{(a^2-1)(n-2) \pm \sqrt{(a^2-1)(a^2n^2-(n-2)^2)}}{2a(n-1)}\,. \tag{10}$$

These states are therefore entirely specified (up to local unitaries) by a single parameter, the local mixedness factor a, which can be accordingly expressed in terms of a single-mode squeezing degree r needed to prepare the state via a network of beam splitters [61, 64, 68–72].

2.2.2 *Svetlichny inequality*

In the Bell scenario, nonlocality can be detected in the state of a composite system by allowing every party to perform a selection of different measurements on their subsystems, each with two or more possible outcomes. From the expectation values of the measured observables one then infers a correlation parameter, whose value is bounded if a local hidden variable theory is assumed. Correlations exceeding the bound reveal the failure of local realism, that is, the presence of nonlocality. We refer the reader to [21, 24, 26, 44, 45] and references therein for an updated account on the subject.

In order to introduce the Svetlichny inequality for genuine multipartite nonlocality [33], it is convenient to start with the bipartite case, i.e. with the traditional Clauser-Horne-Shimony-Holt (CHSH) inequality [26]. Suppose two experimenters Alice

and Bob can each perform either one of two possible dichotomic measurements on their subsystem of a bipartite system. Say, Alice can measure her subsystem in either setting A_0 or A_1, with respective outcome a_x ($x \in \{0,1\}$) and Bob can measure his subsystem in either setting B_0 or B_1 with respective outcome b_y ($y \in \{0,1\}$). Here a_0, a_1, b_0, b_1 can take values ± 1. Defining now $\langle a_x b_y \rangle = \sum_{a,b=\pm 1} ab\, P(ab|xy)$ as the expectation value of the product of outcomes ab for given measurement choices x, y, the Bell-CHSH parameter M_2 can then be written as follows [21, 26], adopting a convenient normalisation [34],

$$M_2 = \frac{1}{2}\left(\langle a_0 b_0 \rangle + \langle a_0 b_1 \rangle + \langle a_1 b_0 \rangle - \langle a_1 b_1 \rangle\right) . \tag{11}$$

Assuming a model with a local hidden variable λ, according to which the expectation values can be factorised as $\langle a_x b_y \rangle = \int \mathrm{d}\lambda q(\lambda) \sum_a a\, P(a|x,\lambda) \sum_b b\, P(b|y,\lambda)$, it is straightforward to see that

$$M_2 \leq 1 , \tag{12}$$

which is known as the CHSH inequality. However, if Alice and Bob share an entangled quantum state ρ, there exist measurement settings such that the parameter M_2 constructed from the expectation values of their experimental data violates the inequality (12), up to the Tsirelson bound

$$M_2 \leq \sqrt{2} , \tag{13}$$

which represents the maximum violation compatible with quantum mechanics.

Consider now a tripartite system, and three observers Alice, Bob, and Charlie. The generalisation of the CHSH inequality to this scenario is known as Mermin-Klyshko inequality [31, 32]. Defining $\langle a_x b_y c_z \rangle = \sum_{a,b,c=\pm 1} abc\, P(abc|xyz)$ as the expectation value of the product of outcomes abc for given measurement choices x, y, z of the three parties, the Mermin-Klyshko parameter can be written as

$$M_3 = \frac{1}{2}\left(\langle a_1 b_0 c_0 \rangle + \langle a_0 b_1 c_0 \rangle + \langle a_0 b_0 c_1 \rangle - \langle a_1 b_1 c_1 \rangle\right) . \tag{14}$$

Once more, $M_3 \leq 1$ for any local hidden variable model, while M_3 can reach up to $\sqrt{2}$ with entangled quantum states. However, a violation of the Mermin-Klyshko inequality can be achieved already by using only bipartite entangled states between

any two of the three parties. To remedy this problem, one can define the Svetlichny parameter S_3 for a tripartite system as $S_3 = (M_3 + \bar{M}_3)/2$, where $\bar{M}_3$ is obtained from M_3 by swapping the 0's and 1's in the settings x, y, z. Explicitly,

$$\begin{aligned} S_3 &= \frac{1}{4}\left(\langle a_1 b_0 c_0\rangle + \langle a_0 b_1 c_0\rangle + \langle a_0 b_0 c_1\rangle - \langle a_1 b_1 c_1\rangle \right. \\ &\quad \left. + \langle a_0 b_1 c_1\rangle + \langle a_1 b_0 c_1\rangle + \langle a_1 b_1 c_0\rangle - \langle a_0 b_0 c_0\rangle\right) . \end{aligned} \tag{15}$$

In this way, a violation of the Svetlichny inequality

$$S_3 \leq 1 \tag{16}$$

ensures that the correlations detected by Alice, Bob, and Charlie cannot be reproduced by any local hidden variable assigned to the joint measurement of any two out of three parties. In this sense, a violation of (16) reveals genuine tripartite nonlocality. Such a violation is possible using quantum mechanical states with genuine tripartite entanglement (i.e. fully inseparable states), such as GHZ states of three qubits [36–39], up to

$$S_3 \leq \sqrt{2} \equiv S_3^Q , \tag{17}$$

which defines the maximum allowed quantum violation S_3^Q.

The Svetlichny inequality can be generalised to detect genuine n-partite nonlocality. Consider a composite system partitioned into n subsystems, each measured by an experimenter (labelled by the superscript $j = 1, \ldots, n$) in two possible settings $O^j_{x_j}$ with respective outcomes $o^j_{x_j}$, where $x_j \in \{0, 1\}$ and $o^j_{x_j} \in \{-1, 1\}$. For $1 \leq k \leq n-1$ the Mermin-Klyshko parameter can be defined recursively in a compact way [34],

$$M_n = \frac{1}{2} M_{n-k}(M_k + \bar{M}_k) + \frac{1}{2}\bar{M}_{n-k}(M_k - \bar{M}_k) , \tag{18}$$

where $M_1 = \langle o^1_0\rangle$, while M_2 and M_3 are given by Eqs. (11) and (14), respectively. The Svetlichny parameter for arbitrary n can be defined accordingly [34],

$$S_n = \begin{cases} M_n, & \text{even } n; \\ \frac{1}{2}(M_n + \bar{M}_n), & \text{odd } n. \end{cases} \tag{19}$$

With the adopted normalisation, violation of the generalised Svetlichny inequality

$$S_n \leq 1 \tag{20}$$

signals genuine n-partite nonlocality. Quantum mechanical violations are possible up to the maximum value

$$S_n \leq 2^{\frac{1}{2}(n-1-(n \mod 2))} \equiv S_n^Q \,, \tag{21}$$

which generalizes the case $n = 3$ reported in Eq. (17).

In the following, we will focus on quantum states invariant under arbitrary permutations of the n subsystems. In this case, let us denote by E_n^m the expectation value of a product of joint measurements with m settings $x_j = 1$ and $(n-m)$ settings $x_j = 0$; for example, E_5^2 can indicate a term like $\langle o_1^1 o_1^2 o_0^3 o_0^4 o_0^5 \rangle$, or any of its permutations. The n-partite Svetlichny parameter S_n of Eq. (19) acquires then the simple form

$$S_n = \frac{1}{2^{\lceil \frac{n}{2} \rceil}} \sum_{m=0}^{n} B_n^m E_n^m \,, \tag{22}$$

where $B_n^m = (-1)^{\left\lceil \frac{n-2(m+1)}{4} \right\rceil} \binom{n}{m}$, with the binomial coefficient $\binom{n}{m} = \frac{n!}{m!(n-m)!}$, and $\lceil \cdot \rceil$ denoting the ceiling function.

2.3 VIOLATION OF SVETLICHNY INEQUALITY FOR GAUSSIAN STATES

2.3.1 *Displaced parity measurements: Multipartite nonlocality*

To test multipartite nonlocality in n-mode continuous variable systems, we first choose *displaced parity measurements* from Sec. 1.2.1 as the operators to be measured on each mode j [10, 53, 58]. It has been proven in [10] that, for an arbitrary (single-mode) quantum state ρ_j, the expectation value of a displaced parity operator $\hat{P}^j(\boldsymbol{\xi}_{x_j}^j)$ is proportional to the Wigner distribution W_ρ of ρ evaluated in the phase space point with coordinates given by the setting $\boldsymbol{\xi}_{x_j}^j$, that is, $\langle \hat{P}^j(\boldsymbol{\xi}_{x_j}^j) \rangle_{\rho_j} = \pi W_{\rho_j}(\boldsymbol{\xi}_{x_j}^j)$. This result extends immediately to multimode states. We can then rewrite all the expectation values appearing in the Svetlichny parameter S_n, defined by Eq. (19), in terms of the Wigner distribution of a n-mode quantum state ρ evaluated at suitable phase space points. For instance, in the tripartite case, the first correlation function in Eq. (15) would read $\langle a_1 b_0 c_0 \rangle = \pi^3 W_\rho(\boldsymbol{\xi}_1^1 \oplus \boldsymbol{\xi}_0^2 \oplus \boldsymbol{\xi}_0^3)$, and

so on [58, 60]. If ρ is a multimode Gaussian state with zero first moments and covariance matrix σ, its Wigner distribution is given by Eq. (1), and the Svetlichny parameter S_n defined in Eq. (19), for displaced parity measurements, depends only on the entries of the covariance matrix σ, as well as on the measurement settings $\{\boldsymbol{\xi}^j_{x_j}\}^{j=1,\ldots,n}_{x_j=0,1}$.

In the following, we investigate the maximum value that the Svetlichny parameter S_n can reach when performing local displaced parity measurements on n-mode permutationally invariant Gaussian states, whose covariance matrix is given by Eq. (9), and characterise the phase space settings leading to a violation of the Svetlichny inequality (20), that is, to a detection of genuine n-partite nonlocality.

Given the permutational symmetry of the states, we can assume that the binary set of available measurement settings is the same for each mode j, so that overall there will be m modes displaced by $\boldsymbol{\xi}_1 = (p_1, q_1)$, and $(n-m)$ modes displaced by $\boldsymbol{\xi}_0 = (p_0, q_0)$. The expectation value E^m_n of such a product of local displaced parity measurements can be then computed exactly, and takes the following expression

$$\begin{aligned} E^m_n = \exp\Big[&-z^-_n(q_0(n-m)+mq_1)^2 - z^+_n(p_0(n-m)+mp_1)^2 \\ &+ (z^-_n - a)\left(q_0^2(n-m)+mq_1^2\right) + (z^+_n - a)\left(p_0^2(n-m)+mp_1^2\right)\Big]. \end{aligned} \tag{23}$$

Plugging the above into Eq. (22), we get a compact formula for the Svetlichny parameter $S_n \equiv S_n(a; q_0, q_1, p_0, p_1)$.

Our next task is to optimise S_n over the local phase space settings at given a, n, i.e., to find

$$S^{\text{opt}}_n(a) = \max_{\{q_{0,1}, p_{0,1}\}} S_n(a; q_0, q_1, p_0, p_1)\,. \tag{24}$$

By evaluating partial derivatives with respect to q_0 and q_1, we can see that the setting $q_0 = 0 = q_1$ yields a stationary point of S_n for any n. A numerical analysis up to $n = 30$ modes confirms that this choice of quadratures maximizes the Svetlichny

parameter S_n. We are thus left to identify the optimal settings for p_0 and p_1, which are obtained by solving the following system of two transcendental equations,

$$\begin{aligned} 0 &= \sum_{m=0}^{n} [amp_1 + z_n^+(m(n-m)p_0 + m(m-1)p_1)] \\ &\quad \times B_n^m e^{-a(mp_1^2+(n-m)p_0^2)-z_n^+[2m(n-m)p_0p_1+m(m-1)p_1^2+(n-m)(n-m-1)p_0^2]}, \\ 0 &= \sum_{m=0}^{n} [a(n-m)p_0 + z_n^+(m(n-m)p_1 + (n-m)(n-m-1)p_0)] \\ &\quad \times B_n^m e^{-a(mp_1^2+(n-m)p_0^2)-z_n^+[2m(n-m)p_0p_1+m(m-1)p_1^2+(n-m)(n-m-1)p_0^2]}. \end{aligned} \tag{25}$$

While an exact solution of these equations appears unfeasible for arbitrary n, we can make some general observations, supported by numerical analysis.

A gallery illustrating the Svetlichny parameter S_n as a function of the phase space settings p_0 and p_1 is presented in Fig. 1 for some representative choices of n, at a fixed value of the state parameter a. The plots show that for any n (and sufficiently large a) there exist regions of phase space settings leading to a violation of the Svetlichny inequality (20) for the states under consideration. With increasing n, even more islands in the parameter space appear that enable such a violation. However, to further investigate the points of maximal violation and to comment on the dependence of the resulting $S_n^{\text{opt}}(a)$ on n and a, as shown in Fig. 2, we need to distinguish between the cases of even and odd n.

For odd $n \geq 3$, motivated by the evident symmetry in the distribution of the peaks in Fig. 1(top), one can verify that the antisymmetric setting $p_0 = \tilde{p}_n(a) = -p_1$ is always an admissible solution for Eqs. (25), which reduce to a single equation whose solution gives the optimal $\tilde{p}_n(a)$ (where the subscript denotes the number of modes, rather than the measurement setting). Numerics confirm that such a solution leads to the largest value of the Svetlichny parameter for odd n in the considered states under displaced parity measurements, i.e., $S_n^{\text{opt}}(a) = S_n(a;0,0,\tilde{p}_n(a),-\tilde{p}_n(a))$. Under these premises, the resulting $S_n^{\text{opt}}(a)$ is plotted as a function of a in Fig. 2(b). As clear from the inset of the Figure, one finds that there exists, for any odd n, a threshold value $\tilde{a}_n$ of a such that $\tilde{p}_n(a) = 0$ and $S_n^{\text{opt}}(a) = 1$ for $1 \leq a \leq \tilde{a}_n$, meaning that no genuine n-partite nonlocality can be detected below the threshold using displaced

parity measurements, despite the fact that pure permutationally invariant Gaussian states are fully inseparable for any n as soon as $a > 1$ [61, 64, 68–72]. This was already noted in [60] in the case $n = 3$. The threshold value $\tilde{a}_n$ to violate the Svetlichny inequality, as well as the optimal setting $\tilde{p}_n(a)$ to reach the largest violation provided $a > \tilde{a}_n$, can be determined analytically in principle by solving Eqs. (25), even though the problem becomes quite untractable for large n. For instance, for $n = 3$ we get $\tilde{a}_3 = \sqrt{\frac{3}{2}}$ and

$$\tilde{p}_3(a) = \sqrt{\frac{1}{8z_3^+(a)} \ln\left[\frac{a + 2z_3^+(a)}{3a - 2z_3^+(a)}\right]}, \tag{26}$$

in agreement with the results of [60][1] However, and quite interestingly, a numerical evaluation reveals that $\tilde{a}_n$ quickly shrinks towards 1 with increasing n [see Fig. 2(b)], which suggests that almost all fully inseparable Gaussian states of the studied class, in case of a large odd number $n \gg 1$ of modes, exhibit a violation of local realism with the adopted measurements.

For even $n \geq 2$ (including the bipartite case $n = 2$, when the Svetlichny parameter S_2 reduces to the Bell-CHSH one M_2), as apparent by the slight skewness in the islands of Fig. 1(bottom), the setting $p_0 = -p_1$ is not anymore a solution of Eqs. (25), which means that an optimisation over two parameters remains to be performed, to obtain $S_n^{\text{opt}}(a) = \max_{\{p_{0,1}\}} S_n(a; 0, 0, p_0, p_1)$. Analytical expressions, if available, are quite cumbersome in this case, so one can comfortably resort to a numerical solution. The resulting $S_n^{\text{opt}}(a)$ is plotted as a function of a in Fig. 2(a). As the inset of the Figure shows, and as numerical calculations confirm, in the case of even n there is no threshold for the violation of the Svetlichny inequality, that is, $S_n^{\text{opt}}(a) > 1$ for all $a > 1$, revealing genuine n-partite nonlocality as soon as the Gaussian states under consideration are fully inseparable.

1 Note that there was a typo in the expression corresponding to $\tilde{p}_3(a)$ in [60], while Eq. (26) gives the correct formula.

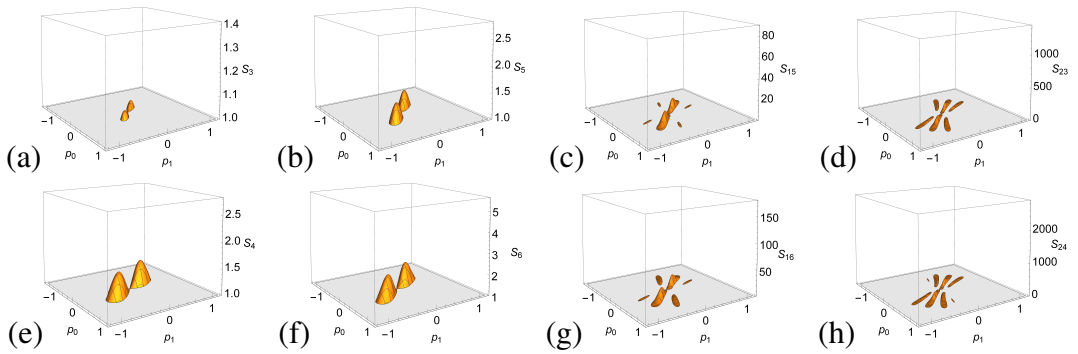

Figure 1: Plots of the Svetlichny parameter $S_n(a)$ for pure permutationally invariant n-mode Gaussian states using displaced parity measurements with $q_0 = 0 = q_1$ and variable settings p_0, p_1, for $a = 1.5$ and representative choices of n. Top row: (a) $n = 3$, (b) $n = 5$, (c) $n = 15$, and (d) $n = 23$. Bottom row: (e) $n = 4$, (f) $n = 6$, (g) $n = 16$, and (h) $n = 24$. The vertical axis in each panel ranges from 1 to the maximum quantum bound S_n^Q, so that only values of S_n violating the Svetlichny inequality (20) are shown. All the plotted quantities are dimensionless.

Finally, by comparing the two cases of even and odd n, i.e. by a justaposition of the two panels of Fig. 2, we observe that $S_{2k}^{\text{opt}}(a) \geq S_{2k+1}^{\text{opt}}(a)$ for any $k \geq 1$, even though the difference between consecutive even and odd cases vanishes asymptotically for $a \gg 1$. Most importantly, however, for any n the maximum Svetlichny parameter achievable with the considered measurements stays well below the maximum value S_n^Q allowed by quantum mechanics, given by Eq. (21) and indicated by dashed lines in Fig. 2. For instance, for $n = 2, 3$ we get $\lim_{a\to\infty} S_n^{\text{opt}}(a) = 4 \times 3^{-9/8} \approx 1.162$ [53, 60], while the maximum quantum violation amounts to $S_n^Q = \sqrt{2} \approx 1.414$. The conclusion we can draw from this extensive analysis is that one can feasibly detect genuine n-partite nonlocality by displaced parity measurements, but such observables are not sensitive enough to reveal an extremal violation of local realism in n-mode Gaussian states.

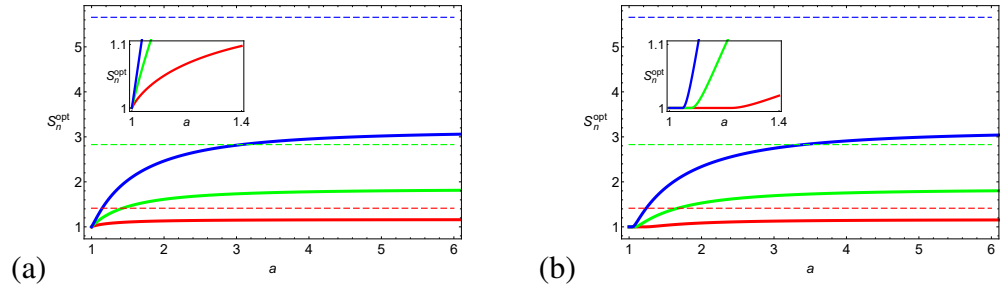

Figure 2: Optimal Svetlichny parameter S_n^{opt} (solid curves) for pure permutationally invariant n-mode Gaussian states using displaced parity measurements, plotted versus the covariance parameter a for (from bottom to top): (a) $n = 2$ (red online), $n = 4$ (green online), $n = 6$ (blue online), and (b) $n = 3$ (red online), $n = 5$ (green online), $n = 7$ (blue online). The insets detail the regime of small a, showing that a threshold for violations of the Svetlichny inequality exists in the odd n case (b), but not in the even n case (a). In both panels, the dashed horizontal lines indicate the maximum value S_n^Q of the Svetlichny parameter allowed by quantum mechanics, given by (from bottom to top) $S_2^Q = S_3^Q = \sqrt{2}$ (dashed red online), $S_4^Q = S_5^Q = 2\sqrt{2}$ (dashed green online), and $S_6^Q = S_7^Q = 4\sqrt{2}$ (dashed blue online), respectively. All the plotted quantities are dimensionless.

2.3.2 *Pseudospin measurements: Maximum tripartite nonlocality*

In the original discussion by Einstein, Podolsky, and Rosen [23], the idealised eigenstate of relative position and total momentum of two particles was argued to possess paradoxical nonlocal properties. In contemporary terms, we can say that such a continuous variable state (which is not normalizable, hence unphysical) is maximally entangled, i.e., it is characterised by a diverging entanglement entropy. Gaussian two-mode squeezed states, generated e.g. by optical parametric amplifiers [46], approach such an ideal limit asymptotically in the regime of large squeezing. For this reason, it is natural to expect that the nonlocality exhibited by these states would reach the maximum allowed by quantum mechanics in the limit of infinite squeezing. This was in fact proven by showing that the bound (13) for the CHSH parameter can be asymptotically saturated by such states, when using *pseudospin measurements* [13].

In the following we show that, by means of optimised pseudospin measurements, the Svetlichny inequality can also be maximally violated on a class of pure permutationally invariant three-mode Gaussian states, up to the limit in (17). This shows that continuous variable Gaussian states can display extremal genuine tripartite quantum nonlocality, which could not be revealed by using displaced parity operators. We emphasize that the measurements considered in this section require us to work directly in the Fock basis, thus losing some of the elegance and compactness of the phase space formalism adopted above. As a result, extending this study beyond three modes appears challenging at present.

For a single mode, the (type-i) pseudospin observable $\hat{S}$ as introduced in Sec. 1.2.2 is defined as [13]

$$\hat{S}(\boldsymbol{\xi}) = \cos\theta\,\hat{S}_z + \sin\theta(e^{-i\varphi}\hat{S}_+ + e^{i\varphi}\hat{S}_-),\,, \tag{27}$$

where $\boldsymbol{\xi} \equiv (\theta, \varphi)$ defines the measurement setting. Moving on to a tripartite scenario, given a three-mode state ρ, we define the correlation function associated with the measurement of pseudospin operators $\hat{S}^j(\boldsymbol{\xi}^j_{x_j})$ on each mode $j \in \{a, b, c\}$ with respective settings $\boldsymbol{\xi}^j_{x_j}$ (where $x_j \in \{0, 1\}$ labels once more two possible settings per mode) as

$$\langle a_{x_a} b_{x_b} c_{x_c}\rangle = \mathrm{tr}\left[\rho\,\hat{S}^a(\boldsymbol{\xi}^a_{x_a})\hat{S}^b(\boldsymbol{\xi}^b_{x_b})\hat{S}^c(\boldsymbol{\xi}^c_{x_c})\right]. \tag{28}$$

Inserting the expression (28) into Eq. (15), we can then construct the Svetlichny parameter S_3 corresponding to pseudospin observables.

We consider a family of pure permutationally invariant three-mode Gaussian states with wavefunction

$$|\psi\rangle = \frac{1}{\sqrt{\cosh r}}\exp\left(\frac{\tanh r}{2}\left(\frac{\hat{a}^\dagger + \hat{b}^\dagger + \hat{c}^\dagger}{\sqrt{3}}\right)^2\right)|000\rangle, \tag{29}$$

where $\hat{j}$ is the annihilation operator on mode j, and $r > 0$ plays the role of a three-mode squeezing parameter. These continuous variable GHZ-like states may be obtained by mixing a single-mode squeezed state [46] with two vacuum states at a balanced "tritter" [61, 79]. Their covariance matrix is local unitarily equivalent to the normal form given in Eq. (9) with an effective parameter $a \equiv \sqrt{\det\boldsymbol{\alpha}} = \frac{1}{3}\sqrt{5 + 4\cosh(2r)}$.

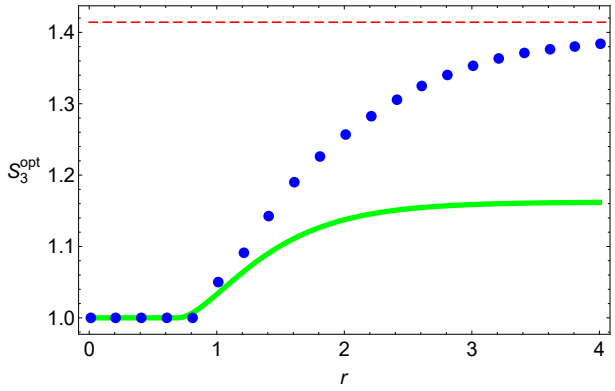

Figure 3: Optimal Svetlichny parameter S_n^{opt} for the 3-mode Gaussian states of Eq. (29), using pseudospin observables (blue points) and displaced parity measurements (solid green line), plotted versus the squeezing parameter r. As in Fig. 2, the dashed horizontal (red) line indicates the maximum value $S_3^Q = \sqrt{2}$ of the Svetlichny parameter allowed by quantum mechanics. All the plotted quantities are dimensionless.

In Fig. 3, we plot the Svetlichny parameter $S_3^{\text{opt}}(r)$ for these states, optimised numerically over all the pseudospin measurement settings $\{\boldsymbol{\xi}_{x_j}^j\}$. Quite interestingly, we see that, in the limit of large r, the violation of the Svetlichny inequality in the considered scenario appears to approach the maximum quantum bound $S_3^Q = \sqrt{2}$. The value of the Svetlichny parameter for the same states using displaced parity measurements (optimised analytically as described in the previous section) is also plotted for comparison. As already remarked, the maximum achievable value of S_3 for three-mode Gaussian states using displaced parity measurements is only ≈ 1.162, and the states of Eq. (29) reach this limit for $r \gg 1$ using such measurements.

We would like to go beyond the numerical analysis to provide a more rigorous evidence for the maximum tripartite quantum nonlocality of the Gaussian states under study. To this aim, we identify specific pseudospin measurement settings, given by

$$(\theta_0^a, \varphi_0^a, \theta_0^b, \varphi_0^b, \theta_0^c, \varphi_0^c) = (0, \tfrac{\pi}{2}, \tfrac{\pi}{4}, \tfrac{\pi}{2}, 0, -\tfrac{\pi}{2}),$$
$$(\theta_1^a, \varphi_1^a, \theta_1^b, \varphi_1^b, \theta_1^c, \varphi_1^c) = (\tfrac{\pi}{2}, \tfrac{\pi}{2}, \tfrac{3\pi}{4}, \tfrac{\pi}{2}, -\tfrac{\pi}{2}, -\tfrac{\pi}{2})\,. \tag{30}$$

With this choice, and after straightforward yet somewhat tedious algebra, we obtain the following expression for the Svetlichny parameter:

$$S_3 = \frac{\sqrt{2}}{4} + \frac{3\sqrt{2}}{2}\mathrm{Re}\Big(\langle\psi|\hat{S}_z^a\hat{S}_+^b\hat{S}_-^c|\psi\rangle - \langle\psi|\hat{S}_z^a\hat{S}_+^b\hat{S}_+^c|\psi\rangle\Big). \tag{31}$$

Eq. (31) can be derived by invoking the permutational invariance of the states $|\psi\rangle$, and observing that any such state is an eigenstate of the total parity $\hat{\Pi} = -\hat{S}_z^a\hat{S}_z^b\hat{S}_z^c$ with eigenvalue $+1$ (that is, it is a superposition of states with an even number of photons). Noting that, for any $j \in \{a,b,c\}$, $\hat{S}_z^j$ preserves the total parity of a state, while $\hat{S}_+^j$ and $\hat{S}_-^j$ act respectively as raising and lowering operators for $\hat{\Pi}$, we obtain that the only nonzero correlation functions contributing to S_3 are $\langle\psi|\hat{S}_z^a\hat{S}_z^b\hat{S}_z^c|\psi\rangle = -\langle\psi|\hat{\Pi}|\psi\rangle = -1$, which does not depend on the squeezing parameter r, together with the squeezing-dependent quantities $\langle\psi|\hat{S}_z^a\hat{S}_+^b\hat{S}_-^c|\psi\rangle$ and $\langle\psi|\hat{S}_z^a\hat{S}_+^b\hat{S}_+^c|\psi\rangle$ and their complex conjugates. All the other nonzero correlation functions are obtained from these by permutation of the indices (a,b,c). Furthermore, it is easy to spot from Eq. (29) that the expansion coefficients of $|\psi\rangle$ in the Fock basis are purely real, which implies that the correlation functions appearing in Eq. (31) are real as well.

Our expression for S_3 can be further simplified noting that the total parity of $|\psi\rangle$ implies $\langle\psi|\hat{S}_z^a\hat{S}_+^b\hat{S}_-^c|\psi\rangle = \langle\psi|\hat{S}_+^b\hat{S}_-^c|\psi\rangle$, while $\langle\psi|\hat{S}_z^a\hat{S}_+^b\hat{S}_+^c|\psi\rangle = -\langle\psi|\hat{S}_+^b\hat{S}_+^c|\psi\rangle$. Then, Eq. (31) may be cast in the elegant form

$$S_3 = \frac{\sqrt{2}}{4}\Big(1 + 3\langle\psi|\hat{S}_x^b\hat{S}_x^c|\psi\rangle\Big), \tag{32}$$

where $\hat{S}_x^j = \hat{S}_+^j + \hat{S}_-^j$. It is thus clear that the state $|\psi\rangle$ would yield maximum violation of the Svetlichny inequality if it could satisfy the condition $\langle\psi|\hat{S}_x^b\hat{S}_x^c|\psi\rangle = 1$. This can only be achieved if $|\psi\rangle$ is a $+1$ eigenstate of $\hat{S}_x^b\hat{S}_x^c$. In the remainder of this section, we report extensive evidence that this is indeed the case in the infinite squeezing limit $r \to \infty$. More precisely, we shall present a semi-analytical proof, supplemented by numerical evidence, that the following limit holds,

$$\lim_{r\to\infty}\Big\||\psi\rangle - \hat{S}_x^b\hat{S}_x^c|\psi\rangle\Big\| = 0. \tag{33}$$

To begin with, we take a series expansion of the exponential in Eq. (29), which yields

$$|\psi\rangle = \frac{1}{\sqrt{\cosh r}} \sum_{n=0}^{\infty} \frac{1}{n!} \left(\frac{\tanh r}{6}\right)^n \left(\hat{a}^\dagger + \hat{b}^\dagger + \hat{c}^\dagger\right)^{2n} |000\rangle. \tag{34}$$

This allows us to find the expansion of $|\psi\rangle$ in the Fock basis,

$$\begin{aligned} |\psi\rangle = \frac{1}{\sqrt{\cosh r}} \sum_{n=0}^{\infty} \frac{1}{n!} \left(\frac{\tanh r}{6}\right)^n \\ \times \sum_{k_1+k_2+k_3=2n} \frac{(2n)!}{\sqrt{k_1!k_2!k_3!}} |k_1, k_2, k_3\rangle. \end{aligned} \tag{35}$$

Our next step is to evaluate the Fock basis expansion of $\hat{S}_x^b \hat{S}_x^c |\psi\rangle$. This is easily done by recalling that the action of $\hat{S}_x^b \hat{S}_x^c$ on a Fock basis element is

$$\hat{S}_x^b \hat{S}_x^c |k_1, k_2, k_3\rangle = \begin{cases} |k_1, k_2+1, k_3+1\rangle & k_2 \text{ even, } k_3 \text{ even;} \\ |k_1, k_2-1, k_3-1\rangle & k_2 \text{ odd, } k_3 \text{ odd;} \\ |k_1, k_2+1, k_3-1\rangle & k_2 \text{ even, } k_3 \text{ odd;} \\ |k_1, k_2-1, k_3+1\rangle & k_2 \text{ odd, } k_3 \text{ even.} \end{cases} \tag{36}$$

Fixing $k_1 + k_2 + k_3 = 2n$, we thus obtain the expansion coefficients

$$\begin{aligned} \langle k_1, k_2, k_3 | \hat{S}_x^b \hat{S}_x^c |\psi\rangle = \frac{1}{\sqrt{\cosh r}} \frac{(2n)!}{n!} \left(\frac{\tanh r}{6}\right)^n \\ \times \begin{cases} \left(\frac{\tanh r}{3}\right) \frac{2n+1}{\sqrt{k_1!(k_2+1)!(k_3+1)!}} & k_2 \text{ even, } k_3 \text{ even;} \\ \left(\frac{3}{\tanh r}\right) \frac{1}{(2n-1)\sqrt{k_1!(k_2-1)!(k_3-1)!}} & k_2 \text{ odd, } k_3 \text{ odd;} \\ \frac{1}{\sqrt{k_1!(k_2+1)!(k_3-1)!}} & k_2 \text{ even, } k_3 \text{ odd;} \\ \frac{1}{\sqrt{k_1!(k_2-1)!(k_3+1)!}} & k_2 \text{ odd, } k_3 \text{ even.} \end{cases} \end{aligned} \tag{37}$$

Thanks to the orthonormality of the Fock states, we can hence write

$$\left\| |\psi\rangle - \hat{S}_x^b \hat{S}_x^c |\psi\rangle \right\|^2 = \frac{1}{\cosh r} \sum_{n=0}^{\infty} \sum_{k_1+k_2+k_3=2n} R_{k_1,k_2,k_3}, \tag{38}$$

where

$$R_{k_1,k_2,k_3} = \left(\frac{(2n)!}{n!}\right)^2 \left(\frac{\tanh r}{6}\right)^{2n} \tag{39}$$
$$\times \begin{cases} \left(\frac{1}{\sqrt{k_1!k_2!k_3!}} - \left(\frac{\tanh r}{3}\right) \frac{2n+1}{\sqrt{k_1!(k_2+1)!(k_3+1)!}}\right)^2 & k_2 \text{ even, } k_3 \text{ even;} \\ \left(\frac{1}{\sqrt{k_1!k_2!k_3!}} - \left(\frac{3}{\tanh r}\right) \frac{1}{(2n-1)\sqrt{k_1!(k_2-1)!(k_3-1)!}}\right)^2 & k_2 \text{ odd, } k_3 \text{ odd;} \\ \left(\frac{1}{\sqrt{k_1!k_2!k_3!}} - \frac{1}{\sqrt{k_1!(k_2+1)!(k_3-1)!}}\right)^2 & k_2 \text{ even, } k_3 \text{ odd;} \\ \left(\frac{1}{\sqrt{k_1!k_2!k_3!}} - \frac{1}{\sqrt{k_1!(k_2-1)!(k_3+1)!}}\right)^2 & k_2 \text{ odd, } k_3 \text{ even.} \end{cases}$$

Since $\lim_{r\to\infty} [\cosh(r)]^{-1} = 0$, in order for Eq. (33) to hold it would be sufficient to have $\sum_n \sum_{k_1+k_2+k_3=2n} R_{k_1,k_2,k_3}$ converging to a finite constant in the limit $r \to \infty$. This is for example the case if the sequence

$$f(n) = \lim_{r\to\infty} \sum_{k_1+k_2+k_3=2n} R_{k_1,k_2,k_3}, \tag{40}$$

converges to zero faster than $n^{-(1+\epsilon)}$, for some $\epsilon > 0$, in the limit $n \to \infty$. Our numerics confirm that this is indeed the case for $\epsilon = \frac{1}{2}$, as shown in Fig. 4. A numerical fit based on $n \lesssim 1000$ yields the asymptotic behaviour $f(n) \simeq 0.282\, n^{-3/2}$, which would provide a convergent sum.

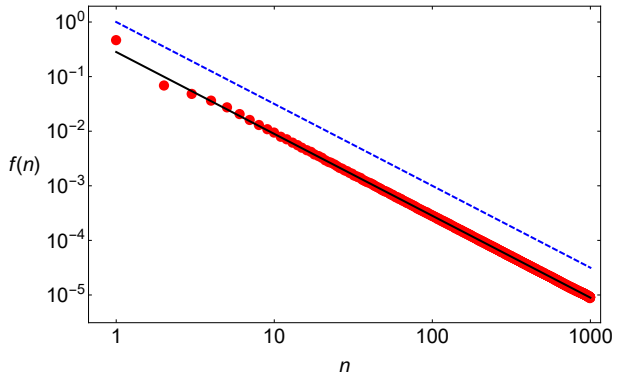

Figure 4: Numerical study of the sequence $f(n)$ as defined in Eq. (40). Red dots indicate the numerically calculated value of $f(n)$. Notice how the asymptotic behaviour for large n appears well approximated by $\simeq 0.282\, n^{-3/2}$ (black solid line), which has been obtained via a power-law fit. The sequence $n^{-3/2}$ is also shown for comparison (blue dashed line). Logarithmic scale is used on both axes. All the plotted quantities are dimensionless.

Summing up, we have provided compelling evidence that the three-mode squeezed states in Eq. (29) asymptotically approach an eigenstate of $\hat{S}_x^b \hat{S}_x^c$ as $r \to \infty$. Correspondingly, this entails that in the same limit one would obtain a maximum quantum violation of the Svetlichny inequality using pseudospin operators with the settings of Eq. (30), that is,

$$\lim_{r\to\infty} S_3(r) = \sqrt{2}. \tag{41}$$

2.4 DISCUSSION

In this Chapter we have studied theoretically the degree of genuine multipartite nonlocality in pure permutationally invariant Gaussian states of n bosonic modes, in terms of the largest amount by which the Svetlichny inequality [33] is violated by specific measurements. When adopting displaced parity measurements [10], we provided a prescription to find the optimal phase space settings in order to observe the most prominent violations of local realism, extending the results of [60]. These measurements nevertheless fail to reveal the maximum Svetlichny nonlocality allowed by quantum mechanics when operating on Gaussian states. For this reason we further considered pseudospin observables [13] and provided convincing evidence that such an ultimate bound is in fact attainable on Gaussian states when using these measurements, in particular in the three-mode instance. Extensions of this result to a higher number of modes, exploiting the symmetries of the states as outlined in our analysis, might be feasible, even though they appear significantly more intricate than the $n = 3$ instance. Also in the case of pseudospin measurements, we identified particular settings which become optimal in the regime of large squeezing. These findings can be useful to guide an experimental demonstration of genuine multipartite continuous variable nonlocality for practical purposes.

Here we have focused on the violation of the Svetlichny inequality [33], which provides a sufficient condition for detecting genuine multipartite nonlocality. More recent studies have led to the identification of a larger set of weaker inequalities, whose violation (even without a violation of Svetlichny inequality) is still sufficient

to demonstrate genuine multipartite nonlocality [44, 45]. Analysing these weaker yet more complex inequalities is considerably more cumbersome in continuous variable systems, and furthermore it is not clear a priori which inequalities can be violated on specific classes of states (and in some cases what is their maximum possible quantum violation), even though the violation of one such inequality has been investigated theoretically for three-mode Gaussian states using displaced parity measurements in [60]. Here we were mainly concerned with identifying conditions to reveal the strongest possible signature of genuine multipartite quantum nonlocality, which justifies our focus on the Svetlichny inequality, and the pursuit of its maximum violation using Gaussian states. Whether such a quantitative violation might be interpreted operationally in terms of a figure of merit for a continuous variable quantum information and communication task would be an interesting topic for further investigation.

Moving forward, it seems worth extending our study to other correlations, such as quantum steering [77, 80, 81], a weaker and asymmetric form of nonlocality which can also be detected by the violation of suitable inequalities [82, 83]. Very recently, displaced parity and pseudospin observables have been considered to detect steerability of bipartite Gaussian states [84, 85], and proven useful to reveal a larger set of steerable states than what can be characterised by using Gaussian measurements alone [80, 86]. Identifying the boundaries of the sets of steerable or nonlocal Gaussian states (in bipartite as well as multipartite continuous variable systems), and the maximum allowed violations of corresponding inequalities when acting with specific classes of feasible measurements, would be helpful to identify optimal resources for fully or partially device-independent quantum communication using continuous variable systems. The next Chapter achieves some progress in such a direction for the bipartite case.

3

QUANTUM STEERING

3.1 OVERVIEW

Quantum information science is experiencing an intensive theoretical development and an impressive experimental progress, leading to revolutionary applications in computation, communication, simulation and sensing technologies [1]. Specific ingredients of quantum systems, including superposition phenomena and different manifestations of nonclassical correlations, are being harnessed for these tasks [21, 22, 82, 83, 87–89]. Characterising the nature and degree of nonclassical correlations in quantum systems amenable to experimental implementation is thus of particular importance, to assess their potential relevance as resources for quantum enhanced tasks. Such a mission has been one of the leading themes of this thesis.

Einstein-Podolsky-Rosen (EPR) *steering* [80, 83, 90] is a type of nonclassical correlation which is strictly intermediate between quantum entanglement [22] and Bell nonlocality [21]. Unlike the latter two, steering is asymmetric, meaning that a bipartite quantum state distributed between two observers Alice and Bob may be steerable from Alice to Bob but not the other way around. Originally regarded as a somehow puzzling manifestation of the EPR paradox [23, 82, 91, 92], steering is now appreciated as a resource [93] for a variety of quantum information protocols, including one-sided device-independent quantum key distribution [94–96], sub-channel discrimination [97], and secure teleportation [98, 99].

Landmark demonstrations of EPR steering have been accomplished in particular in CV systems [95, 100–102], where nonclassical correlations can arise between de-

grees of freedom with a continuous spectrum, such as quadratures of light modes [2, 47]. These experiments, as well as the majority of theoretical studies [76, 80, 82, 86, 91, 96, 103–106], have focused specifically on verification and quantification of steering in Gaussian states of CV systems as revealed by Gaussian measurements. This is motivated on one hand by the fact that Gaussian states, which are thermal equilibrium states of quadratic Hamiltonians, admit a simple and elegant mathematical description [6–8] (see Sec. 1.1), and on the other hand by the fact that Gaussian states can be reliably produced and controlled in a variety of experimental platforms while Gaussian measurements are equally accessible in laboratory by means of homodyne detections [2].

However, it is necessary to go beyond the 'small' world of Gaussian states and measurements in order to unlock the full potential of CV quantum information processing (e.g. for universal quantum computation [107]), and to reach a more faithful characterisation of the fundamental border between classical and quantum world. In this respect, two recent papers showed that there exist bipartite Gaussian states which are not steerable by Gaussian measurements, yet whose EPR steering can be revealed by suitable non-Gaussian measurements in certain parameter regimes [84, 85]. This opens an interesting window on the 'big' non-Gaussian world and suggests that large amounts of useful nonclassical correlations could be overlooked by restricting to an all-Gaussian setting.

In this Chapter, we investigate EPR steering of two-mode CV states as detected by non-Gaussian measurements, specifically pseudospin measurements which have proven useful for studies of Bell nonlocality [13, 14, 17, 18] (as demonstrated in the previous Chapter). After setting up notation and basic concepts in Sec. 3.2, we begin our analysis by specialising to Gaussian states. We consider in particular the prominent family of two-mode squeezed thermal states and identify regions in which their steerability can be detected by pseudospin measurements [13] (but not by Gaussian ones), using a steering criterion derived from the moment matrix [108] associated with such measurements. To accomplish this analysis, which goes significantly beyond the instances considered in the existing literature [84, 85], we derive in Sec. 3.3 an explicit expression for the number basis representation of any two-mode squeezed

thermal state, a result of interest in its own right. We further discuss an extension of our study to arbitrary two-mode Gaussian states by considering an alternative set of pseudospin operators [17], which are nevertheless found less effective than Gaussian measurements for steering detection. Our analysis of EPR steering in Gaussian states by either type of pseudospin measurements is presented collectively in Sec. 3.4 including relevant examples. We then consider in Sec. 3.5 a class of non-Gaussian states defined as mixtures of Gaussian states, which represent the CV counterparts to Werner states [16]. For these states, pseudospin measurements are found to be always more effective than Gaussian ones for steering detection. We finally draw our concluding remarks in Sec. 3.6.

Overall, this Chapter (based on original results published in [4]) represents a comprehensive exploration of EPR steering in CV systems beyond the Gaussian scenario, and may serve as an inspiration for further theoretical and experimental advances on the identification and exploitation of steering for quantum technologies.

3.2 PRELIMINARIES

3.2.1 *Two-mode Gaussian states*

In this Chapter we will focus on a system of $n = 2$ modes, A and B, which can be accessed by two distant observers, respectively called Alice and Bob. Up to local unitaries, and following the notation introduced in Section 1.1, the covariance matrix of any two-mode Gaussian state can be written in the standard form [109, 110]

$$\sigma \equiv \sigma_{AB} = \left(\begin{array}{c|c} \alpha & \gamma \\ \hline \gamma^T & \beta \end{array}\right) = \left(\begin{array}{cc|cc} a & & c & \\ & a & & d \\ \hline c & & b & \\ & d & & b \end{array}\right). \tag{42}$$

The real parameters a, b, c, d, constrained to inequality (3), completely specify the global and marginal degrees of information and all forms of correlation in the state, and can be recast in terms of four local symplectic invariants of the covariance matrix

[111]. The states with $a = b$ are symmetric under swapping of the two modes. A particularly relevant subclass of Gaussian states is that of two-mode squeezed thermal (TMST) states, obtained from Eq. (42) by setting $d = -c$. These include as a special case of pure two-mode squeezed vacuum states, also known as EPR states, which are specified by

$$a = b = \cosh(2s)\,, \quad c = -d = \sinh(2s)\,, \tag{43}$$

in terms of a real squeezing parameter s.

3.2.2 *Steering criteria*

In the quantum information language [80, 103], EPR steering can be formalised in terms of entanglement verification when one of the parties is untrusted, or has uncharacterised devices. Suppose Alice wants to convince Bob, who does not trust her, that they are sharing an entangled state $\hat{\rho}$. Alice can then try and remotely prepare quantum ensembles on Bob's system that could not have been created without a shared entanglement in the first place. If she succeeds, with no need for any assumption on her devices, then entanglement is verified and the state shared by Alice and Bob is certified as $A \to B$ steerable. In formula, a bipartite state $\hat{\rho}$ is $A \to B$ steerable if and only if the probabilities of all possible joint measurements cannot be factorised into a local hidden-variable/hidden-state form [80],

$$\mathcal{P}(a,b|\hat{a},\hat{b},\hat{\rho}) \neq \sum_{\lambda} \mathcal{P}_{\lambda}\mathcal{P}(a|\hat{a},\lambda)\mathcal{P}(b|\hat{b},\hat{\rho}_{\lambda})\,, \quad \forall\, \hat{a},\hat{b}\,, \tag{44}$$

where λ is a real variable, $\{\hat{\rho}_{\lambda}\}$ is an ensemble of marginal states for Bob, $\hat{a},\hat{b}$ denote local observables for Alice and Bob, while a and b are their corresponding outcomes.

Detecting steerability from its definition (44) is challenging. To overcome this problem, several criteria have been developed to provide a more direct and experimentally friendly characterisation of EPR steering [82, 83]. One such criterion, applicable to any (not necessarily Gaussian) CV bipartite state $\hat{\rho}$ with covariance matrix σ, yields that $\hat{\rho}$ is $A \to B$ steerable if [80]

$$\sigma + i(\mathbf{0}^{\oplus N_A} \oplus \boldsymbol{\omega}^{\oplus N_B}) \not\geq 0\,, \tag{45}$$

where N_A (N_B) is the number of modes of Alice's (Bob's) subsystem. This corresponds to a steering test in which Alice and Bob perform Gaussian measurements, that is, they measure (linear combinations of) quadratures such as $\hat{q}_A$, $\hat{p}_A$ and $\hat{q}_B$, $\hat{p}_B$ respectively, by means of homodyne detections. Under the restriction of Gaussian measurements, inequality (45) is also necessary for $A \to B$ steerability if $\hat{\rho}$ is a Gaussian state. For two-mode states ($N_A = N_B = 1$), the condition (45) can be rewritten simply as

$$\det \boldsymbol{\alpha} > \det \boldsymbol{\sigma} \,. \tag{46}$$

In fact, for two-mode Gaussian states with covariance matrix in standard form as in Eq. (42), this necessary and sufficient condition is equivalent to the seminal variance criterion introduced in [91] to demonstrate the EPR paradox [82, 86, 103–105].

As anticipated in Sec. 3.1, however, Gaussian measurements are not always optimal to detect EPR steering of Gaussian states [84, 85]. More generally, one may need to resort to alternative criteria in order to witness EPR steering even in relatively simple states such as two-mode Gaussian states. A rather general approach to steering detection in bipartite states of any (finite or infinite) dimension was put forward in [108] in terms of a hierarchy of inequalities, constructed from the moment matrix corresponding to arbitrary pairs of measurements on Alice's and Bob's sides. As further detailed in the recent review [83], this method is amenable to a numerical implementation via semidefinite programming, however it also provides an easily applicable analytical condition that is sufficient to reveal steering. Namely, a bipartite state $\hat{\rho}$ is $A \to B$ steerable if there exist spin-like measurement operators $\{\hat{s}_A^j\}$ and $\{\hat{t}_B^k\}$ for Alice and Bob, respectively, such that [108]

$$\langle \hat{s}_A^x \otimes \hat{t}_B^x \rangle^2 + \langle \hat{s}_A^y \otimes \hat{t}_B^y \rangle^2 + \langle \hat{s}_A^z \otimes \hat{t}_B^z \rangle^2 > 1. \tag{47}$$

In this Chapter we adopt the criterion (47) to investigate EPR steering of two-mode Gaussian and non-Gaussian states by non-Gaussian pseudospin measurements, defined in the following.

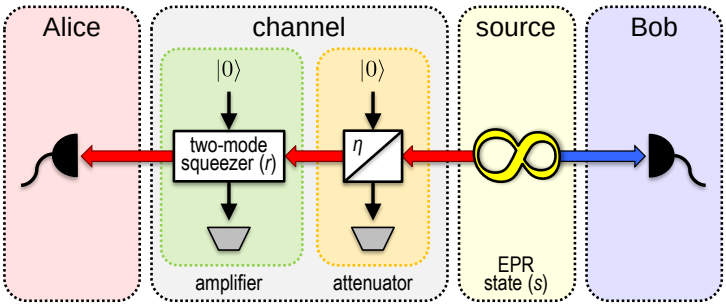

Figure 5: Scheme to generate an arbitrary TMST state [112]. An EPR source (yellow box) prepares a two-mode squeezed vacuum state with squeezing parameter s, Eq. (48). One mode (blue arrow) of the state freely propagates towards Bob while the other mode (red arrow) propagates through a phase-insensitive Gaussian channel (light gray box) towards Alice. The channel can be decomposed [113, 114] into a quantum-limited attenuator realised by a beam splitter with intensity transmissivity η (orange box) followed by a quantum-limited amplifier implemented by a two-mode squeezer with a squeezing parameter r (green box). The state shared by Alice and Bob is then a TMST state $\hat{\rho}_{AB}^{\rm TMST}(s,\eta,r)$ with covariance matrix given by Eq. (52). See text for further details.

3.3 FOCK REPRESENTATION OF TWO-MODE SQUEEZED THERMAL STATES

In this Section we obtain a result of importance in its own right, that is, we derive an explicit expression for the elements of the density matrix of an arbitrary Gaussian TMST state $\hat{\rho}$, with vanishing first moments and covariance matrix σ in standard form given by Eq. (42) with $d=-c$, in the Fock basis $\{|mn\rangle_{AB}\equiv|m\rangle_A|n\rangle_B\}_{m,n=0,1,\ldots}$.

For this purpose we use the trick [112] depicted in Fig. 5 that any TMST state can be prepared by applying a suitable single-mode phase-insensitive Gaussian channel $\mathcal{E}$ to mode A of a two-mode squeezed vacuum state

$$\hat{\rho}_{AB}^{\rm EPR}(s)=|\psi_s\rangle_{AB}\langle\psi_s|,\quad |\psi_s\rangle_{AB}=\frac{1}{\cosh(s)}\sum_{m=0}^{\infty}\tanh^m(s)|mm\rangle_{AB}\,, \tag{48}$$

where s is the squeezing parameter, which possesses a covariance matrix $\sigma_{AB}^{\rm EPR}(s)$ given by Eqs. (42)–(43). Next, we use the fact that any single-mode phase-insensitive Gaussian channel $\mathcal{E}$ can be decomposed into a sequence of a quantum-limited attenu-

ator (i.e., pure-loss) channel $\mathcal{L}_\eta$ with transmissivity η followed by a quantum-limited amplifier $\mathcal{A}_r$ with gain $\cosh^2(r)$ [113, 114], i.e., $\mathcal{E} = \mathcal{A}_r \circ \mathcal{L}_\eta$.

On the level of covariance matrix, the pure-loss channel $\mathcal{L}_\eta$ on mode A can be implemented by mixing the mode with an ancillary mode A', initially in the vacuum state with covariance matrix $\sigma_{A'} = 1$, on a beam splitter described by the symplectic matrix[2]

$$S_\eta^{\mathrm{BS}} = \begin{pmatrix} \sqrt{\eta}1 & -\sqrt{1-\eta}1 \\ \sqrt{1-\eta}1 & \sqrt{\eta}1 \end{pmatrix}. \tag{49}$$

By taking the covariance matrix $\sigma_{AB}^{\mathrm{EPR}}(s) \oplus \sigma_{A'}$ of the three modes A, B and A', transforming modes A and A' via the symplectic matrix (49), and dropping mode A', we get the covariance matrix of the output state of modes A and B after the pure-loss channel,

$$\mathcal{L}_\eta[\sigma_{AB}^{\mathrm{EPR}}(s)] = \begin{pmatrix} (b\eta + 1 - \eta)1 & \sqrt{\eta(b^2-1)}\sigma^z \\ \sqrt{\eta(b^2-1)}\sigma^z & b1 \end{pmatrix}, \tag{50}$$

with $b = \cosh(2s)$. Likewise, the amplifier $\mathcal{A}_r$ can be realised by mixing mode A with another vacuum ancillary mode A'' in a two-mode squeezer with squeezing parameter r, described by the symplectic matrix

$$S_r^{\mathrm{TM}} = \begin{pmatrix} \cosh(r)1 & \sinh(r)\sigma^z \\ \sinh(r)\sigma^z & \cosh(r)1 \end{pmatrix}. \tag{51}$$

By transforming modes A and A'' of the intermediate state with covariance matrix (50) via the symplectic matrix (51), and dropping mode A'', we finally get the output covariance matrix of modes A and B (see Fig. 5), given by [112]

$$\begin{aligned} \sigma_{AB}^{\mathrm{TMST}}(s,\eta,r) &= (\mathcal{A}_r \circ \mathcal{L}_\eta)[\sigma_{AB}^{\mathrm{EPR}}(s)] \\ &= \begin{pmatrix} (\tau b + \zeta)1 & \sqrt{\tau(b^2-1)}\sigma^z \\ \sqrt{\tau(b^2-1)}\sigma^z & b1 \end{pmatrix}, \end{aligned} \tag{52}$$

2 A unitary operation $\hat{U}$ which maps Gaussian states into Gaussian states can be described by a symplectic transformation S which acts by congruence on covariance matrices, $\sigma \mapsto S\sigma S^T$.

with $\tau = \eta\cosh^2(r)$, $\zeta = (1-\eta)\cosh^2(r) + \sinh^2(r)$. In other words, Eq. (52) is the covariance matrix of a TMST state $\hat{\rho}_{AB}^{\mathrm{TMST}}$ in standard form, given by Eq. (42) with

$$\begin{aligned} a &= \eta\cosh^2(r)\cosh(2s) + (1-\eta)\cosh^2(r) + \sinh^2(r)\,, \\ b &= \cosh(2s)\,, \\ -d &= c = \sqrt{\eta}\cosh(r)\sinh(2s)\,. \end{aligned} \tag{53}$$

Since for any admissible values of parameters a, b and $c = -d$ there is always a physical channel $\mathcal{E}$ for which the covariance matrices (52) and (42) coincide, we can always parameterise the standard form covariance matrix of a TMST state as in Eq. (52).

Let us now move to the evaluation of the Fock basis elements of the TMST state, exploiting the parametrisation of Fig. 5. By applying the channel $\mathcal{E}$ to the first mode of the density matrix (48) and using the decomposition $\mathcal{E} = \mathcal{A}_r \circ \mathcal{L}_\eta$, the matrix element to be evaluated boils down to

$$\langle m_1 m_2|\hat{\rho}_{AB}^{\mathrm{TMST}}|n_1 n_2\rangle = (1-\varsigma^2)\varsigma^{m_2+n_2}\langle m_1|(\mathcal{A}_r \circ \mathcal{L}_\eta)(|m_2\rangle\langle n_2|)|n_1\rangle, \tag{54}$$

where we set $\varsigma = \tanh(s)$ and used the linearity of the channel $\mathcal{E}$.

First, we need to calculate how the pure-loss channel $\mathcal{L}_\eta$ transforms the operator $|m\rangle\langle n|$. On the state vector level, a beam splitter unitary $\hat{U}_\eta^{\mathrm{BS}}$ with symplectic matrix (49) transforms the state $|m\rangle_A|0\rangle_{A'}$ as

$$\begin{aligned} |m\rangle_A|0\rangle_{A'} &\rightarrow |\phi\rangle_{AA'} \equiv \hat{U}_\eta^{\mathrm{BS}}|m\rangle_A|0\rangle_{A'} \\ &= \hat{U}_\eta^{\mathrm{BS}}\frac{(\hat{a}_A^\dagger)^m}{\sqrt{m!}}\hat{U}_\eta^{\dagger\mathrm{BS}}|0\rangle_A|0\rangle_{A'} \\ &= \sum_{k=0}^{m}\sqrt{\binom{m}{k}\frac{\eta^k}{(1-\eta)^{k-m}}}|k, m-k\rangle_{AA'}, \end{aligned} \tag{55}$$

where we used the relation $\hat{U}_\eta^{\mathrm{BS}}|0\rangle_A|0\rangle_{A'} = |0\rangle_A|0\rangle_{A'}$, the transformation rule $\hat{U}_\eta^{BS}\hat{a}_A^\dagger\hat{U}_\eta^{\dagger BS} = \sqrt{\eta}\hat{a}_A^\dagger + \sqrt{1-\eta}\hat{a}_{A'}^\dagger$, and the binomial theorem. Hence, if we trace out the ancilla A' from the state $|\phi\rangle_{AA'}$ of Eq. (55), we get the sought expression

$$\mathcal{L}_\eta(|m\rangle\langle n|) = \eta^{\frac{m+n}{2}}\sum_{k=0}^{\min\{m,n\}}\sqrt{\binom{m}{k}\binom{n}{k}}(\eta^{-1}-1)^k|m-k\rangle\langle n-k|. \tag{56}$$

We now need to calculate how the amplifier $\mathcal{A}_r$ acts on the operator $|m\rangle\langle n|$. Similarly to the previous case, a two-mode squeezer unitary $\hat{U}_r^{\rm TM}$ with symplectic matrix (51) transforms the state $|m\rangle_A|0\rangle_{A''}$ as

$$\begin{aligned} |m\rangle_A|0\rangle_{A''} &\rightarrow |\varphi\rangle_{AA''} \equiv \hat{U}_r^{\rm TM}|m\rangle_A|0\rangle_{A''} \\ &= \hat{U}_r^{\rm TM}\frac{(\hat{a}_A^\dagger)^m}{\sqrt{m!}}\hat{U}_r^{\dagger\rm TM}\hat{U}_r^{\rm TM}|0\rangle_A|0\rangle_{A''} \\ &= \frac{1}{[\cosh(r)]^{m+1}}\sum_{l=0}^{\infty}\sqrt{\binom{m+l}{m}}\tanh^l(r)|l+m,l\rangle_{AA''}, \end{aligned} \tag{57}$$

where we used the relations $\hat{U}_r^{\rm TM}|0\rangle_A|0\rangle_{A''} = |\psi_r\rangle_{AA''}$ with $|\psi_r\rangle$ defined in Eq. (48), $\hat{U}_r^{\rm TM}\hat{a}_A^\dagger\hat{U}_r^{\dagger\rm TM} = \cosh(r)\hat{a}_A^\dagger - \sinh(r)\hat{a}_{A''}$, and the binomial theorem. Now, by tracing out the ancilla A'' from the state $|\varphi\rangle_{AA''}$ of Eq. (57), we find that the amplifier transforms the operator $|m\rangle\langle n|$ in the following way

$$\begin{aligned} \mathcal{A}_r(|m\rangle\langle n|) &= \frac{1}{[\cosh(r)]^{m+n+2}}\sum_{l=0}^{\infty}\sqrt{\binom{m+l}{m}\binom{n+l}{n}}[\tanh(r)]^{2l} \\ &\quad\times|m+l\rangle\langle n+l|\,. \end{aligned} \tag{58}$$

Having formulae (56) and (58) in hands we are now in the position to calculate the matrix elements (54) of a TMST state in Fock basis. A rather lengthy algebra finally yields the main result of this Section:

$$\begin{aligned} &\langle m_1m_2|\hat{\rho}_{AB}^{\rm TMST}|n_1n_2\rangle \\ &= \delta_{m_1+n_2,n_1+m_2}\frac{(1-\varsigma^2)}{\cosh^2(r)}\left[\frac{\varsigma\sqrt{\eta}}{\cosh(r)}\right]^{m_2+n_2}[\tanh(r)]^{2(m_1-m_2)} \\ &\quad\times\sum_{k=\max\{0,m_2-m_1\}}^{\min\{m_2,n_2\}}\sqrt{\binom{m_2}{k}\binom{n_2}{k}\binom{m_1}{m_2-k}\binom{n_1}{n_2-k}} \\ &\quad\times\left[\sqrt{\frac{1-\eta}{\eta}}\sinh(r)\right]^{2k}. \end{aligned} \tag{59}$$

This formula, which to the best of our knowledge has not appeared elsewhere, provides the exact Fock basis representation for the most relevant class of two-mode Gaussian states, encompassing and generalising previously known special cases such as the instances where only one of the channels acts on mode A, either the pure-loss $\mathcal{L}_\eta$ (i.e., $r = 0$) or the amplifier $\mathcal{A}_r$ (i.e., $\eta = 1$) [15, 85, 115]. Note that, due

to the presence of the Kronecker symbol, the matrix elements in Eq. (59) vanish if $m_1 + m_2 + n_1 + n_2$ is odd, as it should be [115]. In the Appendix A.1, we explore further applications of Eq. (59) to derive compact expressions for multidimensional Hermite polynomials.

For completeness, we also report the explicit state vectors of all the modes involved in the scheme of Fig. 5 before tracing out the ancillae. Given an initial two-mode squeezed state of the system modes A and B as in Eq. (48) with squeezing s (EPR source), the state of modes A, B and A' after the action of the beam splitter with transmissivity η on A and A' can be written using Eq. (55) as

$$\begin{aligned} |\Phi_{s,\eta}\rangle_{ABA'} &= (\hat{U}^{\rm BS}_{\eta\ AA'} \otimes 1_B)(|\psi_s\rangle_{AB} \otimes |0\rangle_{A'}) \\ &= \sqrt{1-\varsigma^2} \sum_{m=0}^{\infty} \varsigma^m \sum_{k=0}^{m} \sqrt{\binom{m}{k} \frac{\eta^k}{(1-\eta)^{k-m}}} |k, m, m-k\rangle_{ABA'}. \end{aligned} \tag{60}$$

The final state of all modes A, B, A', A'' after the successive action of the two-mode squeezer with squeezing r on A and A'' can then be written using Eq. (57) as

$$\begin{aligned} |\Psi_{s,\eta,r}\rangle_{ABA'A''} &= (\hat{U}^{\rm TM}_{r\ AA''} \otimes 1_{BA'})(|\Phi_{s,\eta}\rangle_{ABA'} \otimes |0\rangle_{A''}) \\ &= \sqrt{1-\varsigma^2} \sum_{m=0}^{\infty} \varsigma^m \sum_{k=0}^{m} \sqrt{\binom{m}{k} \frac{\eta^k}{(1-\eta)^{k-m}}} \frac{1}{[\cosh(r)]^{k+1}} \\ &\times \sum_{l=0}^{\infty} \sqrt{\binom{k+l}{k}} [\tanh(r)]^l |k+l, m, m-k, l\rangle_{ABA'A''}. \end{aligned} \tag{61}$$

By tracing over the ancillary modes, one recovers the TMST state

$$\mathrm{tr}_{A'A''} |\Psi_{s,\eta,r}\rangle_{ABA'A''} \langle \Psi_{s,\eta,r}| \equiv \hat{\rho}^{\rm TMST}_{AB}(s, \eta, r)$$

described by Eq. (53) on the level of covariance matrix and by Eq. (59) on the level of Fock space.

3.4 STEERING OF TWO-MODE GAUSSIAN STATES: GAUSSIAN VERSUS NON-GAUSSIAN MEASUREMENTS

We now investigate EPR steering of two-mode Gaussian states as detected by the criteria presented in Section 3.2.2, looking especially for instances in which superiority

of non-Gaussian measurements over Gaussian ones can be recognised. We focus in particular on the criterion of Eq. (47) [108] evaluated using pseudospin measurements as reported in Sec. 1.2.2.

3.4.1 *Expectation values of pseudospin measurements*

Type-i

Thanks to the results of Sec. 3.3, namely Eq. (59), we are able to evaluate the expectation values of type-i pseudospin operators, defined by Eq. (5) [13], for a general TMST $\hat{\rho}_{AB}^{\mathrm{TMST}}(s,\eta,r)$ parameterised by initial squeezing s, attenuator transmissivity η, and amplifier squeezing r, according to the scheme of Fig. 5. After some algebra, we find

$$\begin{aligned}
\langle \hat{S}_A^x \otimes \hat{S}_B^x \rangle &= \frac{2}{\cosh^2(s)} \sum_{n,l=0}^{\infty} [\tanh(s)]^{4n+1} \left[\Gamma_{nl}(\eta,r)+\mathrm{Y}_{nl}(\eta,r)\right], \\
\langle \hat{S}_A^y \otimes \hat{S}_B^y \rangle &= -\langle \hat{S}_A^x \otimes \hat{S}_B^x \rangle, \\
\langle \hat{S}_A^z \otimes \hat{S}_B^z \rangle &= \langle \hat{\rho}_{AB}^{\mathrm{TMST}}(s,\eta,r) \rangle = \frac{1}{\sqrt{\det \sigma_{AB}^{\mathrm{TMST}}(s,\eta,r)}},
\end{aligned} \tag{62}$$

with

$$\begin{aligned}
\Gamma_{nl}(\eta,r) &= \sum_{k=0}^{n} \eta^{2k+\frac{1}{2}} (1-\eta)^{2n-2k} [\cosh(r)]^{-(4k+3)} [\tanh(r)]^{4l} \\
&\quad \times \sqrt{\binom{2k+2l}{2k}\binom{2k+2l+1}{2k+1}\binom{2n}{2k}\binom{2n+1}{2k+1}}, \\
\mathrm{Y}_{nl}(\eta,r) &= \sum_{k=0}^{n-1} \eta^{2k+\frac{3}{2}} (1-\eta)^{2n-2k-1} [\cosh(r)]^{-(4k+5)} [\tanh(r)]^{4l+2} \\
&\quad \times \sqrt{\binom{2k+2l+2}{2k+1}\binom{2k+2l+3}{2k+2}\binom{2n}{2k+1}\binom{2n+1}{2k+2}}.
\end{aligned}$$

The expressions in Eq. (62) can be evaluated numerically by truncating the sums over n and l to an appropriately large integer depending on the value of the parameters s,η,r.

Before going further, let us note that the steering inequality (47) for type-i pseudospin operators (5) can be interpreted in the context of mapping of CV modes onto

qubits [15, 116–118]. Namely, it is possible to map via a nonliner Jaynes-Cummings interaction a density matrix $\hat{\rho}_A$ of a single mode A onto a density matrix $\hat{\rho}_1$ of a single qubit 1, such that $\langle \hat{S}^j \rangle_{\hat{\rho}_A} \equiv \mathrm{tr}[\hat{S}^j \hat{\rho}_A] = \mathrm{tr}[\sigma^j \hat{\rho}_1] \equiv \langle \sigma^j \rangle_{\hat{\rho}_1}$ [15]. Similarly, if we map locally modes A and B of a two-mode state $\hat{\rho}_{AB}$ onto two qubits 1 and 2, the qubits will end up in a state $\hat{\rho}_{12}$ for which $\langle \hat{S}^i_A \otimes \hat{S}^j_B \rangle_{\hat{\rho}_{AB}} = \langle \sigma^i \otimes \sigma^j \rangle_{\hat{\rho}_{12}}$. Thus the analysis of EPR steering for a two-mode state using type-i pseudospin measurements can be seen as a mapping onto a two-qubit state followed by the analysis of EPR steering for the two-qubit state using conventional spin measurements. Since the mapping does not preserve entanglement [16, 117–119], i.e., some entangled two-mode states are mapped onto separable two-qubit states, we may expect that the same holds true also for steering, that is, a two-mode state can be steerable although the corresponding two-qubit state is unsteerable.

Type-ii

In the case of type-ii pseudospin operators, defined by Eq. (6) [17, 18], we can evaluate analytically their expectation values for all two-mode Gaussian states, specified in general by a standard form covariance matrix σ_{AB} as in Eq. (42) as a function of a, b, c, d. Exploiting the formulation in terms of Wigner functions, Eq. (8), we get

$$\begin{aligned}
\langle \hat{\Pi}^x_A \otimes \hat{\Pi}^x_B \rangle &= \frac{2}{\pi} \arctan \sqrt{\frac{c^2}{ab - c^2}}, \\
\langle \hat{\Pi}^y_A \otimes \hat{\Pi}^y_B \rangle &= \frac{2}{\pi \sqrt{\det \sigma_{AB}}} \arctan \sqrt{\frac{d^2}{ab - d^2}}, \\
\langle \hat{\Pi}^z_A \otimes \hat{\Pi}^z_B \rangle &= \frac{1}{\sqrt{\det \sigma_{AB}}},
\end{aligned} \tag{63}$$

where to obtain the second equation we resorted to Parseval's theorem.

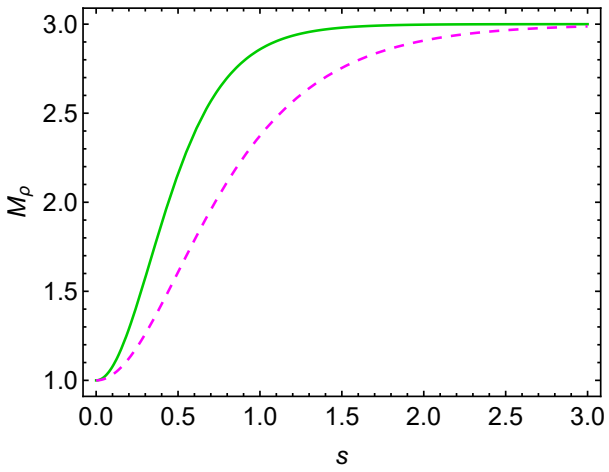

Figure 6: Plot of the left-hand side $M^{(j)}_{\hat{\rho}^{\rm EPR}_{AB}}(s)$ [Eq. (65)] of the squeezing criterion [Eq. (47)] using pseudospin measurements of type j, with $j = \mathrm{i}$ (solid green) and $j = \mathrm{ii}$ (dashed magenta), for a two-mode squeezed vacuum state $\hat{\rho}^{\rm EPR}_{AB}(s)$ [Eq. (48)] as a function of the squeezing parameter s. All the quantities plotted are dimensionless.

3.4.2 *Steering analysis, examples and discussion*

Let us denote the combination of moments in the left-hand side of the EPR steering criterion Eq. (47) evaluated on a state $\hat{\rho}_{AB}$ as $M^{(j)}_{\hat{\rho}_{AB}}$, with $j = \mathrm{i}, \mathrm{ii}$ denoting the pseudospin type. Explicitly,

$$\begin{aligned} M^{(\mathrm{i})}_{\hat{\rho}_{AB}} &= \langle \hat{S}^x_A \otimes \hat{S}^x_B \rangle^2 + \langle \hat{S}^y_A \otimes \hat{S}^y_B \rangle^2 + \langle \hat{S}^z_A \otimes \hat{S}^z_B \rangle^2 , \\ M^{(\mathrm{ii})}_{\hat{\rho}_{AB}} &= \langle \hat{\Pi}^x_A \otimes \hat{\Pi}^x_B \rangle^2 + \langle \hat{\Pi}^y_A \otimes \hat{\Pi}^y_B \rangle^2 + \langle \hat{\Pi}^z_A \otimes \hat{\Pi}^z_B \rangle^2 . \end{aligned} \tag{64}$$

Two-mode squeezed vacuum states

We begin by comparing the two types of pseudospin measurements on a two-mode squeezed vacuum state $\hat{\rho}^{\rm EPR}_{AB}(s)$, defined by Eq. (48) or equivalently by its covariance matrix $\sigma^{\rm EPR}_{AB}(s)$ with elements given in Eq. (43). Referring to the scheme of Fig. 5, this amounts to a pure EPR source without any further noisy channel on A (i.e., $\eta = 1, r = 0$). It is well known that this state is entangled, EPR steerable and

Bell nonlocal as soon as $s > 0$. It thus presents itself as an easy testground for the criterion of Eq. (47).

The expressions in Eq. (64) are straightforward to compute for the two-mode squeezed state, yielding

$$M^{(\mathrm{i})}_{\hat{\rho}^{\mathrm{EPR}}_{AB}}(s) = 1 + 2\tanh^2(2s)\,, \quad M^{(\mathrm{ii})}_{\hat{\rho}^{\mathrm{EPR}}_{AB}}(s) = 1 + (8/\pi^2)\,\mathrm{gd}^2(2s)\,, \tag{65}$$

where $\mathrm{gd}(z) = 2\arctan(e^z) - \pi/2$ is the Gudermannian function. As plotted in Fig. 6, both quantities in Eq. (65) are larger than 1 for any $s > 0$, and increase monotonically as a function of s reaching their maximum value of 3 in the limit $s \to \infty$. This confirms that the criterion of Eq. (47) is able to reveal maximum steerability of the EPR state using either type of pseudospin measurements, in agreement with previous studies of Bell nonlocality [13, 17, 18]. However, we also notice that $M^{(\mathrm{i})}_{\hat{\rho}^{\mathrm{EPR}}_{AB}}(s) \geq M^{(\mathrm{ii})}_{\hat{\rho}^{\mathrm{EPR}}_{AB}}(s)$ in general, which suggests that type-ii observables are less sensitive than type-i ones for steering detection using the adopted criterion. This will be confirmed for more general states in the following.

Two-mode squeezed states with loss on Alice

Next, we consider an important example of noisy Gaussian state, namely a TMST state resulting from the action of a pure-loss channel $\mathcal{L}_\eta$ with transmissivity η on mode A of an EPR state $\hat{\rho}^{\mathrm{EPR}}_{AB}(s)$. This state, that will be denoted by $\hat{\rho}^{\mathrm{TMST}}_{AB}(s,\eta,0)$ according to the notation of Sec. 3.3 (see Fig. 5), arises naturally in quantum key distribution, where $\mathcal{L}_\eta$ models attenuation due to transmission losses. According to Eq. (46), the state $\hat{\rho}^{\mathrm{TMST}}_{AB}(s,\eta,0)$ is $A \to B$ steerable by Gaussian measurements if and only if [80]

$$\eta > \frac{1}{2}\,. \tag{66}$$

However, recently Refs. [84, 85] found that Eq. (66) is not a critical threshold for one-way steerability, as the state $\hat{\rho}^{\mathrm{TMST}}_{AB}(s,\eta,0)$ can be steered from Alice to Bob even at lower values of η if using suitable non-Gaussian measurements. Before presenting the results of our analysis, let us provide a bit more details on the findings of [84, 85].

The authors of [84] considered an equatorial family of type-i pseudospin measurements with $\hat{S}^{\theta} = \cos(\theta)\hat{S}^{x} + \sin(\theta)\hat{S}^{y}$ and applied it together with $\hat{S}^{z}$ to the following nonlinear steering criterion [120]

$$\int_{-\pi}^{\pi} d\theta \, \langle \hat{A}^{\theta}\hat{S}^{\theta} \rangle > \frac{2}{\pi}\left(P_{+}\sqrt{1-Z_{+}^{2}} + P_{-}\sqrt{1-Z_{-}^{2}} \right), \tag{67}$$

where the measurement $\hat{A}^{\theta}$ that Alice performs on her mode is informed by Bob's choice of $\hat{S}^{\theta}$, and $P_{\pm}$ are the probabilities that Alice obtains results ± 1 for her observable $\hat{A}^{z}$, while $Z_{\pm}$ are Bob's respective conditional expectation values. The fulfillment of Eq. (67) implies that steering can be demonstrated from Alice to Bob.

Instead of pseudospin measurements, the authors in Ref. [85] defined a collection of n^2 orthogonal observables $\{\hat{A}^{(n)}\} = \{\lambda_k, \lambda_{kl}^{\pm}\}$ $(k, l = 0, 1, \ldots, n-1)$ where

$$\lambda_k = |k\rangle\langle k|, \qquad \lambda_{kl}^{\pm} = \frac{|k\rangle\langle l| \pm |l\rangle\langle k|}{\sqrt{2}\,(-1)^{\frac{1}{4}\mp\frac{1}{4}}} \quad (k < l)\,. \tag{68}$$

If the correlation matrix $C_{nn'}$ of a two-mode state ρ_{AB}, with elements $(C_{nn'})_{ij} \equiv \langle \hat{A}_i^{(n)} \otimes \hat{B}_j^{(n')} \rangle - \langle \hat{A}_i^{(n)} \rangle \langle \hat{B}_j^{(n')} \rangle$, violates the local uncertainty relations of these non-Gaussian measurements [85], i.e., if

$$\| \, C_{nn'} \, \|_{\rm tr} > \sqrt{\left(n\langle 1_n^A \rangle - \sum_{j=1}^{n} \langle \hat{A}_j^{(n)} \rangle^2 \right)\left(\langle 1_{n'}^B \rangle - \sum_{j=1}^{n'} \langle \hat{B}_j^{(n')} \rangle^2 \right)}, \tag{69}$$

then ρ_{AB} is steerable from Alice to Bob.

To further investigate the EPR steering of the lossy state $\hat{\rho}_{AB}^{\rm TMST}(s, \eta, 0)$ by non-Gaussian measurements, we have evaluated the criterion of Eq. (47) based on pseudospin measurements. Instead of reporting the explicit expressions for the quantities of Eq. (64), we plot in Fig. 7 the threshold curves such that $M_{\hat{\rho}_{AB}^{\rm TMST}}^{(j)}(s, \eta, 0) = 1$, for $j = {\rm i}$ (thick solid green) and $j = {\rm ii}$ (dot-dashed magenta), in the space of parameters (s, η). Steering from Alice to Bob according to the chosen measurements is demonstrated in the region above the corresponding threshold curve. The figure also compares our findings with the thresholds arising from Gaussian measurements [thin solid black, corresponding to saturation of Eq. (66)], from the criterion of Ref. [84] [dashed blue, corresponding to saturation of Eq. (67)], and from the criterion of Ref. [85] [dotted red, corresponding to saturation of Eq. (69)]. We see that our simple criterion based on type-i pseudospin measurements is quite powerful in revealing

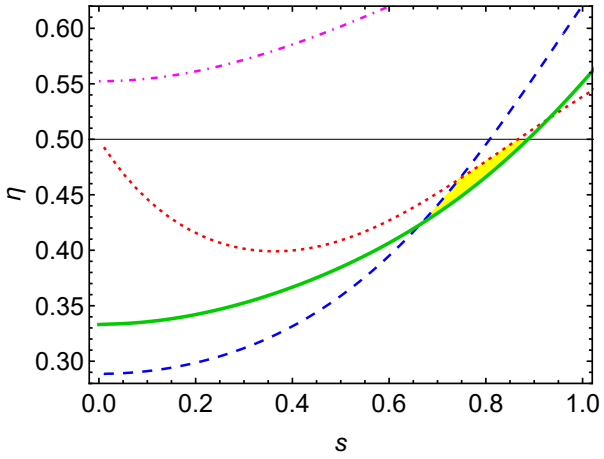

Figure 7: Comparison of EPR steering criteria for the lossy state $\hat{\rho}_{AB}^{\mathrm{TMST}}(s,\eta,0)$ as a function of the initial squeezing s and the attenuator transmissivity η (see Fig. 5). $A \to B$ steering is detected by each criterion in the parameter region above the corresponding threshold curve. The considered criteria are: steerability by Gaussian measurements; Eq. (66) [80] (thin solid black), nonlinear steering criterion with type-i pseudospin measurements, Eq. (67) [84] (dashed blue); local uncertainty relation criterion with two-level orthogonal observables, Eq. (69) [85] (dashed red); moment criterion, Eq. (47) [108], evaluated in this Chapter with type-i pseudospin measurements [13] (thick solid green); moment criterion, Eq. (47) [108], evaluated in this Chapter with type-ii pseudospin measurements [17] (dot-dashed magenta). In the shaded yellow region of parameters, steering is identified only by our criterion based on type-i pseudospin observables. All the quantities plotted are dimensionless.

$A \to B$ steerability down to $\eta \geq 1/3$ for small initial squeezing s, and is in particular better than the criterion of Eq. (67) based on the same measurements for larger s. We also identify a region (shaded yellow in Fig. 7) where our analysis certifies steerability not previously detected by any other criterion based on either Gaussian or non-Gaussian (two-outcome) measurements. For $s \gtrsim 0.9$, however, conventional Gaussian measurements are more suited for steering detection than non-Gaussian ones in the considered state. On the other hand, application of our criterion (47) with type-ii pseudospin measurements is ineffective, as it identifies an $A \to B$ steerable

region which is in fact smaller than the one identified by Gaussian measurements, Eq. (66).

General two-mode squeezed thermal states

Having verified that the EPR steering criterion Eq. (47) with (type-i) pseudospin observables is effective to detect steerability of special Gaussian states beyond the capabilities of Gaussian measurements, we can now extend our analysis to general TMST states, for which no previous steering study based on non-Gaussian measurements has been reported to date. Namely, we consider in general the state $\hat{\rho}_{AB}^{\mathrm{TMST}}(s,\eta,r)$ constructed as in Fig. 5, and investigate EPR steering as a function of the three parameters s (initial squeezing of the EPR source), η (transmissivity of the attenuator channel) and r (squeezing parameter of the amplifier channel). Our analysis is based on numerical evaluation of the formulas in Eq. (62) for the moment criterion $M^{(\mathrm{i})}_{\hat{\rho}_{AB}^{\mathrm{TMST}}}(s,\eta,r) > 1$ using type-i pseudospin measurements, and comparison with the analytical prescription of Eq. (46) relying on Gaussian measurements.

The results are reported in Fig. 8. Panel (a) shows the dependence of the steering thresholds corresponding to non-Gaussian versus Gaussian measurements as a function of the noise parameters r and η, for different fixed values of the initial squeezing s. Panel (a) shows that, even in the presence of both attenuator and amplifier noises on A, EPR steering from Alice to Bob can be demonstrated at lower values of η by using type-i pseudospin measurements as opposed to Gaussian ones, in particular in the region of moderate r. Panel (b) shows in more detail how the analysis of Fig. 7 gets modified by the presence of the additional amplifier noise induced by $\mathcal{L}_r$. While the Gaussian thresholds for steerability remain independent of s, for any fixed r, additional regions of steerability identified by type-i pseudospin measurements appear at intermediate values of s. In general, these results give a quite comprehensive picture of the potential enhancements to EPR steering characterisation for Gaussian states due to non-Gaussian measurements, and go significantly beyond specific examples considered in previous literature [84, 85].

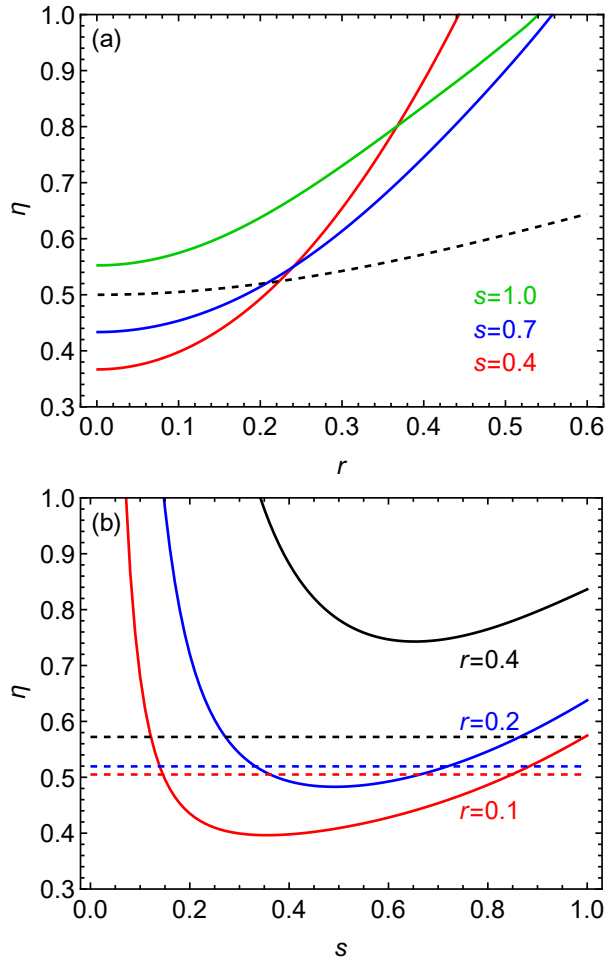

Figure 8: EPR steering of TMST states $\hat{\rho}_{AB}^{\mathrm{TMST}}(s,\eta,r)$. (a) Relation between the threshold for the transmissivity η to detect steering as a function of the amplifier squeezing r, for different initial squeezing s. (b) Relation between the threshold for η to detect steering as a function of s, for different r. Steering is detected in the regions above the corresponding curves. In both panels, solid lines indicate thresholds for the moment criterion Eq. (47) using type-i pseudospin measurements, while dashed lines indicate thresholds for the criterion Eq. (46) using Gaussian measurements. All the quantities plotted are dimensionless.

Arbitrary two-mode Gaussian states

Finally, it would be desirable to extend the previous study to arbitrary two-mode Gaussian states, with covariance matrix σ_{AB} specified by all four independent standard form parameters a, b, c, d as in Eq. (42). However, the construction of Sec. 3.3

to obtain the Fock basis elements of a Gaussian state $\hat{\rho}_{AB}$ is special to the TMST case, $d = -c$, and its possible extension beyond this case appears quite nontrivial. The only possibility we have, based on the tools employed in this Chapter, is to use type-ii pseudospin measurements to investigate the EPR steering of arbitrary two-mode Gaussian states using the moment criterion Eq. (47), thanks to the explicit expressions of Eq. (63). Unfortunately, as anticipated by the special cases investigated in the previous subsections, it turns out that type-ii pseudospin measurements used in the moment criterion of Eq. (47) are always inferior to Gaussian measurements used in the variance criterion of Eq. (46), for all two-mode Gaussian states. This can be proven by maximising the quantity $M^{(\mathrm{ii})}_{\hat{\rho}_{AB}}$, Eq. (64) entering the left-hand side of the moment criterion (47), under the condition that (46) is violated, that is, that the state is unsteerable by Gaussian measurements. We find

$$\max_{\{a,b,c,d\}} M^{(\mathrm{ii})}_{\hat{\rho}_{AB}}(a,b,c,d)\Big|_{a^2\leq(ab-c^2)(ab-d^2)} = 1\,, \tag{70}$$

which is obtained for $a = b = 1$, $c = d = 0$, i.e., when ρ_{AB} reduces to the product of vacuum states for A and B, with $\sigma_{AB} = 1_A \oplus 1_B$. This shows that the moment criterion (47) can never detect EPR steering using type-ii pseudospin measurements if the state is not already steerable by Gaussian measurements. In fact, the steerability region as detected by $M^{(\mathrm{ii})}_{\hat{\rho}_{AB}} > 1$ is strictly smaller than the one defined by Eq. (46), as demonstrated in the instance of Fig. 7. However, this does not exclude that the type-ii pseudospin operators might be useful to detect EPR steering of Gaussian states beyond Gaussian measurements if other criteria, possibly involving higher order moments, are considered.

3.5 STEERING OF CONTINUOUS VARIABLE NON-GAUSSIAN WERNER STATES

Up to now, we focused on the investigation of EPR steering for Gaussian states using non-Gaussian measurements. A next logical step is to include also non-Gaussian states into consideration. Here, we probe this scenario by analyzing steerability for a paradigmatic example of mixed non-Gaussian states given by the class of CV Werner states [16]. In past literature, the CV Werner states have been studied from the point

of view of inseparability, nonlocality and optical nonclassicality [16], as well as quantum discord [121]. In this Section we complement the list by analyzing EPR steering of these states as detected by the inequality (47) with type-i pseudospin operators (5).

A CV Werner state is defined as the convex mixture

$$\hat{\rho}^W = p\,\hat{\rho}^{\rm EPR}_{AB}(s) + (1-p)\,[\hat{\rho}^{\rm th}_A(u)\otimes\hat{\rho}^{\rm th}_B(u)], \tag{71}$$

where $0 \le p \le 1$, $\hat{\rho}^{\rm EPR}_{AB}(s)$ is the two-mode squeezed vacuum state (48), and

$$\hat{\rho}^{\rm th}_j(u) = [1-\tanh^2(u)]\sum_{m=0}^{\infty}\tanh^{2m}(u)|m\rangle_j\langle m|, \quad j=A,B \tag{72}$$

is a thermal state with $\tanh^2(u) = \langle n_j\rangle/(1+\langle n_j\rangle)$, where $\langle n_j\rangle$ is the mean number of thermal photons in mode j. For $u=s$, the state (71) can be interpreted as originating from transmission of one mode of the two-mode squeezed vacuum state (48) through a non-Gaussian channel which, with probability p, transmits the mode unaltered and, with probability $1-p$, replaces the mode with a thermal state (72) with $u=s$. In addition, in the limit $s\to\infty$ the latter Werner state provides a direct analogy to the original discrete-variable Werner state [27], because it becomes a mixture of a maximally entangled EPR state and a maximally mixed state in the infinite-dimensional Hilbert space.

Moving to the determination of the region of parameters p,s, and u, for which the steering inequality (47) is satisfied, we first need to derive the expectation values $\langle\hat{S}^j_A\otimes\hat{S}^j_B\rangle$, $j=x,y,z$, of pairs of type-i pseudospin operators (5) on the CV Werner state (71). Straightforward algebra reveals that the expectation values attain the following simple form [16],

$$\begin{aligned}\langle\hat{S}^x_A\otimes\hat{S}^x_B\rangle &= -\langle\hat{S}^y_A\otimes\hat{S}^y_B\rangle = pv\,,\\ \langle\hat{S}^z_A\otimes\hat{S}^z_B\rangle &= pw+1-w\,,\end{aligned} \tag{73}$$

where $v=\tanh(2s)$ and $w=\tanh^2(2u)$. Making use of the expectation values (73), one then finds that the steering inequality (47) boils down to

$$p^2 + \frac{2w(1-w)}{2v^2+w^2}p - \frac{w(2-w)}{2v^2+w^2} > 0, \tag{74}$$

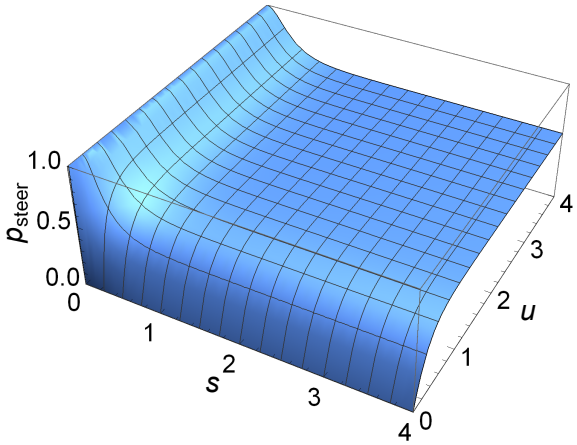

Figure 9: Threshold probability $p_{\text{steer}} \equiv p^{(\text{i})}_{\text{steer}}$ [Eq. (75)] characterising the EPR steering of the CV Werner state (71) as a function of the squeezing parameter s and the thermal noise parameter u. According to inequality (47), the state is steerable by type-i pseudospin measurements if $p > p^{(\text{i})}_{\text{steer}}$. All the quantities plotted are dimensionless.

which is equivalent to

$$p > p^{(\text{i})}_{\text{steer}} \equiv \frac{\sqrt{w\left(w - 2v^2 w + 4v^2\right)} - w(1-w)}{2v^2 + w^2}. \tag{75}$$

The region of fulfilment of the steering inequality (47) for the CV Werner state (71) with type-i pseudospin measurements is depicted in Fig. 9. By comparing it with the results of [15], one can see that the threshold $p^{(\text{i})}_{\text{steer}}$ for detecting steering is lower than the one for detecting Bell nonlocality, as it should be expected given the hierarchy existing between these two forms of nonclassical correlations. Furthermore, for $u = s$ and in the strong squeezing limit, the inequality (75) reduces to $p > 1/\sqrt{3}$, which coincides with the threshold for steering of a two-qubit Werner state when Alice has exactly three inputs [92].

We can also check the steerable region predicted by the inequality (47) when using type-ii pseudospin operators (6). By linearity, the expectation values $\langle \hat{\Pi}^j_A \otimes \hat{\Pi}^j_B \rangle$, $j = x, y, z$, of pairs of type-ii pseudospin operators on the CV Werner state can be

obtained as convex combinations of the corresponding expectation values on the two Gaussian states entering the definition (71). Exploiting Eqs. (63), we find

$$\begin{aligned}\langle \hat{\Pi}_A^x \otimes \hat{\Pi}_B^x \rangle &= \langle \hat{\Pi}_A^y \otimes \hat{\Pi}_B^y \rangle = \frac{2p}{\pi}\mathrm{gd}(2s), \\ \langle \hat{\Pi}_A^z \otimes \hat{\Pi}_B^z \rangle &= p + (1-p)\mathrm{sech}^2(2u)\,.\end{aligned} \tag{76}$$

Using the expectation values (76), one then finds that the steering inequality (47) is fulfilled using type-ii pseudospin measurements when

$$p > p_{\mathrm{steer}}^{(\mathrm{ii})} \equiv \frac{\sqrt{w\left(\pi^2 w + 8(2-w)\mathrm{gd}^2(2s)\right)} - \pi w(1-w)}{(8/\pi)\mathrm{gd}^2(2s) + \pi w^2}. \tag{77}$$

We find that the threshold $p_{\mathrm{steer}}^{(\mathrm{ii})}$ is only slightly higher than $p_{\mathrm{steer}}^{(\mathrm{i})}$ in the regime of small s, however they both converge to $1/\sqrt{3}$ in the asymptotic limit $u = s \to \infty$. Therefore both types of pseudospin observables are equally effective in this regime.

For the sake of comparison, we can finally look at the region of parameters p, s, and u in which the CV Werner state is steerable by Gaussian measurements. For this purpose, we need the covariance matrix of the state $\hat{\rho}^W$, which is simply given by the linear combination of the covariance matrices of the Gaussian states appearing in the convex mixture (71),

$$\sigma_{AB}^W = p\sigma_{AB}^{\mathrm{EPR}}(s) + (1-p)\cosh(2u)(1_A \oplus 1_B)\,. \tag{78}$$

Explicitly, σ_{AB}^W is in the standard form (42) with $a = b = p\cosh(2s) + (1-p)\cosh(2u)$ and $c = -d = p\sinh(2s)$. According to (46), the state is steerable by Gaussian measurements when $a > a^2 - c^2$, which amounts to

$$p > p_{\mathrm{steer}}^{(\mathrm{G})} \equiv \frac{\sqrt{c_s^2(1-2c_u)^2 - 2c_s c_u + c_u(4-3c_u)} + c_s(2c_u-1) - 2c_u^2 + c_u}{4c_s c_u - 2\left(c_u^2+1\right)}\,, \tag{79}$$

where $c_s = \cosh(2s)$ and $c_u = \cosh(2u)$. Remarkably, one sees that $p_{\mathrm{steer}}^{(\mathrm{G})} > p_{\mathrm{steer}}^{(\mathrm{i})}$ for any $s, u > 0$, meaning that non-Gaussian pseudospin measurements are always superior to Gaussian measurements for the characterisation of EPR steering in the non-Gaussian CV Werner states. In particular, when $u = s$ we find $p_{\mathrm{steer}}^{(\mathrm{G})} = 1/\sqrt{1+\mathrm{sech}(2s)}$, which tends to 1 in the limit $s \to \infty$, meaning that, although the state is steerable for $p > 1/\sqrt{3}$ as confirmed by either (75) or (77), Gaussian measurements can never detect steering in this asymptotic case unless $p = 1$,

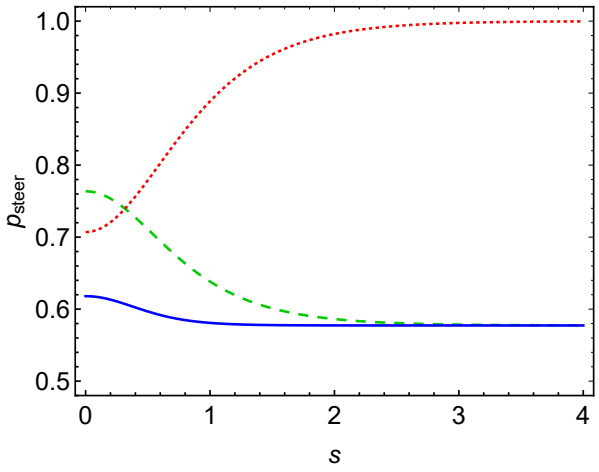

Figure 10: Threshold probabilities characterising the EPR steering of the CV Werner state (71) with $u = s$. The state is steerable by type-i pseudospin measurements when $p > p^{(\text{i})}_{\text{steer}}$ [Eq. (75)] (solid blue line), by type-ii pseudospin measurements when $p > p^{(\text{ii})}_{\text{steer}}$ [Eq. (77)] (dashed green line), and by Gaussian measurements when $p > p^{(\text{G})}_{\text{steer}}$ (dotted red line) [Eq. (79)]. All the quantities plotted are dimensionless.

i.e. when the state (71) trivially reduces to the EPR state (48). A comparison between the EPR steering thresholds (75), (77), and (79) for the CV Werner state with $u = s$ is provided in Fig. 10.

3.6 DISCUSSION

In this Chapter we investigated EPR steering [80] of continuous variable bipartite states, as revealed by a simple nonlinear criterion [108] involving the second moments of pseudospin measurements [13, 17]. Our analysis led to the identification of sizeable regions of parameters in which Gaussian states, in particular two-mode squeezed thermal states, can only be steered by non-Gaussian measurements, complementing and extending recent findings [84, 85]. We also showed that non-Gaussian (pseudospin) measurements are more effective than Gaussian (quadrature) measurements for witnessing steering of non-Gaussian continuous variable Werner states [16], whose steerability properties were found comparable to their discrete-

variable counterparts [92]. While pseudospin observables are experimentally hard to measure with current technology, our results can stimulate further research to identify accessible non-Gaussian measurements for enhanced steering detection in CV states. Since steering is a fundamental resource for quantum communication [86, 93–96, 98, 99, 104], this can lead in turn to further advances in the engineering of secure quantum network architectures based on continuous variable systems. It would be interesting in the future to investigate generalisations of our study to multipartite settings [81, 101, 122], analyzing in particular relaxations to strict monogamy inequalities for steering which hold in the all-Gaussian setting [76, 102, 106, 123].

In the first part of the Chapter, we also obtained a result of independent interest, that is the Fock representation of arbitrary two-mode squeezed thermal states. In this respect, recall that a standard approach [124–126] to the derivation of the elements of a quantum state in the Fock basis makes use of the fact that the Husimi Q quasi-probability distribution of the state is proportional to a generating function of the elements. For a Gaussian state, the generating function is Gaussian and thus it is at the same time a generating function for multidimensional Hermite polynomials [127]. This implies that, up to a normalisation factor, the Fock basis elements of Gaussian states are equal to multidimensional Hermite polynomials (see AppendixA.1 for details). Since for higher orders the polynomials are obtained as multiple derivatives of a multivariate Gaussian function, they are very complex, and thus in practical tasks one has to evaluate them numerically using a recurrence relation [115]. Here, we undertook a different route by calculating the Fock basis elements directly with the help of an expression of a two-mode squeezed thermal state via a two-mode squeezed vacuum state with one mode exposed to a phase-insensitive Gaussian channel, and a decomposition of the latter channel into a sequence of a pure-loss channel and a quantum-limited amplifier [112–114]. This led to a rather simple formula for the density matrix elements in terms of a single finite sum as given in Eq. (59). On a more general level, given the correspondence outlined above, our approach may also serve as an inspiration to derive new relations for multidimensional Hermite polynomials. An explicit instance is discussed in Appendix A.1.

4

REACTION-COORDINATE MAPPING

4.1 OVERVIEW

This thesis was concerned so far with *static* characterisation and detection of different types of correlations in CV quantum states. On the other hand, characterising the *dynamics* of open quantum systems in structured environments is central to nearly all aspects of quantum research—from modelling the chemistry of biomolecules [128–130], to understanding thermodynamics in the quantum regime [131], or assisting in the design of nano-structures for quantum technology applications [132–134]. Unfortunately, treating open systems in complex environments is extremely challenging, the main reason being the absence of a clear-cut timescale separation between system and evironmental dynamics [135]. Various tools exist to deal with such problems, including exact path-integral methods [136–138], stochastic Schrödinger equations [139, 140], unitary transformations [141, 142], or Markovian embeddings [143–146]. In this Chapter, we shall focus on the latter; specifically, on the "reaction-coordinate mapping" [147].

In a seminal paper by Garg *et al.* [128] a very simple *ansatz* was put forward for the structure of the environment modulating the rate of an electron-transfer process in a biomolecule. Essentially, it assumes that a distinct collective environmental coordinate—the *reaction* coordinate (RC)—couples strongly to the donor–acceptor system, which can be thought-of as a two-level spin. In this construction, the combined effect of all other environmental degrees of freedom would merely cause semi-classical friction on the spin–RC composite. It is then possible to view the spin as

an open system and work out its dissipative dynamics via, e.g., exact path-integral methods.

Interestingly, the ansatz can be turned on its head [144, 146, 148] and viewed as a Markovian embedding technique. Namely, an arbitrarily complicated environment may be iteratively decomposed by first, extracting a collective environmental coordinate and working out the coupling of the resulting 'augmented system' to the remaining 'residual environment'. By repeating this procedure sufficiently many times, one ends up with an open-system model with the simplest friction-like Ohmic dissipation [144, 145], albeit with a much larger system size. Whenever the residual friction (i.e., dissipation strength) is perturbatively small, the problem can be rigorously solved via standard weak-coupling Markovian master equations[3]. This provides a simple route to tackle otherwise intractable open quantum systems, especially when a single iteration of the procedure suffices for the problem at hand.

The reaction-coordinate mapping has been applied extensively to open quantum systems strongly coupled to both bosonic [146, 149–157] and fermionic [158–160] reservoirs. Its relative ease of use and the neat physical picture that emerges from it, in terms of, e.g., system–environment correlation-sharing structure [146, 149], make it particularly appealing as a general-purpose open-system tool. Unfortunately, relying on perturbative master equations imposes a priori severe limitations on the parameter ranges in which the method can be used. Intriguingly, however, it has resisted benchmarking at finite temperatures over a wide friction range [146, 149, 158], which made us wonder where are its true limitations[4].

In this Chapter, based on original material published in [5], we set out precisely to "push" the method to the limit, by deliberately taking the forbidden large friction limit in a minimal heat-transport setup. Our biggest advantage is that we work with an exactly solvable model [161]; we can thus always benchmark the accuracy of the mapping without having to approximate the exact dynamics numerically. Under steady-state conditions, we find that the RC mapping does work accurately even un-

3 A Fokker–Plank equation may be derived in the opposite large-friction limit [128, 146].

4 Recently, the RC mapping has been shown to break down at large friction in the zero-temperature limit [157]. Our calculations here are, however, limited to *finite* temperatures.

der extremely large friction, in spite of the fact that the underlying master equation breaks down. We also find that overdamped dynamics, resulting in strong residual friction, is accurately captured by this method. Importantly, however, when the residual friction is strong and one relies on weak-coupling master equations to compute heat (or particle) currents across the non-equilibrium open system of interest, the results can be completely flawed and yet, appear physically consistent. This observation can have important consequences when using the reaction-coordinate mapping to explore the thermodynamics of strongly coupled nanoscale open systems; verifying that the method approximates the state of an open system correctly is certainly not enough to trust it with the calculation of quantum-thermodynamic variables.

As a by-product of our master-equation analysis of the augmented system subjected to friction, we derive here a (global) Born–Markov secular quantum master equation for a general linear network of harmonic nodes coupled to arbitrarily many equilibrium environments. This generalises the customarily used *local* master equations applied to quantum transport problems through weakly interacting networks [162]. We also write the ensuing non-equilibrim steady state, and explicit formulas for the corresponding stationary heat currents. Finally, we discuss the *dos and don'ts* of the often confusing Hamiltonian frequency-renormalisation counter-terms that appear in quantum Brownian motion [163–165], as it is particularly important to use them consistently when performing the reaction-coordinate mapping.

This Chapter is structured as follows: In Sec. 4.2.1, we introduce our simple model and discuss very briefly the reaction-coordinate mapping. In Sec. 4.2.2, we provide the general quantum master equation that we shall later apply on our augmented system. Rather than reproducing the standard textbook derivation from the microscopic system–bath(s) model, we limit ourselves to provide here the key steps, and write down instead the full equations of motion explicitly, along with their stationary solutions, and the corresponding steady-state heat currents. In Sec. 4.2.3 we outline the exact solution of both our original problem and that of the augmented system undergoing (arbitrarily strong) friction. We then proceed to discuss the steady-state (cf. Sec. 4.3.1) and dynamical (cf. Sec. 4.3.2) benchmarks to the reaction-coordinate mapping, commenting both on the approximation to the state of the system and to

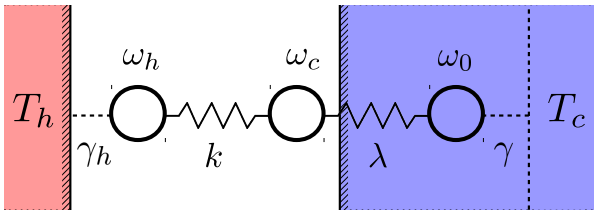

Figure 11: Sketch of the non-equilibrium quantum wire with nodes at frequencies ω_h and ω_c and internal coupling k. The dissipative interaction between node ω_h and the corresponding (hot) bath, at T_h, is characterised by an Ohmic spectral density, e.g., $J_h(\omega) \sim \gamma_h \omega$. As a result, the corresponding environmental correlation time is short. Furthermore, the dissipation strength γ_h is assumed to be perturbatively weak. On the contrary, the (cold) bath at T_c features long-lived correlations due to the structured spectral density $J_c(\omega) = \gamma\lambda^2\omega/\left[\gamma^2\omega^2 + \left(\omega^2 - \omega_0^2\right)^2\right]$. The resulting dynamics can be mimicked exactly by coupling a reaction coordinate at frequency ω_0 to the system with strength λ. This composite makes up the augmented system which, in turn, couples to a residual reservoir—customarily assumed to be in equilibrium also at T_c—via $\tilde{J}_c(\omega) \sim \gamma\,\omega$. This guarantees that the residual environmental correlations for the augmented system are short-lived. However, if the 'friction' coefficient γ in $J_c(\omega)$ is large, so is the residual dissipation strength. Crucially, this clashes with the weak-coupling approximation which underpins *any* perturbative quantum master equation that could be written for the augmented three-node system.

the stationary heat currents flowing across it. Finally, in Sec. 4.4, we wrap up and draw our conclusions.

4.2.1 *A two-node non-equilibrium quantum wire*

Full Hamiltonian

As already advanced, our model consists of a two-node chain (or "quantum wire") of harmonic oscillators with a linear spring-like coupling of strength k (see Fig. 11), that is

$$\boldsymbol{H}_w = \sum\nolimits_{\alpha\in\{h,c\}} \left(\frac{1}{2}\omega_\alpha^2 \boldsymbol{X}_\alpha^2 + \frac{\boldsymbol{P}_\alpha^2}{2}\right) + \frac{k}{2}(\boldsymbol{X}_h - \boldsymbol{X}_c)^2. \tag{80}$$

Note that here and in what follows, we set all masses to one. We shall also take $\hbar = k_B = 1$. The wire is kept out of equilibrium by two linear bosonic baths at temperatures T_α. Throughout, $\alpha \in \{h, c\}$ stands for 'hot' or 'cold', i.e., $T_h > T_c$. Their Hamiltonians can thus be cast as $\boldsymbol{H}_{T_\alpha} = \sum_\mu \omega_\mu \boldsymbol{a}_\mu^{(\alpha)\,\dagger} \boldsymbol{a}_\mu^{(\alpha)}$, where $\boldsymbol{a}_\mu^{(\alpha)\,\dagger}$ ($\boldsymbol{a}_\mu^{(\alpha)}$) is a creation (annihilation) operator of bath α in the collective bosonic environmental mode at frequency ω_μ. In turn, the dissipative interactions between the wire and the baths are

$$\boldsymbol{H}_{\mathrm{diss},\,\alpha} = \boldsymbol{X}_\alpha \otimes \boldsymbol{B}_\alpha \coloneqq \boldsymbol{X}_\alpha \sum\nolimits_\mu g_\mu^{(\alpha)}\, \boldsymbol{x}_\mu^{(\alpha)} \qquad \alpha \in \{h, c\}, \tag{81}$$

where the quadratures $\sqrt{2\omega_\mu}\, \boldsymbol{x}_\mu^{(\alpha)} \coloneqq \boldsymbol{a}_\mu^{(\alpha)\,\dagger} + \boldsymbol{a}_\mu^{(\alpha)}$ and, as usual, the coupling constants $g_\mu^{(\alpha)}$ make up the spectral densities

$$J_\alpha(\omega) \coloneqq \pi \sum\nolimits_\mu \frac{g_\mu^{(\alpha)\,2}}{2\omega_\mu} \delta(\omega - \omega_\mu) \qquad \alpha \in \{h, c\}\,. \tag{82}$$

Importantly, each system–bath coupling $\boldsymbol{H}_{\mathrm{diss},\alpha}$ requires us to introduce a renormalisation term in the bare Hamiltonian of the wire $\boldsymbol{H}_w \mapsto \boldsymbol{H}_w + \boldsymbol{\delta H}_{w\text{–}\alpha}$, which compensates for the environmental distortion on the system's potential [165]. If we were not to include such terms and let $T_h = T_c = T$ be arbitrarily large, the exact stationary state would approach $\boldsymbol{\varrho}_w(\infty) \sim \exp\left[-(\boldsymbol{H}_w - \boldsymbol{\delta H}_{w\text{–}h} - \boldsymbol{\delta H}_{w\text{–}c})/T\right]$ instead of the classical limit $\boldsymbol{\varrho}_w(\infty) \sim \exp\left(-\boldsymbol{H}_w/T\right)$; this should be seen as an important deficiency of the model [163]. Specifically, these extra terms are

$$\boldsymbol{\delta H}_{w\text{–}\alpha} = \boldsymbol{X}_\alpha^2 \sum\nolimits_\mu \frac{g_\mu^{(\alpha)\,2}}{2\omega_\mu^2} = \boldsymbol{X}_\alpha^2 \int_0^\infty \frac{\mathrm{d}\omega}{\pi}\, \frac{J_\alpha(\omega)}{\omega} \coloneqq \frac{\delta_\alpha}{2} \boldsymbol{X}_\alpha^2, \tag{83}$$

and the full Hamiltonian of our system is, therefore,

$$\boldsymbol{H} = \boldsymbol{H}_{T_h} + \boldsymbol{H}_{\mathrm{diss},\,h} + \boldsymbol{\delta H}_{w\text{–}h} + \boldsymbol{H}_w + \boldsymbol{\delta H}_{w\text{–}c} + \boldsymbol{H}_{\mathrm{diss},\,c} + \boldsymbol{H}_{T_c}. \tag{84}$$

We take an Ohmic spectrum for the coupling to the 'hot bath', i.e., $J_h(\omega) = \gamma_h\,\omega\,\theta(\omega/\Lambda_h)$, where $\theta(x)$ is some rapidly decaying function for arguments $x > 1$, which places an upper bound on the excitation energies. For practical reasons we choose the algebraic cutoff $\theta(x) = (1+x^2)^{-1}$, although other choices would not alter our results as long as Λ_h is large. Such $J_h(\omega)$ is referred-to as 'overdamped' in the context of energy transfer in molecular systems [149]. For the coupling of the wire to the cold bath, we take instead the 'underdamped' spectrum

$$J_c(\omega) = \frac{\gamma\,\lambda^2\,\omega}{\gamma^2\omega^2 + (\omega^2 - \omega_0^2)^2}, \tag{85}$$

which displays a peak around ω_0, whose height and width are essentially controlled by λ and γ, respectively[5]. This is precisely the effective spectral density resulting from the aforementioned ansatz by Garg *et al.* [128]. The frequency-renormalisation shifts δ_α for these expectral densities are explicitly given by $\delta_h = \gamma_h\Lambda_h$ and $\delta_c = \lambda^2/\omega_0^2$.

The decay of the environmental correlation functions $\langle \boldsymbol{B}_\alpha(t)\,\boldsymbol{B}_\alpha(0)\rangle$ gives an idea of the bath's memory time, and to which extent a simple Markovian relaxation process can be a good approximation to the actual dynamics. Specifically [166]

$$\langle \boldsymbol{B}_\alpha(t)\,\boldsymbol{B}_\alpha(0)\rangle = \int_0^\infty \frac{\mathrm{d}\omega}{\pi}\,J_\alpha(\omega)\left(\coth\frac{\omega}{2T_\alpha}\cos\omega t - i\sin\omega t\right). \tag{86}$$

While, at finite temperatures, a spectral density like our $J_h(\omega)$ typically leads to very short correlation times, consistent with the Markovian approximation, a spectrum such as (85) can give rise to very long-lived correlations and thus, to a much more complex dynamics. However, at sufficiently low temperatures—a regime which we shall not explore here—the bath correlation times can become comparable to the typical system dynamics even for an Ohmic spectral density.

5 Note that in the limit of very large γ this becomes $J_c(\omega) \sim \frac{\lambda^2}{\gamma\omega}$.

The reaction-coordinate mapping in a nutshell

To circumvent this problem one may try to exploit the fact that Eq. (85) is the effective spectral density for a system which couples indirectly—namely, through a bosonic mode, or reaction coordinate, of frequency ω_0—to a residual reservoir with a purely Ohmic spectrum [128]; the coupling between the auxiliary mode and the system being of strength λ (see Fig. 11). Put in other words, the dynamics

$$\frac{\mathrm{d}}{\mathrm{d}t}\boldsymbol{\varrho}_w(t) = -i\,\mathrm{tr}_{\bar{w}}\,[\tilde{\boldsymbol{H}},\tilde{\boldsymbol{\rho}}] \tag{87}$$

generated by

$$\begin{aligned}\tilde{\boldsymbol{H}} \coloneqq \boldsymbol{H}_{T_h} + \boldsymbol{H}_{\mathrm{diss},\,h} + \boldsymbol{\delta H}_{w\text{–}h} + \boldsymbol{H}_w + \boldsymbol{\delta H}_{w\text{–}c} \\ - \lambda\,\boldsymbol{X}_c\boldsymbol{X}_{\mathrm{RC}} + \frac{1}{2}\left(\omega_0^2\,\boldsymbol{X}_{\mathrm{RC}}^2 + \boldsymbol{P}_{\mathrm{RC}}^2\right) + \boldsymbol{\delta H}_{\mathrm{RC\text{–}res}} \\ + \boldsymbol{X}_{\mathrm{RC}}\sum\nolimits_{\mu}\tilde{g}_{\nu}^{(c)}\tilde{\boldsymbol{x}}_{\nu}^{(c)} + \sum\nolimits_{\nu}\omega_{\nu}\,\tilde{\boldsymbol{a}}_{\nu}^{(c)\,\dagger}\tilde{\boldsymbol{a}}_{\nu}^{(c)},\end{aligned} \tag{88}$$

exactly coincides with that of

$$\frac{\mathrm{d}}{\mathrm{d}t}\boldsymbol{\varrho}_w(t) = -i\,\mathrm{tr}_{\bar{w}}[\boldsymbol{H},\boldsymbol{\rho}], \tag{89}$$

when the coefficients $\{g_{\mu}^{(c)}\}$ in $\boldsymbol{H}_{\mathrm{diss},\,c}$ correspond to Eq. (85) [by virtue of (82)] and the $\{\tilde{g}_{\nu}^{(c)}\}$ in the sixth term on the right-hand side of Eq. (88), to $\tilde{J}_c(\omega) = \gamma\,\omega$; technically, some suitable cutoff function $\theta(\omega/\tilde{\Lambda}_c)$ with would be required, the mapping being exact only in the limit $\tilde{\Lambda}_c \to \infty$. Here, $\mathrm{tr}_{\bar{w}}$ amounts to tracing over all degrees of freedom except for the wire. The boldface symbols with tilde correspond to operators completely or partly supported in the residual reservoir; in our case, the quadratures $\{\tilde{\boldsymbol{x}}_{\nu}^{(c)}\}$, the creation and annihilation $\{\tilde{\boldsymbol{a}}_{\nu}^{\dagger\,(c)},\tilde{\boldsymbol{a}}_{\nu}^{(c)}\}$ operators in modes at frequency ω_{ν}; and the joint state of the hot bath, the wire, the reaction coordinate, and the residual reservoir $\tilde{\boldsymbol{\rho}}(t)$. Finally, the newly introduced operators $\boldsymbol{X}_{\mathrm{RC}}$ and $\boldsymbol{P}_{\mathrm{RC}}$ stand for the canonical degrees of freedom of the RC. Note that we have included as well the renormalisation term $\boldsymbol{\delta H}_{\mathrm{RC\text{–}res}}$ arising from the coupling between the RC and the residual bath [cf. Eq. (83)]. Accessible and rigorous derivations of the equivalence between Eqs. (89) and (87) can be readily found in the literature [128, 144, 146, 150].

There is, however, an important caveat regarding the initial condition for the augmented system. It is common practice to assume that the residual reservoir is in equilibrium at temperature T_c, just like the original physical bath (see Fig. 11); and to initialise the auxiliary RC in a thermal state at T_c, uncorrelated from the rest [146, 149]. Note that the dynamics generated by Eqs. (87) and (89) only agree if $\boldsymbol{\rho}(0) = \tilde{\boldsymbol{\rho}}(0)$, i.e.,

$$\boldsymbol{\varrho}_{T_h} \otimes \boldsymbol{\varrho}_w(0) \otimes \boldsymbol{\varrho}_{T_c} = \boldsymbol{\varrho}_{T_h} \otimes \boldsymbol{\varrho}_w(0) \otimes \tilde{\boldsymbol{\varrho}}_{\mathrm{RC}\,+\,\mathrm{res}}(0)\,. \tag{90}$$

In particular, this means that the composite 'RC + residual reservoir' should start instead in a joint thermal state at temperature T_c; that is, $\tilde{\boldsymbol{\varrho}}_{\mathrm{RC}\,+\,\mathrm{res}}(0) = \boldsymbol{\varrho}_{T_c}$, which is *not* of the form $\boldsymbol{\varrho}_{\mathrm{RC}}(0) \otimes \tilde{\boldsymbol{\varrho}}_{T_c}$. Hence, there could be large initial correlations between the RC and the residual reservoir, especially at low T_c. Importantly, the absence of correlations with the environment is central to the derivation of the most common quantum master equations [166]. Luckily, in many cases of practical interest the residual interactions $\tilde{g}_\mu^{(c)}$ are sufficiently weak so that the dynamics is faithfully captured under this simple assumption. As we show in Sec. 4.3.2 below, this is indeed the case when working in the overdamped limit. Furthermore, given its uniqueness [167], the non-equilibrium steady state (NESS) of our linear wire is always correctly reproduced by the augmented system, regardless of the initial condition for the RC.

Before moving on, let us briefly recapitulate: Our original problem consists of two interacting oscillators locally coupled to two heat baths. The coupling to one of them is of the form (85), which complicates the analysis as it is likely to produce non-Markovian dissipation (i.e., with long memory times). Luckily this precise dissipative dynamics can be exactly mimicked by replacing the problematic thermal contact with one auxiliary oscillator undergoing purely Markovian dissipation. In a suitable parameter range, this 'augmented' three-oscillator model can thus be tackled via a standard master equation (as we do in Sec. 4.2.2 below), which would allow us to recover the original dynamics by just tracing out the auxiliary coordinate. The "twist" of this project is that we push such master equation far beyond its range of applicability—namely, we allow for a very strong residual dissipation on the augmented system—and benchmark its prediction for the steady state of the wire against

the *exact* stationary solution of the problem. This can always be obtained with the methods outlined in Sec. 4.2.3, since our $\boldsymbol{H}$ in Eq. (88) is fully linear.

4.2.2 *Markovian master equation and its stationary solution*

The (global) GKLS master equation

We will now outline the derivation of the adjoint quantum master equation for an arbitrary linear network of N harmonic nodes, locally coupled to M baths. This is a Born–Markov secular master equation [166] in the standard Gorini–Kossakowski–Lindblad–Sudarshan (GKLS) form [168, 169]. In this project we shall only be interested in applying it to a simple 1D chain of three (and, in Sec. 4.3.2, also two) harmonic oscillators with heat baths coupled at both ends. Nonetheless, the general equation is of independent interest, as it can be applied to many problems in quantum transport.

It is important to stress that we treat dissipation *globally*, as opposed to the widespread 'local' or 'additive' approach [162]. That is, we acknowledge that even if each bath couples *locally* to one node of the network, the ensuing dissipation affects the system *as a whole*, due to the internal interactions. Indeed, the local approach is known to lead to severe physical inconsistencies [153, 170–173]. Rigorously, such local equations are only acceptable when understood as either the lowest-order term in a perturbative expansion of a global master equation in the internal coupling strength [174, 175], or as a limiting case of a discrete collisional process [176–178]. In any case, addressing dissipation locally is often the only practical way forward in large interacting non-linear open systems—exact diagonalisation of the full many-body Hamiltonian is, otherwise, required. Remarkably, finding, e.g., the NESS, which sets the transport properties of any interacting linear network, with the "plug-and-play" stationary solution below [i.e., Eqs. (98) and (100)] only requires the diagonalisation of the corresponding $N \times N$ interaction matrix.

The Hamiltonian of a general linear network can be cast as

$$\boldsymbol{H}_N = \frac{1}{2}\left(\vec{\boldsymbol{X}}^T V \vec{\boldsymbol{X}} + \vec{\boldsymbol{P}}^T \vec{\boldsymbol{P}}\right), \tag{91}$$

assuming again that masses are $M = 1$. Here, $\vec{\boldsymbol{X}}$ and $\vec{\boldsymbol{P}}$ are N-dimensional vectors containing the position and momentum operators of each node, and V is real and symmetric. Let P be the orthogonal transformation that brings (91) into the diagonal form $\boldsymbol{H}_N = \frac{1}{2}\left(\vec{\boldsymbol{\eta}}^T \Omega^2 \vec{\boldsymbol{\eta}} + \vec{\boldsymbol{\pi}}^T \vec{\boldsymbol{\pi}}\right)$, where $\Omega_{ij} = \Omega_i \delta_{ij} > 0$ is a diagonal matrix formed of the normal mode frequencies corresponding to the conjugate variables $\left\{\boldsymbol{\eta}_i, \boldsymbol{\pi}_i\right\}_{i\in\{1,\cdots,N\}}$ (i.e., $\vec{\boldsymbol{\eta}} \coloneqq P^T \vec{\boldsymbol{X}}$).

The standard derivation of a Born–Markov secular master equation [161, 166, 171] now requires to decompose the 'system–environment' couplings [in our case, $\boldsymbol{X}_i$ for the M nodes coupled to local baths, as per Eq. (81)] as eigen-operators of $\boldsymbol{H}_N$. That is $\boldsymbol{X}_i = \sum_j \boldsymbol{L}_i(\Omega_j) + \boldsymbol{L}_i(\Omega_j)^\dagger$ so that $[\boldsymbol{H}_N, \boldsymbol{L}_i(\Omega_j)] = -\Omega_j \boldsymbol{L}_i(\Omega_j)$. These non-Hermitian operators, turn out to be simply

$$\boldsymbol{L}_i(\Omega_j) = \frac{P_{ij}}{\sqrt{2\Omega_j}} \boldsymbol{b}_j\,, \qquad \boldsymbol{L}_i(-\Omega_j) \coloneqq \boldsymbol{L}_i(\Omega_j)^\dagger\,, \tag{92}$$

where $\boldsymbol{b}_j = \sqrt{\Omega_j/2}\left(\boldsymbol{\eta}_j + i\boldsymbol{\pi}_j/\Omega_j\right)$. With these definitions, the equation of motion for an arbitrary Heisenberg-picture (Hermitian) operator $\boldsymbol{O}(t)$ under the Born–Markov and secular approximations reads [166]

$$\begin{aligned}
\frac{\mathrm{d}\boldsymbol{O}(t)}{\mathrm{d}t} &= i\left[\boldsymbol{H}_N, \boldsymbol{O}(t)\right] \\
&+ \sum\nolimits_{i=1}^{M}\Bigg(\sum\nolimits_{j=1}^{N} \Gamma_i(\Omega_j)\left(\boldsymbol{L}_i(-\Omega_j)\,\boldsymbol{O}(t)\,\boldsymbol{L}_i(\Omega_j) - \frac{1}{2}\left\{\boldsymbol{L}_i(-\Omega_j)\,\boldsymbol{L}_i(\Omega_j), \boldsymbol{O}(t)\right\}_+\right) \\
&+ \sum\nolimits_{j=1}^{N} \Gamma_i(\Omega_j)\, e^{-\Omega_j/T_j}\left(\boldsymbol{L}_i(\Omega_j)\,\boldsymbol{O}(t)\,\boldsymbol{L}_i(-\Omega_j) - \frac{1}{2}\left\{\boldsymbol{L}_i(\Omega_j)\,\boldsymbol{L}_i(-\Omega_j), \boldsymbol{O}(t)\right\}_+\right)\Bigg),
\end{aligned} \tag{93}$$

with $\{\cdot,\cdot\}_+$ denoting the anticommutator and the decay rates being given by $\Gamma_i(\Omega_j) \coloneqq 2\,J_i(\Omega_j)\left(1 - e^{-\Omega_j/T_i}\right)^{-1}$, so that $\Gamma_i(-\Omega_j)/\Gamma_i(\Omega_j) = \exp\left(-\Omega_j/T_i\right)$, thus reflecting local detailed balance.

The main appeal of Eq. (93) is that it is guaranteed to generate a completely positive and trace-preserving dynamics for the system [168, 169], unlike other frequently used weak-coupling master equations [179, 180]. Furthermore, under mild ergodicity assumptions, it admits a unique stationary solution [181] which, in the case of a single environmental temperature T, is the thermal equilibrium state $\boldsymbol{\varrho}_N(t) \propto \exp\left(-\boldsymbol{H}_N/T\right)$ [182]. Importantly, this means that no renormalisation needs to be

done on the Hamiltonian $\boldsymbol{H}_N$ to recover the correct equilibrium state in the high-temperature limit. For that reason, when applying Eq. (93) to the three-node augmented system, we take

$$\boldsymbol{H}_3 = \boldsymbol{H}_w + \boldsymbol{\delta H}_{w\text{–}c} - \lambda \boldsymbol{X}_c \boldsymbol{X}_{\mathrm{RC}} + \frac{1}{2}\left(\omega_0^2 \boldsymbol{X}_{\mathrm{RC}}^2 + \boldsymbol{P}_{\mathrm{RC}}^2\right) \tag{94}$$

as the system Hamiltonian; i.e, we discard the renormalisation terms $\boldsymbol{\delta H}_{h\text{–}w}$ and $\boldsymbol{\delta H}_{\mathrm{RC\text{–}res}}$ in Eq. (88), corresponding to the thermal contact with the hot and the residual environment, respectively.

However, the term $\boldsymbol{\delta H}_{w\text{–}c}$ is—by construction—part of the augmented system after the reaction-coordinate mapping [146, 150]. As we shall see in Sec. 4.3.2 below, disregarding this latter term in the augmented-system Hamiltonian, e.g., on the basis of δ_c being small, can yield the wrong dynamics for the wire at intermediate times, even if the short-time evolution and the steady state are reproduced accurately.

Equations of motion for the covariances

Applying Eq. (93) to the symmetrised covariances $\left\langle \frac{1}{2}\{\boldsymbol{r}_j(t), \boldsymbol{r}_k(t)\}_+ \right\rangle \coloneqq [c_{\mathrm{me}}^{(N)}]_{jk}(t)$, where $\vec{\boldsymbol{r}} = (\boldsymbol{\eta}_1, \boldsymbol{\pi}_1, \cdots, \boldsymbol{\eta}_N, \boldsymbol{\pi}_N)^T$, yields a closed algebra for the 'covariance matrix' of the network $c_{\mathrm{me}}^{(N)}(t)$, where the sub-index 'me' stands for 'master equation' and allows to differentiate it from the 'ex' (for 'exact') covariance matrix, that we will compute in Sec. 4.2.3 below. Specifically, we have

$$\frac{\mathrm{d}}{\mathrm{d}t}\langle \boldsymbol{\eta}_j^2 \rangle = \sum\nolimits_{i=1}^{M} \frac{P_{ij}^2}{2\Omega_j} \Delta_i(\Omega_j) \langle \boldsymbol{\eta}_j^2 \rangle + \langle \{\boldsymbol{\eta}_j, \boldsymbol{\pi}_j\}_+ \rangle + \sum\nolimits_{i=1}^{M} \frac{P_{ij}^2}{4\Omega_j^2} \Sigma_i(\Omega_j) \tag{95a}$$

$$\frac{\mathrm{d}}{\mathrm{d}t}\langle \{\boldsymbol{\eta}_j, \boldsymbol{\pi}_j\}_+ \rangle = -2\Omega_j^2 \langle \boldsymbol{\eta}_j^2 \rangle + 2\langle \boldsymbol{\pi}_j^2 \rangle + \sum\nolimits_{i=1}^{M} \frac{P_{ij}^2}{2\Omega_j} \Delta_i(\Omega_j) \langle \{\boldsymbol{\eta}_j, \boldsymbol{\pi}_j\}_+ \rangle \tag{95b}$$

$$\frac{\mathrm{d}}{\mathrm{d}t}\langle \boldsymbol{\pi}_j^2 \rangle = \sum\nolimits_{i=1}^{M} \frac{P_{ij}^2}{2\Omega_j} \Delta_i(\Omega_j) \langle \boldsymbol{\pi}_j^2 \rangle - \Omega_j^2 \langle \{\boldsymbol{\eta}_j, \boldsymbol{\pi}_j\}_+ \rangle + \sum\nolimits_{i=1}^{M} \frac{P_{ij}^2}{4} \Sigma_i(\Omega_j), \tag{95c}$$

together with the asymptotically vanishing covariances (for $j \neq k$)

$$\frac{\mathrm{d}}{\mathrm{d}t}\langle \boldsymbol{\eta}_j \boldsymbol{\eta}_k \rangle = \langle \boldsymbol{\eta}_j \boldsymbol{\pi}_k \rangle + \langle \boldsymbol{\eta}_k \boldsymbol{\pi}_j \rangle + \sum\nolimits_{i=1}^{M} \left(\frac{P_{ij}^2}{4\Omega_j} \Delta_i(\Omega_j) + \frac{P_{ik}^2}{4\Omega_k} \Delta_i(\Omega_k) \right) \langle \boldsymbol{\eta}_j \boldsymbol{\eta}_k \rangle \tag{96a}$$

$$\frac{\mathrm{d}}{\mathrm{d}t}\langle \boldsymbol{\eta}_j \boldsymbol{\pi}_k \rangle = \langle \boldsymbol{\pi}_j \boldsymbol{\pi}_k \rangle - \Omega_k^2 \langle \boldsymbol{\eta}_j \boldsymbol{\eta}_k \rangle + \sum\nolimits_{i=1}^{M} \left(\frac{P_{ij}^2}{4\Omega_j} \Delta_i(\Omega_j) + \frac{P_{ik}^2}{4\Omega_k} \Delta_i(\Omega_k) \right) \langle \boldsymbol{\eta}_j \boldsymbol{\pi}_k \rangle \tag{96b}$$

$$\frac{\mathrm{d}}{\mathrm{d}t}\langle \boldsymbol{\pi}_j \boldsymbol{\pi}_k \rangle = -\Omega_j^2 \langle \boldsymbol{\eta}_j \boldsymbol{\pi}_k \rangle - \Omega_k^2 \langle \boldsymbol{\eta}_k \boldsymbol{\pi}_j \rangle + \sum\nolimits_{i=1}^{M} \left(\frac{P_{ij}^2}{4\Omega_j} \Delta_i(\Omega_j) + \frac{P_{ik}^2}{4\Omega_k} \Delta_i(\Omega_k) \right) \langle \boldsymbol{\pi}_j \boldsymbol{\pi}_k \rangle, \tag{96c}$$

where $\Sigma_i(\Omega_j) \coloneqq \Gamma_i(-\Omega_j) + \Gamma_i(\Omega_j)$ and $\Delta_i(\Omega_j) \coloneqq \Gamma_i(-\Omega_j) - \Gamma_i(\Omega_j)$. For completeness, the equations of motion for the first-order moments $\langle \boldsymbol{\eta}_j \rangle$ and $\langle \boldsymbol{\pi}_j \rangle$ are given by

$$\frac{\mathrm{d}}{\mathrm{d}t}\langle \boldsymbol{\eta}_j \rangle = \langle \boldsymbol{\pi}_j \rangle + \sum\nolimits_{i=1}^{M} \frac{P_{ij}^2}{4\Omega_j} \Delta_i(\Omega_j) \langle \boldsymbol{\eta}_j \rangle \tag{97a}$$

$$\frac{\mathrm{d}}{\mathrm{d}t}\langle \boldsymbol{\pi}_j \rangle = -\Omega_j^2 \langle \boldsymbol{\eta}_j \rangle + \sum\nolimits_{i=1}^{M} \frac{P_{ij}^2}{4\Omega_j} \Delta_i(\Omega_j) \langle \boldsymbol{\pi}_j \rangle . \tag{97b}$$

Since our Hamiltonian (91) is quadratic in position and momenta, any Gaussian initial state of the network will remain Gaussian at all times. In turn, given that Gaussian states (see Sec. 1.1) are fully characterised by their first- and second-order moments [183] (that is, $\langle \boldsymbol{r}_j(t) \rangle$ and $\left\langle \frac{1}{2}\{\boldsymbol{r}_j(t), \boldsymbol{r}_k(t)\}_+ \right\rangle$), Eqs. (95)–(97) thus provide a full dynamical description of the problem. Furthermore, since $\langle \boldsymbol{r}_j(\infty) \rangle = \langle \boldsymbol{r}_j(\infty)\, \boldsymbol{r}_k(\infty) \rangle = 0$ for $j \neq k$, we can concentrate only on Eqs. (95) as far as the NESS is concerned. Explicitly, this is given by

$$\langle \boldsymbol{\eta}_j^2(\infty) \rangle = -\frac{\tilde{\Sigma}(\Omega_j)}{2\tilde{\Delta}(\Omega_j)\,\Omega_j}, \tag{98a}$$

$$\left\langle \frac{1}{2}\{\boldsymbol{\eta}_j(\infty), \boldsymbol{\pi}_j(\infty)\}_+ \right\rangle = 0, \tag{98b}$$

$$\langle \boldsymbol{\pi}_j^2(\infty) \rangle = -\frac{\tilde{\Sigma}(\Omega_j)\,\Omega_j}{2\tilde{\Delta}(\Omega_j)}, \tag{98c}$$

where $\tilde{\Sigma}(\Omega_j) \coloneqq \sum_{i=1}^{M} P_{ij}^2/(2\Omega_j)\,\Sigma_i(\Omega_j)$ and $\tilde{\Delta}(\Omega_j) \coloneqq \sum_{i=1}^{M} P_{ij}^2/(2\Omega_j)\,\Delta_i(\Omega_j)$. One can then transform $c^{(N)}(t)$ into the covariance matrix[6] $C_{\rm me}^{(N)}(t)$, defined in terms of the original variables $\vec{\boldsymbol{R}} = (\boldsymbol{X}_1, \boldsymbol{P}_1, \cdots, \boldsymbol{X}_N, \boldsymbol{P}_N)^T$ by means of $C_{\rm me}^{(N)}(t) = Q\, c_{\rm me}^{(N)}(t)\, Q^T$, where

$$Q = \begin{pmatrix} P_{11} & 0 & P_{12} & 0 & \cdots \\ 0 & P_{11} & 0 & P_{12} & \cdots \\ P_{21} & 0 & P_{22} & 0 & \cdots \\ 0 & P_{21} & 0 & P_{22} & \cdots \\ \vdots & \vdots & \vdots & \vdots & \ddots \end{pmatrix}. \tag{99}$$

Importantly, under the secular approximation underpinning the GKLS equation, all the position–momentum covariances $\langle \boldsymbol{X}_i(\infty)\, \boldsymbol{P}_j(\infty)\rangle$ vanish in steady state. As a result, local current operators defined within the harmonic network would invariably average to zero [174]. We shall elaborate more on this in Sec. 4.3.1 below. In order to compute the correct stationary heat currents, one can alternatively define the adjoint dissipation super-operators $\mathcal{L}_i^\dagger$ for each heat bath by rewriting Eq. (93) as $\mathrm{d}\boldsymbol{O}(t)/\mathrm{d}t \coloneqq i[\boldsymbol{H}_N, \boldsymbol{O}] + \sum_{i=1}^{M} \mathcal{L}_i^\dagger\, \boldsymbol{O}$. That way, we can cast the steady-state heat current flowing from the ith bath into the network as $\dot{\mathcal{Q}}_{i,\rm me}^{(N)} \coloneqq \langle \mathcal{L}_i^\dagger\, \boldsymbol{H}_N(\infty)\rangle$ [184, 185]. In our case, this evaluates to

$$\dot{\mathcal{Q}}_{i,\rm me}^{(N)} \;=\; \sum\nolimits_{j=1}^{N} \frac{P_{ij}^2}{2\Omega_j}\, \Delta_i(\Omega_j) \left(\frac{1}{2}\Omega_j^2 \langle \boldsymbol{\eta}_j^2(\infty)\rangle + \frac{1}{2}\langle \boldsymbol{\pi}_j^2(\infty)\rangle \right) + \frac{P_{ij}^2}{4}\, \Sigma_i(\Omega_j)\,. \tag{100}$$

In Sec. 4.3.1 below, we shall apply the general equations (98) and (100) to the simple three-oscillator chain making up the augmented system for our quantum wire (cf. Fig. 11), and compare them with the *exact* stationary state and heat currents (see Sec. 4.2.3). In turn, in Sec. 4.3.2, we compare the reduced dynamics of the augmented system with the time-evolution of the two-node wire in a parameter regime where Eqs. (95)–(97) are also directly applicable to the original problem.

6 Note that in this Chapter we adopt a different convention from the previous ones, so that here the covariance matrix C is defined as one half of the covariance matrix σ introduced in Sec. 1.1.

A note on the underlying approximations

To conclude this section, let us briefly comment on the approximations underlying the microscopic derivation of Eq. (93) [166]. First and foremost, it is a second-order perturbative expansion of the exact master equation in the system–environment(s) coupling [180]. Therefore, it is only meaningful under the assumption of weak dissipation. In addition, the Markov approximation has been performed by neglecting any memory effects in the dissipative process, since environmental correlations are assumed to be very short-lived. Note that it may well be the case that environmental correlations are indeed short while the dissipation is strong; recall that the bath memory time is essentially determined by the "shape" of the spectral density [cf. Eq. (86)]. In such situation, the Markov approximation would be valid, but the weak coupling assumption would be violated.

The completely positive GKLS form (93) is attained after performing the secular approximation which, in our case requires that all normal-mode frequencies Ω_j be well separated as compared to the dissipation rates (i.e., $\min_{j\neq k}\{|\Omega_j - \Omega_k|, 2\Omega_j\} \gg \max_{i\in\{1,\cdots,M\}}\{\gamma_i\}$). Once again, this approximation is incompatible with arbitrarily large dissipation rates γ_i, but may also be easily violated under weak dissipation [161, 174]. For that reason, the full Redfield equation [179, 180]—containing all non-secular terms—is often used instead when performing the RC mapping [146, 149, 150]. As we will see in Sec. 4.3 below, even if *both* the weak coupling and the secular approximation are violated on the augmented system, the two-node reduction of the resulting state may still provide an excellent approximation to the exact steady state of the wire.

As a final remark, notice that Eq. (93) does not include the so-called Lamb shift term [166]. This is a Hamiltonian-like contribution to the master equation, dissipative in origin. The Lamb shift is often neglected for being a 'small' contribution when compared with the bare Hamiltonian $\boldsymbol{H}_N$ [150]. It is safe to say that, when working with a GKLS quantum master equation, the Lamb shift is entirely irrelevant

for the thermodynamics of steady-state energy-conversion processes[7]. Interestingly, however, when the Redfield equation is used instead (e.g., due to the inadequacy of the secular approximation), the Lamb shift can have noticeable effects [158]. Note that this term is not related to the frequency renormalisation discussed in Sec. 4.2.1 above.

4.2.3 *Exact stationary solution*

The stationary state of our two-node wire can be obtained *exactly*, with no other assumptions than a factorised initial state of the form $\boldsymbol{\rho}(0) = \boldsymbol{\varrho}_{T_h} \otimes \boldsymbol{\varrho}_w(0) \otimes \boldsymbol{\varrho}_{T_c}$, and no restrictions on $\boldsymbol{\varrho}_w(0)$. Importantly, the problem can be solved analytically regardless of the spectral densities at the boundaries. These linear open systems have been extensively studied in the literature [186–192], as they are among the few which admit an exact solution under strong dissipation. Full details about the calculation of the steady state and stationary heat currents for the Hamiltonian in Eq. (84) were given by González *et al.* [161], and here we limit ourselves to outline the key steps.

The exact dynamics of the wire obeys the following quantum Langevin equations [164, 193]

$$\frac{\mathrm{d}^2}{\mathrm{d}t^2}\boldsymbol{X}_\alpha + (\omega_\alpha^2 + \delta_\alpha)\,\boldsymbol{X}_\alpha + k\,(\boldsymbol{X}_\alpha - \boldsymbol{X}_{\bar{\alpha}}) = \boldsymbol{F}_\alpha(t) + \int_{t_0}^{t} \mathrm{d}s\, \chi_\alpha(t-s)\,\boldsymbol{X}_\alpha(s), \quad (101)$$

where $\alpha \in \{h, c\}$ and $\bar{c} \coloneqq h$ and $\bar{h} \coloneqq c$. As we can see, the coherent evolution of the two coupled (and renormalised) oscillators is affected by environmental driving and dissipation (terms on the right-hand side). Importantly, the upper limit of the integral can be extended to infinity by supplementing the dissipation kernel $\chi_\alpha(t)$ with a Heavisde step function $\Theta(t)$ [i.e., $\chi_\alpha(t) \mapsto \chi_\alpha(t)\,\Theta(t)$] [194]. Since we are

7 Indeed, all the standard quantum-thermodynamic arguments based on the contractivity of the dissipative dynamics and uniqueness of the (thermal) fixed point of any of the dissipators of a GKLS equation [182, 184] hold regardless of whether or not the Lamb shift is included in $\mathcal{L}_i$. In particular, one *always* finds $\mathcal{L}_i\, e^{-\boldsymbol{H}_N/T_i} = 0$, i.e., the fixed point of the dynamics is a thermal state with respect to the *unshifted* Hamiltonian.

interested in the steady state of the wire, our aim will be to compute the covariance matrix $C_{\rm ex}^{(2)}$ at any finite time t while setting $t_0 \to -\infty$.

With this in mind, we can now Fourier-transform Eqs. (101), which yields

$$\begin{pmatrix} -\omega^2 + \omega_h^2 + \delta_h + k - \hat{\chi}_h(\omega) & -k \\ -k & -\omega^2 + \omega_c^2 + \delta_c + k - \hat{\chi}_c(\omega) \end{pmatrix} \begin{pmatrix} \hat{\boldsymbol{X}}_h \\ \hat{\boldsymbol{X}}_c \end{pmatrix} := A(\omega) \begin{pmatrix} \hat{\boldsymbol{X}}_h \\ \hat{\boldsymbol{X}}_c \end{pmatrix} = \begin{pmatrix} \hat{\boldsymbol{F}}_h \\ \hat{\boldsymbol{F}}_c \end{pmatrix}. \tag{102}$$

Here, the "hatted" symbols are in the frequency domain, i.e., $\hat{f}(\omega) := \int_{-\infty}^{\infty} \mathrm{d}t\, e^{i\omega t} f(t)$. Therefore, $(\hat{\boldsymbol{X}}_h, \hat{\boldsymbol{X}}_c)^T = A^{-1}(\omega)\,(\hat{\boldsymbol{F}}_h, \hat{\boldsymbol{F}}_c)^T$, so that the objects we wish to compute are

$$\begin{aligned} &\left\langle \frac{1}{2}\{\boldsymbol{X}_\alpha(t'), \boldsymbol{X}_\beta(t'')\} \right\rangle \\ &= \int_{-\infty}^{\infty} \frac{\mathrm{d}\omega'}{2\pi} \int_{-\infty}^{\infty} \frac{\mathrm{d}\omega''}{2\pi} \sum_{\delta\gamma} [A^{-1}]_{\alpha\gamma}(\omega')\, [A^{-1}]_{\beta\delta}(\omega'') \left\langle \tfrac{1}{2}\{\hat{\boldsymbol{F}}_\gamma(\omega'), \hat{\boldsymbol{F}}_\delta(\omega'')\} \right\rangle e^{-i\omega' t'}\, e^{-i\omega'' t''} \end{aligned} \tag{103}$$

for $t' = t'' = t$. The position–momentum and momentum–momentum covariances can be obtained by differentiating Eq. (103), which is equivalent to multiplying the integrand by $(-i\omega')$ and $(-\omega'\omega'')$, respectively. To carry out the integration in (103) explicitly, we only need the Fourier transform of the dissipation kernels $\hat{\chi}_\alpha(\omega)$ and the power spectrum of the environmental forces $\langle \frac{1}{2}\{\hat{\boldsymbol{F}}_\alpha(\omega'), \hat{\boldsymbol{F}}_\beta(\omega'')\}\rangle$. These are given by [194]

$$\mathrm{Im}\,\hat{\chi}_\alpha = J_\alpha(\omega)\,\Theta(\omega) - J_\alpha(-\omega)\,\Theta(-\omega) \tag{104a}$$

$$\mathrm{Re}\,\hat{\chi}_\alpha = \frac{1}{\pi}\,\mathrm{P}\int_{-\infty}^{\infty} \mathrm{d}\omega'\, \frac{\mathrm{Im}\,\hat{\chi}_\alpha(\omega')}{\omega' - \omega} \tag{104b}$$

$$\left\langle \frac{1}{2}\{\hat{\boldsymbol{F}}_\alpha(\omega'), \hat{\boldsymbol{F}}_\beta(\omega'')\} \right\rangle = \frac{1}{2\pi}\, \coth\!\left(\frac{\omega'}{2T_\alpha}\right) \mathrm{Im}\,\hat{\chi}_\alpha \delta_{\alpha\beta}\, \delta(\omega' + \omega''), \tag{104c}$$

where P denotes 'principal value', $\delta_{\alpha\beta}$ is a Kronecker delta and $\delta(x)$ is a Dirac delta. The integration in Eq. (104b) can be readily performed for the overdamped

and underdamped spectral densities of interest, i.e., $J_h(\omega) = \gamma_h \Lambda_h^2 \omega/(\omega^2 + \Lambda_h^2)$ and $J_c(\omega) = \gamma\lambda^2\omega/[\gamma^2\omega^2 + (\omega^2 - \omega_0^2)^2]$, which yields

$$\hat{\chi}_h(\omega) = \frac{\Lambda_h^2 \gamma_h}{\Lambda_h - i\omega} \tag{105a}$$

$$\hat{\chi}_c(\omega) = \frac{\lambda^2}{\omega_0^2 - i\gamma\omega - \omega^2}\,. \tag{105b}$$

Note that Eq. (105a) may also be used for the dissipation kernel of the residual bath acting on the augmented system, by merely replacing γ_h with γ and taking a large cutoff.

Summing up, Eqs. (103)–(105) are all we need to fill in the full stationary 4×4 covariance matrix $C_{\rm ex}^{(2)}(\infty)$. Note that it is indeed possible to solve the problem not only exactly, but also analytically [189, 195]. In turn, the 6×6 NESS $C_{\rm ex}^{(3)}(\infty)$ of the augmented system can be found in a completely analogous way [195], by just replacing the 'vector of forces' $(\hat{\boldsymbol{F}}_h, \hat{\boldsymbol{F}}_c)^T$ by $(\hat{\boldsymbol{F}}_h, 0, \hat{\boldsymbol{F}}_{\rm res})^T$ and $A(\omega)$, with

$$B(\omega) = \begin{pmatrix} -\omega^2 + \omega_h^2 + \delta_h + k - \hat{\chi}_h(\omega) & -k & 0 \\ -k & -\omega^2 + \omega_c^2 + \delta_c + k & -\lambda \\ 0 & -\lambda & -\omega^2 + \omega_0^2 + \delta_{\rm res} - \hat{\chi}_{\rm res}(\omega) \end{pmatrix}. \tag{106}$$

To conclude this section, let us introduce the exact stationary heat currents, for comparison with Eq. (100). A direct calculation shows that the change in the energy of our wire (or the augmented system) due to dissipative interactions with bath α—i.e, $\dot{Q}_{\alpha,{\rm ex}}^{(N)} = i\langle[\boldsymbol{H}_{w\text{–}\alpha}, \boldsymbol{H}_w]\rangle$—can be cast as [190, 196]

$$\dot{Q}_{h,{\rm ex}}^{(2)} = -k\langle \boldsymbol{X}_c \boldsymbol{P}_h\rangle_{N=2} = k\langle \boldsymbol{X}_h \boldsymbol{P}_c\rangle_{N=2} = -\dot{Q}_{c,{\rm ex}}^{(2)} \tag{107a}$$

$$\dot{Q}_{h,{\rm ex}}^{(3)} = -k\langle \boldsymbol{X}_c \boldsymbol{P}_h\rangle_{N=3} = \lambda\langle \boldsymbol{X}_c \boldsymbol{P}_{\rm RC}\rangle_{N=3} = -\dot{Q}_{\rm res,ex}^{(3)}\,. \tag{107b}$$

4.3.1 *Steady state and stationary heat currents*

We are now ready to put the reaction-coordinate mapping to the test. Using Eqs. (103)–(105), we can compute the exact stationary covariance matrix of the original (two-node wire) problem $C_{\mathrm{ex}}^{(2)}(\infty)$, as well as that of the augmented (three-node) system, $C_{\mathrm{ex}}^{(3)}(\infty)$. Alternatively, we can look for the steady state of the augmented system according to the GKLS master equation, i.e., $C_{\mathrm{me}}^{(3)}$. Benchmarking the RC mapping thus amounts to assessing how "close" is the relevant 4×4 submatrix of $C_{\mathrm{me}}^{(3)}(\infty)$ to the exact stationary state $C_{\mathrm{ex}}^{(2)}(\infty)$. We conclude by noting that the covariance dynamics can also be obtained non-perturbatively in the system–baths couplings by means of stochastic propagation and averaging, in linear and weakly non-linear continuous-variable systems [197, 198].

We thus need to be able to *quantify* the distance between two covariance matrices C_1 and C_2. To that end, we resort to the Uhlmann fidelity [199, 200] $\mathcal{F}(C_1, C_2)$ which, for arbitrary N-mode Gaussian states with vanishing first-order moments, is

$$\mathcal{F}(C_1, C_2) = \left(\frac{F}{\sqrt[4]{\det\,(C_1 + C_2)}} \right)^2 \tag{108a}$$

$$F := \left(\det \left(2 \left(\sqrt{1 + \frac{\left(C_{\mathrm{aux}}\,\Theta\right)^{-2}}{4}} + 1 \right) C_{\mathrm{aux}} \right) \right)^{1/4} \tag{108b}$$

$$C_{\mathrm{aux}} := \Theta^T \left(C_1 + C_2\right)^{-1} \left(\frac{\Theta}{4} + C_2\,\Theta\,C_1 \right) \tag{108c}$$

$$\Theta := \bigoplus_{i=1}^{N} \begin{pmatrix} 0 & 1 \\ -1 & 0 \end{pmatrix}. \tag{108d}$$

This is a meaningful distance measure, since $\mathcal{F}(C_1, C_2) = 1$ only holds if the states are identical, and $0 < \mathcal{F}(C_1, C_2) \leq 1$.

Steady states

In Fig. 12(a) we illustrate our steady-state benchmark for the RC mapping (solid line). Strikingly, we find that the reduction of $C_{\mathrm{me}}^{(3)}(\infty)$ onto the wire degrees of freedom remains nearly identical to the exact stationary state $C_{\mathrm{ex}}^{(2)}(\infty)$, even at extremely large residual dissipation strengths γ. In the figure, for instance, the fidelity between the two states falls below 95% only at $\gamma \gtrsim 60$. When it comes to the approximations that justify the GKLS master equation (93) (cf. Sec. 4.2.2), this is completely off-limits. Indeed, note that the normal-mode frequencies of the augmented system are, in this example, $\Omega_1 \simeq 1.31$, $\Omega_2 \simeq 3.13$, and $\Omega_3 \simeq 4.02$, which renders the secular approximation problematic already at residual dissipations as small as $\gamma \sim 0.1$. More importantly, $\gamma \simeq 60$ can by no means be considered small and hence, a perturbative expansion of the generator of the dissipative dynamics is out of the question. Our extensive numerics show that this surprising observation is not due to a lucky parameter choice but rather, a generic feature. It is also consistent with the excellent agreement previously reported in other (non-linear) models [146, 149, 157], between the reduction of the master-equation-propagated augmented system and the numerical solution to the original problem.

As surprising as this observation may seem, there is nothing contradictory in it—indeed, the GKLS master equation does break down for $\gamma \gtrsim 0.1$, which corresponds to $\log(\gamma/\gamma_h) \gtrsim 5$ [area to the right of the dotted line in Fig. 12(a)]. We can see this in Fig. 12(a), when instead of looking at the reduction of $C_{\mathrm{me}}^{(3)}(\infty)$ onto the wire, we consider the full augmented system and compare it with the exact three-node solution $C_{\mathrm{ex}}^{(3)}(\infty)$ (dashed line). Specifically, $\mathcal{F}(C_{\mathrm{ex}}^{(3)}(\infty), C_{\mathrm{me}}^{(3)}(\infty)) < 0.95$ for $\gamma > 0.15$, as expected. We are thus not claiming that Markovian master equations in Lindblad form are generally valid for strong coupling situations. What we find is that non-equilibrium energy transfer processes through open quantum systems in complex environments can be captured faithfully over a much wider parameter range than previously thought, by combining the RC mapping with a GKLS master equation (RC–GKLS mapping).

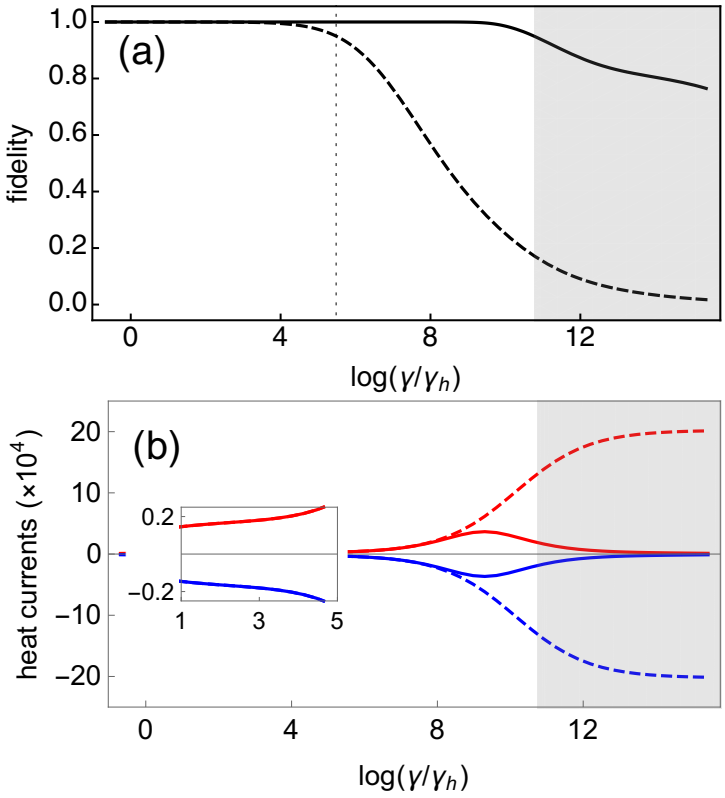

Figure 12: (a) (solid) Uhlmann fidelity between $C_{\rm ex}^{(2)}(\infty)$ and the relevant two-node reduction of $C_{\rm me}^{(3)}(\infty)$. This is achieved simply by eliminating rows and columns related to the reaction-coordinate variables $\boldsymbol{X}_{\rm RC}$ and $\boldsymbol{P}_{\rm RC}$ from the 6×6 matrix $C_{\rm me}^{(3)}(\infty)$. The abscissa corresponds to the natural log of the friction coefficient γ of the underdamped spectral density in Eq. (85), at the interface between the wire and the cold bath (normalised by the dissipation strength into the hot bath γ_h). Only in the shaded-grey area the fidelity drops below 95%. (dashed) Fidelity between $C_{\rm ex}^{(3)}(\infty)$ and $C_{\rm me}^{(3)}(\infty)$ as a function of the normalised friction γ/γ_h. This falls below 95% to the right of the dotted line. (b) Steady-state heat currents coming from the hot (red) and cold (blue) baths *into* the wire as a function of γ/γ_h for the same parameters as in panel (a). The solid lines correspond to the exact calculation from Eq. (107a), while the dashed ones result from applying the GKLS master equation to the augmented system, as per Eq. (100). The inset is a zoom into the low friction limit and the shaded-grey area is the same as in (a). In both panels, the wire is characterised by $\omega_h = 1$, $\omega_c = 3$, and $k = 0.8$; the overdamped Ohmic spectral density at the hot interface, by $\gamma_h = 10^{-3}$ and $\Lambda_h = 10^3$; the underdamped spectral density at the cold interface, by $\lambda = 0.9$ and $\omega_0 = 4$; and the baths, by temperatures $T_h = 3.3$ and $T_c = 1.2$.

We still need, however, to provide some physical intuition backing this observation. To that end, let us take a *detour* to comment on recent literature on locality of temperature in quantum many-body lattice systems [201–204]. It is clear that the reduction of the global thermal state of a large lattice onto a small local subspace can deviate substantially from a local thermal state—this is due to the non-vanishing interactions between the subsystem in question and the rest of the lattice. However, the (non-thermal) state of such sub-lattice may be approximated arbitrarily well as follows: One first envelopes it with a 'boundary' or 'buffer' region, taken from the surrounding lattice; such augmented system is then set to a thermal state at the global temperature of the full system and then, the auxiliary buffer is traced out [201]. The result is in good agreement with the local state of interest so long as the boundary is thick enough, relative to some relevant correlation length scale [203, 204]. Something similar happens in our example: imposing incorrect (thermal) boundary conditions on an augmented system, we can reproduce the state of the wire faithfully; the techniques only breaks down when the boundary–environment interactions become sufficiently large, so that correlations start to appear between the wire and the residual environment. Making this intuition more precise by studying the correlation sharing structure between wire, RC, and residual bath, goes, however, beyond the scope of this project.

Steady-state heat currents

Besides faithfully reproducing the NESS of an open quantum system, one would also like to learn about the stationary heat currents that it supports, especially when viewing it as a 'continuous thermal device' for quantum thermodynamics [185]. To do so from the RC-mapped picture, we need to gauge the energy per unit time crossing the boundary between either bath and the augmented system; this can only be achieved by using to the corresponding GKLS dissipators $\mathcal{L}_i$ [cf. Eq. (100)]. Under strong coupling, however, these are certainly *not* valid generators of the dissipative dynamics. A priori, one should thus expect a substantial mismatch between the GKLS stationary heat currents and their exact values in this regime. In Fig. 12(b) we can indeed see that for $\gamma \sim 60$—where $C^{(2)}_{\mathrm{ex}}(\infty)$ and the reduction of $C^{(3)}_{\mathrm{me}}(\infty)$ dif-

fer only by 5%—the master equation overestimates the heat currents by an order of magnitude, and fails to capture, even qualitatively, their behaviour for larger friction γ.

Note that resorting to the dissipators is indeed the only feasible way to estimate heat currents; $C^{(3)}_{\mathrm{me}}(\infty)$ is lacking the key covariances $\langle \boldsymbol{X}_c \boldsymbol{P}_h \rangle$ and $\langle \boldsymbol{X}_c \boldsymbol{P}_{\mathrm{RC}} \rangle$ needed to evaluate the dissipative change in the energy of the heat baths [cf. Eq. (107a)]. In fact, this has been criticised as one of the most unsatisfactory features of GKLS-type quantum master equations [174]. Alternatively, one could think of waiving the secular approximation to work instead with a Redfield master equation [179, 180]. Although the aforementioned covariances would then cease to be zero, the calculation would continue to yield quantitatively wrong results at very large γ—this time simply due to the breakdown of the basic weak-coupling assumption. Ultimately, however, the Redfield approach might improve the GKLS results under moderate residual dissipation [150, 158]. Therefore, even in the light of the promising observation made in Sec. 4.3.1 above, great care must still be taken when relying on the RC–GKLS mapping to discuss quantum thermodynamics under non-Markovian dissipation.

4.3.2 *Dynamics*

One can now ask whether the resilience of the RC–GKLS mapping to strong residual dissipation is exclusively a steady-state feature, or whether it holds throughout the entire dissipative evolution. Unfortunately, we do not have an exact dynamical benchmark—at most, we are able to solve here for the steady state of the exact Eq. (101). We, therefore, chose parameters so that the original two-node problem *can* be described via a GKLS quantum master equation. We recall, however, that this type of equation can in principle be solved non-perturbatively at finite times with stochastic propagation techniques [197, 198].

In particular, we scale ω_0 and λ in the structured spectral density $J_c(\omega)$ in Eq. (85) as $\lambda^2 = \alpha_1 \alpha_2 \gamma$ and $\omega_0^2 = \gamma \alpha_2$. Taking once again the large friction limit $\gamma \gg 1$ leads to the overdamped spectrum $J_c(\omega) \sim \alpha_1 \alpha_2 \omega / (\omega^2 + \alpha_2^2)$ [205].

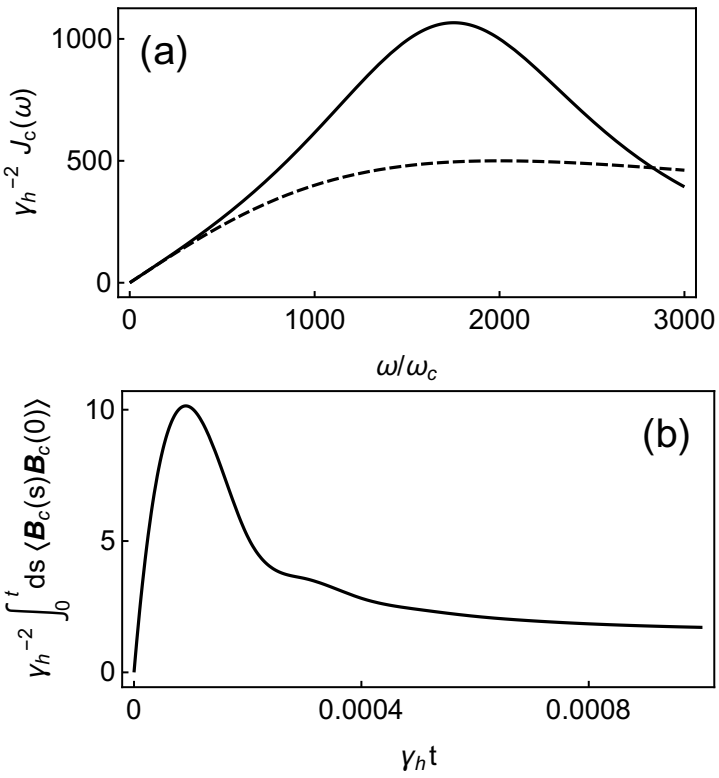

Figure 13: (a) (solid) Structured spectral density $J_c(\omega)$ with scaled ω_0 and λ so as to approximate an overdamped profile in the limit of large γ. In particular, $\lambda^2 = \alpha_1\,\alpha_2\,\gamma$ and $\omega_0^2 = \alpha_2\,\gamma$, with $\alpha_1 = \gamma_h = 10^{-3}$, $\alpha_2 = \Lambda_h = 10^3$, and $\gamma = 10^3$. The limiting Ohmic spectrum (dashed) for $\gamma \to \infty$ has been added for comparison. (b) Integrated bath correlation function for the spectral density $J_c(\omega)$ scaled as in (a). The time elapsed until saturation in the above curve characterises the memory of the cold bath. Hence, if the relevant dynamics occurs over time scales larger than $\gamma_h t \simeq 10^{-3}$ [cf. Fig. 14(a) below], we can safely work under the Markov approximation.

For our calculations, we will take the numerical values $\alpha_1 = \gamma_h$ and $\alpha_2 = \Lambda_h$. Note that $J_c(\omega) \sim \alpha_1\,\alpha_2\,\omega/(\omega^2 + \alpha_2^2)$ looks like the Ohmic-algebraic $J_h(\omega)$ introduced above, except for a missing factor α_2 in the numerator. Hence, while α_1 takes the numerical value of γ_h, it must have units of frequency *squared* instead of frequency. It is $\alpha_1/\alpha_2 \ll \gamma_h$ which plays the role of the dissipation strength in this case. In Fig. 13(a) we plot both the resulting spectral density (solid) along with the Ohmic limiting case of $\gamma \to \infty$ (dashed). As it can be seen, for our choice of parameters, the corresponding wire–bath coupling ends up being at most $O(\gamma_h) \ll 1$, which

would justify the weak-coupling approximation and the use of a perturbative master equation.

The next step towards a GKLS equation is to certify the validity of the Markov approximation: we must ensure that the decay of the bath correlation functions computed in Eq. (86) is sufficiently fast when compared to the dynamics of the wire. In Fig. 13(b) we plot the integrated correlation $\int_0^t \mathrm{d}s\, \langle \boldsymbol{B}_c(s)\, \boldsymbol{B}_c(0)\rangle$, whose saturation time ($\gamma_h \tau_c \sim 5\times 10^{-4}$) is just below the relevant time scale for the dissipative evolution of the wire ($\gamma_h \tau_w \sim 10^{-3}$) [compare with Fig. 14(a)]. We thus confidently say that the Markov approximation holds. For the parameters chosen, the secular approximation is also not a problem (cf. caption of Fig. 14). Namely, the normal-mode frequencies of the wire are $\Omega_1 = 0.34$ and $\Omega_2 = 0.97$, while the dissipation rates are both $O(\gamma_h)$, which is perturbative.

We thus take the time evolution of the two-node wire according to the master equation (93), as valid approximation to the exact dissipative dynamics, and a good benchmark for the RC mapping. Just like we did in Sec. 4.3.1, we also apply a GKLS master equation to the resulting three-node augmented system; again in spite of the fact that it is totally unjustified (the residual dissipation is $\gamma = 10^3$). As pointed out in Sec. 4.2.1, initially, we assume no correlations between the reaction coordinate, the wire, and either of the two baths, and initialise the RC in a thermal state at the original temperature of the cold bath.

Our results are plotted in Fig. 14. As we can see, the RC–GKLS mapping (open dots) accurately approximates the dynamics of the covariances of the wire (solid black line), and it does so during the entire evolution. However, as expected from the results in Fig. 12(a), it fails to capture the covariances of the reaction coordinate itself. We show this in Fig. 14(d) by comparing the stationary value of $\langle \boldsymbol{X}_{\mathrm{RC}}^2 \rangle$ as predicted by the master equation, with its exact asymptotic value. It is remarkable, however, that the covariances for the wire are perfectly reproduced in spite of the extremely large friction $\gamma = 10^3$. This contrasts with the degradation of fidelity illustrated in Fig. 12(a), and is entirely due to our choice of friction-dependent λ and ω_0.

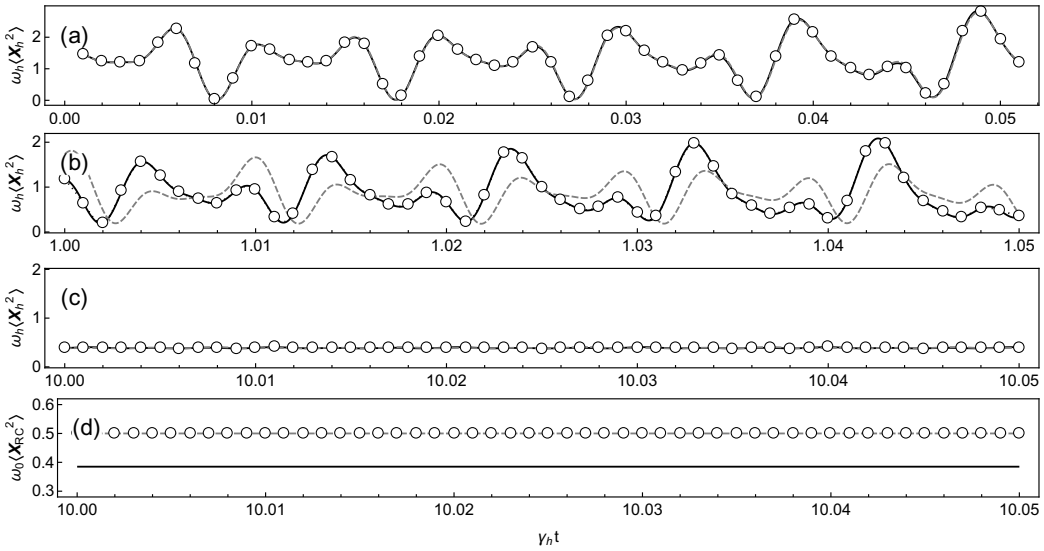

Figure 14: (a)–(c) Time evolution of $\langle \boldsymbol{X}_h^2 \rangle$ at different stages of the dynamics, according to a master equation applied directly on the two-node wire (solid black), on the three-node augmented system (open circles), and on an augmented system whose cold frequency has *not* been suitably shifted as per the RC mapping (grey dashed). (d) (solid black) exact steady-state value of $\langle \boldsymbol{X}_{\mathrm{RC}}^2 \rangle$ superimposed to the asymptotic value of this covariance according to the master equation, acting on a shifted (open circles) and unshifted (dashed grey) augmented system. Here, $\omega_h = 0.1$, $\omega_c = 0.5$, $k = 0.4$, $T_h = 0.6$, $T_c = 0.5$, and the rest of parameters are the same as in Fig. 13.

Finally, we also take the opportunity here to illustrate the vital importance of the frequency shift $\boldsymbol{\delta H}_{w\text{–}c}$ on the augmented system (cf. Sec. 4.2.1). Note that before the mapping we do not include any shifts in the Hamiltonian of the wire, since we are tackling the original problem via a master equation. However, for the mapping to be an identity, the frequency of the 'cold oscillator' must be shifted as in $\omega_c \mapsto \omega_c^2 + \lambda^2/\omega_0^2$ when applying the master equation to the augmented system. For our choice of parameters this means tuning it from 0.5 to 0.501, which might seem totally negligible. Indeed, the short-time dynamics [cf. Fig. 14(a)] and the stationary state [cf. Fig. 14(c)] remain virtually unaffected when the shift is not taken into account (dashed grey lines). At intermediate times, however, the effects of the shift become evident, as shown in Fig. 14(b)—neglecting it does cause the RC–GKLS mapping to break down.

4.4 DISCUSSION

In this Chapter we have benchmarked the reaction-coordinate mapping in an exactly solvable linear model, consisting of a two-node chain of harmonic oscillators. These are individually coupled to two baths at different temperatures and thus, support a steady-state heat current. The mapping takes this setup into a three-oscillator augmented system, which is also exactly solvable. The idea, however, is to tackle the augmented system via a weak-coupling Markovian master equation. What we found can be summarised as follows:

- The reduction of the stationary state of the augmented system onto the degrees of freedom of the two-node wire—according to the master equation—resembles very closely the exact steady state. This can be so, even in regimes of parameters for which the approximations underpinning the master equation break down; specifically, the secular approximation and even the basic weak-coupling assumption.

- Even when the stationary state of the wire is captured faithfully by the master-equation approach, the joint state of all three nodes of the augmented system can differ very substantially from the exact solution of the augmented problem. This happens whenever the underlying approximations cease to be justified.

- More importantly, the non-equilibrium steady state of the wire may be accurately reproduced by the master equation acting on the augmented system and yet, the stationary heat currents obtained from it can be quantitatively and even qualitatively wrong.

- At least in the overdamped limit, the reaction-coordinate mapping succeeds in approximating the state of the wire not only asymptotically, but throughout the entire dissipative dynamics.

In addition, we discussed the subtleties surrounding the frequency renormalisation shifts appearing as a result of the system–environment(s) coupling, and illustrated the importance of using them consistently. We also presented in full detail a consistent

Markovian master equation in GKLS form that generalises previous results [161], and can be directly applied to an arbitrary network of of N harmonic oscillators locally connected to M heat baths at different temperatures. We explicitly provided the corresponding (Gaussian) non-equilibrium steady state, and the expression for the M stationary heat currents flowing across the network. Note that we have focused exclusively on continuous-variable systems in Gaussian states and hence, extending our conclusions to finite-dimensional or non-linear models would require further work.

Our results have two important consequences when dealing with virtually intractable problems involving nano- and micro-scale systems in non-Markovian baths, such as biological environments. On the one hand, they raise hopes of relying on the combination of 'reaction-coordinate mapping' and 'weak-coupling master equations' beyond the strict range of applicability of the latter. Although the mapping had been successfully applied to open-systems strongly coupled to highly structured environments [146, 149–154, 156, 158–160, 206], our findings suggest that non-Markovian noise featuring broader power spectra—which so far was though to be out of reach for the mapping—may also be modelled in the exact same manner. On the other hand, however, weak-coupling master equations should *not* be trusted beyond their range of applicability when calculating boundary heat currents—even if these appear to be thermodynamically consistent, they may be serious overestimations. It is pertinent to keep this it in mind when using the reaction-coordinate mapping to extend quantum thermodynamics into the strong coupling regime, an interesting line which currently attracts an increasing attention [147, 150–152, 158, 159, 206]. Put simply, being able to replicate accurately the exact numerical propagation of an open system with the reaction-coordinate technique does not guarantee that the boundary heat (or particle) currents calculated from the corresponding master equation are equally accurate. This is the main message from this Chapter.

We also note that a closely-related systematic technique has been recently put forward to emulate dissipation into structured environments through GKLS-type master equations [207], which can be used to deal with the strong friction regime. When it comes to extensions of our analysis, it may be possible to improve on the boundary

currents by taking the secular approximation back and working with the full Redfield equation [157, 158]. It would thus be interesting to generalise Eqs. (95)–(98) and (100) to allow for non-secular contributions, and benchmarking those instead. After all, as already mentioned the reaction-coordinate mapping is often combined with Redfield rather than GKLS quantum master equations [146, 149, 150, 157, 158]. It is important to bear in mind, however, that Redfield equations may not only violate complete positivity, but even positivity alone [179, 180], which seriously compromises the consistency of any quantum-thermodynamic variables derived from it. This generalisation lies, however, beyond the scope of this project, and will be tackled elsewhere.

5

CONCLUSIONS

In this thesis we have investigated fundamental properties of continuous variable quantum systems in both static and dynamical conditions.

We began by studying theoretically the degree of genuine multipartite nonlocality in pure permutationally invariant Gaussian states of n bosonic modes, in terms of the largest amount by which the so-called Svetlichny inequality can be violated by specific measurements. When adopting displaced parity measurements, we identified the optimal phase space settings that correspond to the largest violations of local realism. These measurements nevertheless do not suffice to reach the maximum Svetlichny nonlocality allowed by quantum mechanics when operating on Gaussian states. Therefore we further considered pseudospin observables and demonstrated that such an ultimate bound is in fact attainable on Gaussian states when using these measurements, in particular in the three-mode instance. Also in the case of pseudospin measurements, we identified particular settings which become optimal in the regime of asymptotically large squeezing.

We then turned our attention to other correlations, in particular EPR steering, an asymmetric form of nonlocality which can also be detected by the violation of suitable inequalities. Recent works had shown that non-Gaussian measurements can be useful to detect steerability of Gaussian states in regimes where Gaussian measurements are not sufficient. Here, we performed a systematic investigation of EPR steering in two-mode Gaussian states by pseudospin measurements, by testing a nonlinear criterion based on second moments of the pseudospin correlation matrix. We identified significant regions of parameters in which Gaussian states can only be

steered by non-Gaussian measurements. We further showed that non-Gaussian measurements are more effective than Gaussian ones to witness steering of non-Gaussian continuous variable Werner states, which were shown to exhibit features comparable to their discrete variable counterparts.

These results just summarised provide useful insights on the role of non-Gaussian measurements in benchmarking different forms of quantum correlations of Gaussian and non-Gaussian states. Given that both EPR steering and Bell nonlocality play essential roles in partially or fully device-independent quantum cryptography, our results find useful applications in the design of secure quantum network architectures based on continuous variable systems.

Our investigation was not limited to static detection of continuous variable quantum resources. In fact, our final study focused on characterising the dynamics of open quantum systems in structured environments. We considered in particular heat transport in an exactly solvable model, consisting of a two-node chain of harmonic oscillators connecting two baths at different temperatures. Our objective was to assess the validity of the reaction-coordinate mapping for the considered model; this technique aims to mimic the original problem by means of an augmented system via a weak-coupling Markovian master equation, which includes a suitably chosen collective environmental coordinate (reaction-coordinate), coupled to a simpler effective reservoir. We found that the stationary state of the original problem can be reproduced accurately by a weak-coupling treatment even when the residual dissipation on the augmented system is very strong, and the agreement holds throughout the entire dynamics under large residual dissipation in the overdamped regime. These observations can be crucial when using the reaction-coordinate mapping to study the largely unexplored strong-coupling regime in quantum thermodynamics.

Overall, the results obtained and the techniques developed in this thesis contribute to advance our understanding of continuous variable quantum information theory and quantum thermodynamics. It would be interesting to further combine methods from the three main chapters of this thesis and analyse the dynamical creation and distribution of steering and nonlocality in continuous variable open quantum systems modelled using the reaction-coordinate mapping.

This perspective is left open for future work.

A

APPENDIX

A.1 COMPACT EXPRESSION FOR MULTIDIMENSIONAL HERMITE POLYNOMIALS

The method used in Sec. 3.3 for the derivation of the Fock basis elements of TMST states, given by Eq. (59), can be a cornerstone for a wider algebra programme aimed at the derivation of new compact expressions for multidimensional Hermite polynomials based on quantum mechanics.

Making use of the results of Refs. [124–126], it can be shown [115] that, for a TMST state $\hat{\rho}_{AB}^{\mathrm{TMST}}$ with covariance matrix σ_{AB} given by the right-hand side of Eq. (42), where $d = -c$, the Fock basis elements can be written formally as

$$\langle m_1 m_2|\hat{\rho}_{AB}^{\mathrm{TMST}}|n_1 n_2\rangle = \frac{4H^{(\boldsymbol{\Theta})}_{m_1,m_2,n_1,n_2}(\mathbf{0})}{\sqrt{\det\left(\sigma_{AB}+1\right)}\sqrt{m_1!m_2!n_1!n_2!}}. \tag{A.1}$$

Here $H^{(\boldsymbol{\Theta})}_{m_1,m_2,n_1,n_2}(\mathbf{0})$ is the four-dimensional Hermite polynomial at the origin, which can be calculated from the expression [127]

$$\begin{aligned} H^{(\boldsymbol{\Theta})}_{m_1,m_2,n_1,n_2}(\boldsymbol{x}) = (-1)^{\sum_{i=1}^{2} n_i+m_i} \exp\left(\frac{1}{2}\boldsymbol{x}^T\boldsymbol{\Theta}\boldsymbol{x}\right) \\ \times \frac{\partial^{\sum_{i=1}^{2} n_i+m_i}}{\partial x_1^{m_1}\partial x_2^{m_2}\partial x_3^{n_1}\partial x_4^{n_2}} \exp\left(-\frac{1}{2}\boldsymbol{x}^T\boldsymbol{\Theta}\boldsymbol{x}\right), \end{aligned} \tag{A.2}$$

and $\boldsymbol{\Theta}$ is a real symmetric matrix defining the polynomial, which is of the form:

$$\boldsymbol{\Theta} = -\begin{pmatrix} 0 & e & f & 0 \\ e & 0 & 0 & g \\ f & 0 & 0 & e \\ 0 & g & e & 0 \end{pmatrix}, \tag{A.3}$$

where

By comparing the right-hand sides of Eq. (A.1) and Eq. (59) and taking into account the relation

$$\frac{1-\varsigma^2}{\cosh^2(r)} = \frac{4}{\sqrt{\det\left(\sigma_{AB}+1\right)}}, \tag{A.4}$$

which follows from Eqs. (53), one finds that the Hermite polynomials $H^{(\mathbf{\Theta})}_{m_1,m_2,n_1,n_2}(\mathbf{0})$ can be expressed as

$$\begin{aligned} &H^{(\mathbf{\Theta})}_{m_1,m_2,n_1,n_2}(\mathbf{0}) \\ &= \sqrt{m_1!m_2!n_1!n_2!}\,\delta_{m_1+n_2,n_1+m_2}\left[\frac{\varsigma\sqrt{\eta}}{\cosh(r)}\right]^{m_2+n_2}\left[\tanh(r)\right]^{2(m_1-m_2)} \\ &\times \sum_{k=\max\{0,m_2-m_1\}}^{\min\{m_2,n_2\}} \sqrt{\binom{m_2}{k}\binom{n_2}{k}\binom{m_1}{m_2-k}\binom{n_1}{n_2-k}} \\ &\times\left[\sqrt{\frac{1-\eta}{\eta}}\sinh(r)\right]^{2k}. \end{aligned} \tag{A.5}$$

If we now reverse Eqs. (53), we can express after some algebra the parameters $\sqrt{\eta}, \varsigma$, as well as all functions of the squeezing parameter r which appear on the right-hand side of Eq. (A.5), as functions of the covariance matrix parameters a, b and c, which finally yields the following formula for four-dimensional Hermite polynomials defined by the matrix $\mathbf{\Theta}$ in Eq. (A.3):

$$\begin{aligned} H^{(\mathbf{\Theta})}_{m_1,m_2,n_1,n_2}(\mathbf{0}) &= \sqrt{m_1!m_2!n_1!n_2!}\,\delta_{m_1+n_2,n_1+m_2}\,e^{m_2+n_2}f^{m_1-m_2} \\ &\times \sum_{k=\max\{0,m_2-m_1\}}^{\min\{m_2,n_2\}} \sqrt{\binom{m_2}{k}\binom{n_2}{k}\binom{m_1}{m_2-k}\binom{n_1}{n_2-k}}\left(\frac{fg}{e^2}\right)^k. \end{aligned} \tag{A.6}$$

Note that, in the usual practice, Hermite polynomials are evaluated numerically using a recurrence relation. Our last formula (A.6) shows that, in some cases, this is not necessary and one can obtain them just as a single finite sum instead. This can make analytical calculations with multidimensional Hermite polynomials more tractable and numerical calculations more efficient.

Over the years, there have been many attempts to find the proper description of quantum oscillators. In this section, we first introduce the Dirac approach, then the Susskind-Glogower operator, and finally the pseudospin operator.

In classical electromagnetic theory, the electric field of a single mode can be written as

$$\mathbf{E}(\mathbf{r},t) = \frac{1}{2}\mathbf{e}_x E_0[e^{i\mathbf{k}\cdot\mathbf{r}-\omega t+\phi} + e^{-i\mathbf{k}\cdot\mathbf{r}-\omega t+\phi}]\,. \tag{A.7}$$

and its equivalent expression in quantum mechanics

$$\hat{E}(\mathbf{r},t) = \frac{1}{2}\vec{e}_x E_0[\hat{a}e^{i\mathbf{k}\cdot\mathbf{r}-\omega t} + \hat{a}^\dagger e^{-i\mathbf{k}\cdot\mathbf{r}-\omega t}]\,. \tag{A.8}$$

By comparing Eq. (A.7) and Eq. (A.8), Dirac [208] decomposed ladder operatos into polar form,

$$\hat{a} = e^{i\hat{\phi}}\sqrt{\hat{n}}\,. \tag{A.9}$$

$$\hat{a}^\dagger = \sqrt{\hat{n}}e^{-i\hat{\phi}}\,. \tag{A.10}$$

where $\hat{\phi}$ is Hermitian and $e^{i\hat{\phi}}$ is a unitary operator. We shall find that this is not correct. From the commutation relation $\left[\hat{a},\hat{a}^\dagger\right] = 1$, we have

$$e^{i\hat{\phi}}\hat{n} - \hat{n}e^{i\hat{\phi}} = e^{i\hat{\phi}} \tag{A.11}$$

then the commutation relation for $\hat{n}$ and $\hat{\phi}$ is obtained by expanding the exponentials in Eq. (A.11),

$$[\hat{n},\hat{\phi}] = i \tag{A.12}$$

However, if we take the matrix elements of this relation in the Fock basis, we have

$$[n'-n]\langle n'|\hat{\phi}|n\rangle = i\delta_{n'n} \tag{A.13}$$

This is not correct since when $n' = n$, the right side is i, while the left side is zero. The root of the problem is that we are not taking into account the periodic nature of $\hat{\phi}$.

Another reason that such attempt fails is that $\hat{\phi}$ is not Hermitian and $e^{i\hat{\phi}}$ is not a unitary operator. From Eq. (A.9) and Eq. (A.10), we have

$$e^{i\hat{\phi}} = \hat{a}\frac{1}{\sqrt{\hat{n}}} \tag{A.14}$$

$$e^{-i\hat{\phi}} = \frac{1}{\sqrt{\hat{n}}}\hat{a}^\dagger \tag{A.15}$$

which gives,

$$e^{i\hat{\phi}}e^{-i\hat{\phi}} = 1 \tag{A.16}$$

$$e^{-i\hat{\phi}}e^{i\hat{\phi}} = \hat{a}\frac{1}{\hat{n}}\hat{a}^\dagger \neq 1 \tag{A.17}$$

The root of the problem is that only positive integer values of the operator $\hat{n}$ have been included [209].

What if we include negative integers in this case as shown in [210], we will still get back to the contradiction encountered in Eq. (A.13).

Now we introduce the Susskind-Glogower approach, where the "one-sided" unitary phase operator is defined as

$$\hat{E} = \frac{1}{\sqrt{\hat{n}+1}}\hat{a} \tag{A.18}$$

$$\hat{E}^\dagger = \hat{a}^\dagger\frac{1}{\sqrt{\hat{n}+1}} \tag{A.19}$$

where $\hat{E}$ and $\hat{E}^\dagger$ are analogs of the phase operator $e^{\pm i\hat{\phi}}$. When applied to the number states, we get

$$\hat{E} = \sum_{n=0}^{\infty}|n\rangle\langle n+1| \qquad \hat{E}^\dagger = \sum_{n=0}^{\infty}|n+1\rangle\langle n| \tag{A.20}$$

From (A.20), we can define trigonometric functions of phase such that,

$$\hat{C} = \frac{1}{2}(\hat{E} + \hat{E}^\dagger) \qquad \hat{S} = \frac{1}{2i}(\hat{E} - \hat{E}^\dagger) \tag{A.21}$$

These operators are Hermitian and are observables, and they do become classical phase functions in the limit of large amplitudes [209]. We shall also notice that these operators satisfy commutation relations, but do not commute for the vacuum, since

$$[\hat{C}, \hat{n}] = i\hat{S} \qquad [\hat{S}, \hat{n}] = -i\hat{C} \qquad [\hat{C}, \hat{S}] = \frac{i}{2}|0\rangle\langle 0| \tag{A.22}$$

The problem can be fixed by introducing the parity operator in the Susskind-Glogower operator. These new operators are knows as pseudospin operators, introduced in Pan et al paper [13], they are defined as

$$\hat{S}_- = \frac{\hat{I} + (-1)^{\hat{N}}}{2\sqrt{\hat{N}+1}}\hat{a} \qquad \hat{S}_+ = \hat{a}^\dagger \frac{\hat{I} + (-1)^{\hat{N}}}{2\sqrt{\hat{N}+1}} \tag{A.23}$$

where $(-1)^{\hat{N}}$ is the parity operator, and $\hat{S}_\pm$ are the analogs of $\hat{E}$ and $\hat{E}^\dagger$. We can rewrite Eq. (A.23) in number basis as

$$\hat{S}_- = \sum_{n=0}^{\infty} |2n\rangle\langle 2n+1| = (\hat{S}_+)^\dagger \tag{A.24}$$

One of the nice properties of pseudospin is that they satisfy commutation relations,

$$[\hat{S}_Z, \hat{S}_\pm] = \pm 2\hat{S}_\pm \qquad [\hat{S}_+, \hat{S}_-] = \hat{S}_Z \tag{A.25}$$

where the operator $\hat{S}_Z = -(-1)^{\hat{N}}$. As we have shown in Eq. (A.24) these operators satisfy the same commutation relations as for the spin $\frac{1}{2}$ system, and therefore the pseudospin operator $\hat{S} = (S_x, S_y, S_z)$, where $\hat{S}_x \pm i\hat{S}_y = 2\hat{s}_\pm$ is the counterpart of the spin operator σ, as discussed in Sec. 1.2.2.

On the other hand, the parity operator introduced in the pseudospin operator might seem to be confusing as, strictly speaking, we cannot assign parity to photons since they have zero mass at rest. However, we can still deduce the parity of the photon to be $(-1)^L$, where L is angular momentum, by observing single photon transitions between atomic states. As discussed above, the pseudospin system is the counterpart

of the spin $\frac{1}{2}$ system, so the next question is, how does the spin matrices act on Fock space. In Appendix A.3, we show that the spin matrices are given in Segal-Bargmann representation, or Bargmann-Fock representation, that is,

Table 1.: spin 1/2 operators

matrix form	**Bargmann-Fock representation**
$\hat{\sigma}_- = 2\begin{pmatrix} 0 & 0 \\ 1 & 0 \end{pmatrix}$	$\hat{F}_{\sigma-} = 2\hat{a}$ Or $\hat{F}_{\sigma-} = 2\sum_{n=0}^{\infty} \sqrt{n+1}\|n\rangle\langle n+1\|$
$\hat{\sigma}_+ = 2\begin{pmatrix} 0 & 1 \\ 0 & 0 \end{pmatrix}$	$\hat{F}_{\sigma+} = 2\hat{a}^\dagger\hat{n}$ Or $\hat{F}_{\sigma+} = 2\sum_{n=0}^{\infty} n\sqrt{n+1}\|n+1\rangle\langle n\|$

If we compare the spin 1/2 operators $\hat{F}_{\sigma\pm}$ in Fock representation to the pseudospin operators in Eq. (A.23) and (A.24), the spin 1/2 operator does not contain either parity operator, or even/odd part in Fock representation. One suggested interpretation of pseudospin operators is that [13]

"*it is a kind of spin operators acting upon the parity space of photons*"

In other words, new intrinsic uncertainty for photons might be formulated.

A.3 LIE ALGEBRA sl_2 AND ITS REPRESENTATION

The Lie algebra sl_2, generated by e, f, h is subjected to the following commutation relations

$$[e, f] = h, \quad [h, e] = 2e, \quad [h, f] = -2f$$

In 2-dimensional vector representation, it is written as

$$\begin{aligned} \mathfrak{sl}_2 &\longrightarrow \mathrm{Mat}_2(C) \\ e &\longrightarrow E = \begin{pmatrix} 0 & 1 \\ 0 & 0 \end{pmatrix} \\ f &\longrightarrow F = \begin{pmatrix} 0 & 0 \\ 1 & 0 \end{pmatrix} \\ h &\longrightarrow H = \begin{pmatrix} 1 & 0 \\ 0 & -1 \end{pmatrix} \end{aligned}$$

Note that the Lie algebra of su_2 and sl_2 have the same complexification and hence we can construct the representation of both, such that

$$\begin{aligned} \mathfrak{sl}_2 &\longrightarrow \mathfrak{su}_2 \\ e &\longrightarrow \tfrac{P+iJ}{2i} \\ f &\longrightarrow \tfrac{P-iJ}{2i} \\ h &\longrightarrow -iH \end{aligned}$$

Or vice versa,

$$\begin{aligned} P &= \begin{pmatrix} 0 & i \\ i & 0 \end{pmatrix} = i(e+f) \\ J &= \begin{pmatrix} 0 & 1 \\ -1 & 0 \end{pmatrix} = e-f \\ H &= \begin{pmatrix} i & 0 \\ 0 & -i \end{pmatrix} = ih \end{aligned}$$

where P, J, H are generators of su_2.

Given that the Fock space is an infinite-dimensional space of polynomilas in one variable x, the vector space has a basis such that

$$\left\{x^0, x^1, x^2, ..., x^n, ...\right\}$$

so that any polynomial $p(x)$ can be written as

$$p(x) = p_0 + p_1 x + p_2 x^2 + ... + p_n x^n$$

Now we have the map that defines the Fock representation of sl_2

$$\begin{aligned} e &\longrightarrow E = \tfrac{d}{dx} \\ f &\longrightarrow F = -x^2 \tfrac{d}{dx} \\ h &\longrightarrow H = -2x \tfrac{d}{dx} \end{aligned}$$

Combining the above representations, we have the following spin matrices su_2 acting on the Fock space

$$P = \begin{pmatrix} 0 & i \\ i & 0 \end{pmatrix} = i(e+f) = i(1-x^2)\tfrac{d}{dx}$$
$$J = \begin{pmatrix} 0 & 1 \\ -1 & 0 \end{pmatrix} = e-f = (1+x^2)\tfrac{d}{dx}$$
$$H = \begin{pmatrix} i & 0 \\ 0 & -i \end{pmatrix} = ih = -2x\tfrac{d}{dx}$$

One may introduce annihilation and creation operators on the Segal–Bargmann space by setting

$$\hat{a} = \frac{d}{dx}, \qquad \hat{a}^\dagger = x, \qquad \hat{n} = \hat{a}^\dagger \hat{a} = x\frac{d}{dx}$$

then we have

$$P = \begin{pmatrix} 0 & i \\ i & 0 \end{pmatrix} \longrightarrow i(\hat{a} - \hat{a}^\dagger \hat{n})$$
$$J = \begin{pmatrix} 0 & -1 \\ 1 & 0 \end{pmatrix} \longrightarrow \hat{a} + \hat{a}^\dagger \hat{n}$$
$$H = \begin{pmatrix} i & 0 \\ 0 & -i \end{pmatrix} \longrightarrow -2i\hat{n}$$

BIBLIOGRAPHY

[1] J. P. Dowling and G. J. Milburn, "Quantum technology: the second quantum revolution", Phil. Trans. Roy. Soc. A **361**, 1655 (2003).

[2] A. Serafini, *Quantum continuous variables* (Taylor & Francis, Oxford, 2017).

[3] B. Xu, T. Tufarelli, and G. Adesso, "Genuine multipartite nonlocality of permutationally invariant gaussian states", Physical Review A **95**, 012124 (2017).

[4] Y. Xiang, B. Xu, L. Mišta Jr, T. Tufarelli, Q. He, and G. Adesso, "Investigating einstein-podolsky-rosen steering of continuous-variable bipartite states by non-gaussian pseudospin measurements", Physical Review A **96**, 042326 (2017).

[5] L. A. Correa, B. Xu, B. Morris, and G. Adesso, "Pushing the limits of the reaction-coordinate mapping", The Journal of Chemical Physics **151**, 094107 (2019).

[6] G. Adesso and F. Illuminati, "Entanglement in continuous-variable systems: recent advances and current perspectives", J. Phys. A: Math. Theor. **40**, 7821 (2007).

[7] C. Weedbrook, S. Pirandola, R. García-Patrón, N. J. Cerf, T. C. Ralph, J. H. Shapiro, and S. Lloyd, "Gaussian quantum information", Rev. Mod. Phys. **84**, 621 (2012).

[8] G. Adesso, S. Ragy, and A. R. Lee, "Continuous variable quantum information: gaussian states and beyond", Open Syst. Inf. Dyn. **21**, 1440001 (2014).

[9] R. Simon, N. Mukunda, and B. Dutta, "Quantum-noise matrix for multimode systems: u(n) invariance, squeezing, and normal forms", Phys. Rev. A **49**, 1567 (1994).

[10] K. Banaszek and K. Wódkiewicz, "Direct probing of quantum phase space by photon counting", Phys. Rev. Lett. **76**, 4344 (1996).

[11] K. Banaszek, C. Radzewicz, K. Wódkiewicz, and J. S. Krasinski, "Direct measurement of the wigner function by photon counting", Phys. Rev. A **60**, 674 (1999).

[12] B Stoklasa, L Motka, J Rehacek, Z Hradil, L. L. Sánchez-Soto, and G. Agarwal, "Experimental violation of a bell-like inequality with optical vortex beams", New J. Phys. **17**, 113046 (2015).

[13] Z. B. Chen, J. W. Pan, G. Hou, and Y. D. Zhang, Phys. Rev. Lett. **88**, 040406 (2002).

[14] Z. B. Chen and Y. D. Zhang, Phys. Rev. A **65**, 044102 (2002).

[15] R. Filip and L. Mišta, Jr., "Violation of bell's inequalities for a two-mode squeezed vacuum state in lossy transmission lines", Phys. Rev. A **66**, 044309 (2002).

[16] L. Mišta, Jr., R. Filip, and J. Fiurášek, "Continuous-variable werner state: separability, nonlocality, squeezing, and teleportation", Phys. Rev. A **65**, 062315 (2002).

[17] G. Gour, F. C. Khanna, A. Mann, and M. Revzen, "Optimization of bell's inequality violation for continuous variable systems", Phys. Lett. A **324**, 415 (2004).

[18] M. Revzen, P. A. Mello, A. Mann, and L. M. Johansen, "Bell's inequality violation with non-negative wigner functions", Phys. Rev. A **71**, 022103 (2005).

[19] A. Ferraro and M. G. A. Paris, "Nonlocality of two- and three-mode continuous variable systems", Journal of Optics B: Quantum and Semiclassical Optics **7**, 174 (2005).

[20] J. Martin and V. Vennin, "Obstructions to bell cmb experiments", Phys. Rev. D **96**, 063501 (2017).

[21] N. Brunner, D. Cavalcanti, S. Pironio, V. Scarani, and S. Wehner, "Bell nonlocality", Rev. Mod. Phys. **86**, 419 (2014).

[22] R. Horodecki, P. Horodecki, M. Horodecki, and K. Horodecki, "Quantum entanglement", Rev. Mod. Phys. **81**, 865 (2009).

[23] A. Einstein, B. Podolsky, and N. Rosen, "Can quantum-mechanical description of physical reality be considered complete?", Phys. Rev. **47**, 777 (1935).

[24] J. S. Bell, "On the einstein-podolsky-rosen paradox", Physics **1**, 195 (1964).

[25] N. Gisin, G. Ribordy, W. Tittel, and H. Zbinden, "Quantum cryptography", Rev. Mod. Phys. **74**, 145 (2002).

[26] J. F. Clauser, M. A. Horne, A. Shimony, and R. A. Holt, "Proposed experiment to test local hidden-variable theories", Phys. Rev. Lett. **23**, 880 (1969).

[27] R. F. Werner, "Quantum states with einstein-podolsky-rosen correlations admitting a hidden-variable model", Phys. Rev. A **40**, 4277 (1989).

[28] B. Hensen, H. Bernien, A. E. Dréau, A. Reiserer, N. Kalb, M. S. Blok, J. Ruitenberg, R. F. Vermeulen, R. N. Schouten, C. Abellán, et al., "Loophole-free bell inequality violation using electron spins separated by 1.3 kilometres", Nature **526**, 682 (2015).

[29] M. Giustina et al., "Significant-loophole-free test of bell's theorem with entangled photons", Phys. Rev. Lett. **115**, 250401 (2015).

[30] L. K. Shalm et al., "Strong loophole-free test of local realism", Phys. Rev. Lett. **115**, 250402 (2015).

[31] N. D. Mermin, "Extreme quantum entanglement in a superposition of macroscopically distinct states", Phys. Rev. Lett. **65**, 1838 (1990).

[32] D. N. Klyshko, "The bell and ghz theorems: a possible three-photon interference experiment and the question of nonlocality", Phys. Lett. A **172**, 399 (1993).

[33] G. Svetlichny, "Distinguishing three-body from two-body nonseparability by a bell-type inequality", Phys. Rev. D **35**, 3066 (1987).

[34] D. Collins, N. Gisin, S. Popescu, D. Roberts, and V. Scarani, "Bell-type inequalities to detect true n-body nonseparability", Phys. Rev. Lett. **88**, 170405 (2002).

[35] J.-D. Bancal, N. Brunner, N. Gisin, and Y.-C. Liang, "Detecting genuine multipartite quantum nonlocality: a simple approach and generalization to arbitrary dimensions", Phys. Rev. Lett. **106**, 020405 (2011).

[36] Z. Zhao, T. Yang, Y.-A. Chen, A.-N. Zhang, M. Żukowski, and J.-W. Pan, "Experimental violation of local realism by four-photon greenberger-horne-zeilinger entanglement", Phys. Rev. Lett. **91**, 180401 (2003).

[37] S. Ghose, N. Sinclair, S. Debnath, P. Rungta, and R. Stock, "Tripartite entanglement versus tripartite nonlocality in three-qubit greenberger-horne-zeilinger-class states", Phys. Rev. Lett. **102**, 250404 (2009).

[38] A. Ajoy and P. Rungta, "Svetlichny's inequality and genuine tripartite nonlocality in three-qubit pure states", Phys. Rev. A **81**, 052334 (2010).

[39] J. Lavoie, R. Kaltenbaek, and K. J. Resch, "Experimental violation of svetlichny's inequality", New J. Phys. **11**, 073051 (2009).

[40] M. Seevinck and G. Svetlichny, "Bell-type inequalities for partial separability in n-particle systems and quantum mechanical violations", Phys. Rev. Lett. **89**, 060401 (2002).

[41] P. Mitchell, S. Popescu, and D. Roberts, "Conditions for the confirmation of three-particle nonlocality", Phys. Rev. A **70**, 060101 (2004).

[42] N. S. Jones, N. Linden, and S. Massar, "Extent of multiparticle quantum nonlocality", Phys. Rev. A **71**, 042329 (2005).

[43] J.-D. Bancal, C. Branciard, N. Gisin, and S. Pironio, "Quantifying multipartite nonlocality", Phys. Rev. Lett. **103**, 090503 (2009).

[44] R. Gallego, L. E. Würflinger, A. Acín, and M. Navascués, "Operational framework for nonlocality", Phys. Rev. Lett. **109**, 070401 (2012).

[45] J.-D. Bancal, J. Barrett, N. Gisin, and S. Pironio, "Definitions of multipartite nonlocality", Phys. Rev. A **88**, 014102 (2013).

[46] S. Barnett and P. M. Radmore, *Methods in theoretical quantum optics*, Vol. 15 (Oxford University Press, 2002).

[47] S. L. Braunstein and P. van Loock, "Quantum information with continuous variables", Rev. Mod. Phys. **77**, 513 (2005).

[48] U. Leonhardt and J. A. Vaccaro, "Bell correlations in phase space: application to quantum optics", J. Mod. Opt. **42**, 939 (1995).

[49] A. Gilchrist, P. Deuar, and M. D. Reid, "Contradiction of quantum mechanics with local hidden variables for quadrature phase amplitude measurements", Phys. Rev. Lett. **80**, 3169 (1998).

[50] H. Nha and H. J. Carmichael, "Proposed test of quantum nonlocality for continuous variables", Phys. Rev. Lett. **93**, 020401 (2004).

[51] R. García-Patrón, J. Fiurášek, N. J. Cerf, J. Wenger, R. Tualle-Brouri, and P. Grangier, "Proposal for a loophole-free bell test using homodyne detection", Phys. Rev. Lett. **93**, 130409 (2004).

[52] R. García-Patrón, J. Fiurášek, and N. J. Cerf, "Loophole-free test of quantum nonlocality using high-efficiency homodyne detectors", Phys. Rev. A **71**, 022105 (2005).

[53] H. Jeong, W. Son, M. S. Kim, D. Ahn, and v. Brukner, "Quantum nonlocality test for continuous-variable states with dichotomic observables", Phys. Rev. A **67**, 012106 (2003).

[54] P. van Loock and S. L. Braunstein, "Greenberger-horne-zeilinger nonlocality in phase space", Phys. Rev. A **63**, 022106 (2001).

[55] A. Ferraro and M. G. A. Paris, J. Opt. B: Quantum Semiclass. Opt. **7**, 174 (2005).

[56] A. Acín, N. J. Cerf, A. Ferraro, and J. Niset, "Tests of multimode quantum nonlocality with homodyne measurements", Phys. Rev. A **79**, 012112 (2009).

[57] J. Li, T. Fogarty, C. Cormick, J. Goold, T. Busch, and M. Paternostro, "Tripartite nonlocality and continuous-variable entanglement in thermal states of trapped ions", Phys. Rev. A **84**, 022321 (2011).

[58] S.-W. Lee, M. Paternostro, J. Lee, and H. Jeong, "Testing genuine multipartite nonlocality in phase space", Phys. Rev. A **87**, 022123 (2013).

[59] J. Zhang, T. Zhang, A. Xuereb, D. Vitali, and J. Li, "More nonlocality with less entanglement in a tripartite atom-optomechanical system", Ann. Phys. (Berlin) **527**, 147 (2015).

[60] G. Adesso and S. Piano, "Theory of genuine tripartite nonlocality of gaussian states", Phys. Rev. Lett. **112**, 010401 (2014).

[61] P. van Loock and S. L. Braunstein, "Multipartite entanglement for continuous variables: a quantum teleportation network", Phys. Rev. Lett. **84**, 3482 (2000).

[62] P. van Loock and A. Furusawa, "Detecting genuine multipartite continuous-variable entanglement", Phys. Rev. A **67**, 052315 (2003).

[63] T. Aoki, N. Takei, H. Yonezawa, K. Wakui, T. Hiraoka, A. Furusawa, and P. van Loock, "Experimental creation of a fully inseparable tripartite continuous-variable state", Phys. Rev. Lett. **91**, 080404 (2003).

[64] G. Adesso, A. Serafini, and F. Illuminati, "Quantification and scaling of multipartite entanglement in continuous variable systems", Phys. Rev. Lett. **93**, 220504 (2004).

[65] R. Y. Teh and M. D. Reid, "Criteria for genuine n-partite continuous-variable entanglement and einstein-podolsky-rosen steering", Phys. Rev. A **90**, 062337 (2014).

[66] G. Adesso, A. Serafini, and F. Illuminati, "Multipartite entanglement in three-mode gaussian states of continuous-variable systems: quantification, sharing structure, and decoherence", Phys. Rev. A **73**, 032345 (2006).

[67] G. Adesso, A. Serafini, and F. Illuminati, "Optical state engineering, quantum communication, and robustness of entanglement promiscuity in three-mode gaussian states", New J. Phys. **9**, 60 (2007).

[68] G. Adesso and F. Illuminati, "Continuous variable tangle, monogamy inequality, and entanglement sharing in gaussian states of continuous variable systems", New J. Phys. **8**, 15 (2006).

[69] T. Hiroshima, G. Adesso, and F. Illuminati, "Monogamy inequality for distributed gaussian entanglement", Phys. Rev. Lett. **98**, 050503 (2007).

[70] G. Adesso and F. Illuminati, "Strong monogamy of bipartite and genuine multipartite entanglement: the gaussian case", Phys. Rev. Lett. **99**, 150501 (2007).

[71] G. Adesso and F. Illuminati, "Genuine multipartite entanglement of symmetric gaussian states: strong monogamy, unitary localization, scaling behavior, and molecular sharing structure", Phys. Rev. A **78**, 042310 (2008).

[72] G. Adesso and F. Illuminati, "Equivalence between entanglement and the optimal fidelity of continuous variable teleportation", Phys. Rev. Lett. **95**, 150503 (2005).

[73] H. Yonezawa, T. Aoki, and A. Furusawa, Nature **431**, 430 (2004).

[74] T. Aoki, G. Takahashi, T. Kajiya, J.-i. Yoshikawa, S. L. Braunstein, P. Van Loock, and A. Furusawa, "Quantum error correction beyond qubits", Nature Phys. **5**, 541 (2009).

[75] A. M. Lance, T. Symul, W. P. Bowen, B. C. Sanders, and P. K. Lam, "Tripartite quantum state sharing", Phys. Rev. Lett. **92**, 177903 (2004).

[76] Y. Xiang, I. Kogias, G. Adesso, and Q. He, "Multipartite gaussian steering: monogamy constraints and quantum cryptography applications", Phys. Rev. A **95**, 010101 (2017).

[77] S. Armstrong, M. Wang, R. Y. Teh, Q. Gong, Q. He, J. Janousek, H.-A. Bachor, M. D. Reid, and P. K. Lam, "Multipartite einstein–podolsky–rosen steering and genuine tripartite entanglement with optical networks", Nature Phys. **11**, 167 (2015).

[78] R. Neigovzen, C. Rodó, G. Adesso, and A. Sanpera, "Multipartite continuous-variable solution for the byzantine agreement problem", Phys. Rev. A **77**, 062307 (2008).

[79] M. Żukowski, A. Zeilinger, and M. A. Horne, "Realizable higher-dimensional two-particle entanglements via multiport beam splitters", Phys. Rev. A **55**, 2564 (1997).

[80] H. M. Wiseman, S. J. Jones, and A. C. Doherty, "Steering, entanglement, nonlocality, and the einstein-podolsky-rosen paradox", Phys. Rev. Lett. **98**, 140402 (2007).

[81] Q. Y. He and M. D. Reid, "Genuine multipartite einstein-podolsky-rosen steering", Phys. Rev. Lett. **111**, 250403 (2013).

[82] M. D. Reid, P. D. Drummond, W. P. Bowen, E. G. Cavalcanti, P. K. Lam, H. A. Bachor, U. L. Andersen, and G. Leuchs, "Colloquium: the einstein-podolsky-rosen paradox: from concepts to applications", Rev. Mod. Phys. **81**, 1727 (2009).

[83] D. Cavalcanti and P. Skrzypczyk, "Quantum steering: a review with focus on semidefinite programming", Rep. Prog. Phys. **80**, 024001 (2017).

[84] S. Wollmann, N. Walk, A. J. Bennet, H. M. Wiseman, and G. J. Pryde, "Observation of genuine one-way einstein-podolsky-rosen steering", Phys. Rev. Lett. **116**, 160403 (2016).

[85] S.-W. Ji, J. Lee, J. Park, and H. Nha, "Quantum steering of Gaussian states via non-Gaussian measurements", Sci. Rep. **6**, 29729 (2016).

[86] I. Kogias, A. Lee, S. Ragy, and G. Adesso, "Quantification of gaussian quantum steering", Phys. Rev. Lett. **114**, 060403 (2015).

[87] A. Streltsov, G. Adesso, and M. B. Plenio, "Quantum coherence as a resource", arXiv:1609.02439v3 (2017).

[88] K. Modi, A. Brodutch, H. Cable, T. Paterek, and V. Vedral, "The classical-quantum boundary for correlations: discord and related measures", Rev. Mod. Phys. **84**, 1655 (2012).

[89] G. Adesso, T. R. Bromley, and M. Cianciaruso, "Measures and applications of quantum correlations", J. Phys. A.: Math. Theor. **49**, 473001 (2016).

[90] E. Schrödinger, "Discussion of probability relations between separated systems (I)", Proc. Camb. Phil. Soc. **31**, 553 (1935).

[91] M. D. Reid, "Demonstration of the einstein-podolsky-rosen paradox using nondegenerate parametric amplification", Phys. Rev. A **40**, 913 (1989).

[92] E. G. Cavalcanti, S. J. Jones, H. M. Wiseman, and M. D. Reid, "Experimental criteria for steering and the einstein-podolsky-rosen paradox", Phys. Rev. A. **80**, 032112 (2009).

[93] R. Gallego and L. Aolita, "Resource theory of steering", Phys. Rev. X **5**, 041008 (2015).

[94] C. Branciard, E. G. Cavalcanti, S. P. Walborn, V. Scarani, and H. M. Wiseman, "One-sided device-independent quantum key distribution: security, feasibility, and the connection with steering", Phys. Rev. A **85**, 010301 (2012).

[95] N. Walk, S. Hosseini, J. Geng, O. Thearle, J. Y. Haw, S. Armstrong, S. M. Assad, J. Janousek, T. C. Ralph, T. Symul, H. M. Wiseman, and P. K. Lam, "Experimental demonstration of gaussian protocols for one-sided device-independent quantum key distribution", Optica **3**, 634 (2016).

[96] I. Kogias, Y. Xiang, Q. Y. He, and G. Adesso, "Unconditional security of entanglement-based continuous-variable quantum secret sharing", Phys. Rev. A **95**, 012315 (2017).

[97] M. Piani and J. Watrous, "Necessary and sufficient quantum information characterization of einstein-podolsky-rosen steering", Phys. Rev. Lett. **114**, 060404 (2015).

[98] M. D. Reid, "Signifying quantum benchmarks for qubit teleportation and secure quantum communication using einstein-podolsky-rosen steering inequalities", Phys. Rev. A **88**, 062338 (2013).

[99] Q. Y. He, L. Rosales-Zárate, G. Adesso, and M. D. Reid, "Secure continuous variable teleportation and Einstein-Podolsky-Rosen steering", Phys. Rev. Lett. **115**, 180502 (2015).

[100] V. Händchen, T. Eberle, S. Steinlechner, A. Samblowski, T. Franz, R. F. Werner, and R. Schnabel, "Observation of one-way einstein-podolsky-rosen steering", Nat. Photon. **6**, 596 (2012).

[101] S. Armstrong, M. Wang, R. Y. Teh, Q. Gong, Q. Y. He, J. Janousek, H.-A. Bachor, M. D. Reid, and P. K. Lam, "Multipartite einstein-podolsky-rosen steering and genuine tripartite entanglement with optical networks", Nat. Phys. **11**, 167 (2015).

[102] X. Deng, Y. Xiang, C. Tian, G. Adesso, Q. Y. He, Q. Gong, X. Su, C. Xie, and K. Peng, "Demonstration of monogamy relations for einstein-podolsky-rosen steering in gaussian cluster states", Phys. Rev. Lett. **118**, 230501 (2017).

[103] S. J. Jones, H. M. Wiseman, and A. C. Doherty, "Entanglement, einstein-podolsky-rosen correlations, bell nonlocality, and steering", Phys. Rev. A **76**, 052116 (2007).

[104] Q. Y. He, Q. H. Gong, and M. D. Reid, "Classifying directional gaussian entanglement, einstein-podolsky-rosen steering, and discord", Phys. Rev. Lett. **114**, 060402 (2015).

[105] I. Kogias and G. Adesso, "Einstein–podolsky–rosen steering measure for two-mode continuous variable states", J. Opt. Soc. Am. B **32**, A27 (2015).

[106] L. Lami, C. Hirche, G. Adesso, and A. Winter, "Schur complement inequalities for covariance matrices and monogamy of quantum correlations", Phys. Rev. Lett. **117**, 220502 (2016).

[107] N. C. Menicucci, P. van Loock, M. Gu, C. Weedbrook, T. C. Ralph, and M. A. Nielsen, "Universal quantum computation with continuous-variable cluster states", Phys. Rev. Lett. **97**, 110501 (2006).

[108] I. Kogias, P. Skrzypczyk, D. Cavalcanti, A. Acín, and G. Adesso, "Hierarchy of steering criteria based on moments for all bipartite quantum systems", Phys. Rev. Lett. **115**, 210401 (2015).

[109] R. Simon, "Peres-horodecki separability criterion for continuous variable systems", Phys. Rev. Lett. **84**, 2726 (2000).

[110] L.-M. Duan, G. Giedke, J. I. Cirac, and P. Zoller, "Inseparability criterion for continuous variable systems", Phys. Rev. Lett. **84**, 2722 (2000).

[111] G. Adesso, A. Serafini, and F. Illuminati, "Extremal entanglement and mixedness in continuous variable systems", Phys. Rev. A **70**, 022318 (2004).

[112] S. Pirandola, G. Spedalieri, S. L. Braunstein, N. J. Cerf, and S. Lloyd, "Optimality of gaussian discord", Phys. Rev. Lett. **113**, 140405 (2014).

[113] F. Caruso, V. Giovannetti, and A. S. Holevo, New J. Phys. **8**, 310 (2006).

[114] R. García-Patrón, C. Navarrete-Benlloch, S. Lloyd, J. H. Shapiro, and N. J. Cerf, Phys. Rev. Lett. **108**, 110505 (2012).

[115] L. Mišta, Jr., D. McNulty, and G. Adesso, "No-activation theorem for gaussian nonclassical correlations by gaussian operations", Phys. Rev. A **90**, 022328 (2014).

[116] B. Kraus and J. I. Cirac, "Discrete entanglement distribution with squeezed light", Phys. Rev. Lett. **92**, 013602 (2004).

[117] M. Paternostro, W. Son, and M. S. Kim, "Complete conditions for entanglement transfer", Phys. Rev. Lett. **92**, 197901 (2004).

[118] G. Adesso, S. Campbell, F. Illuminati, and M. Paternostro, "Controllable gaussian-qubit interface for extremal quantum state engineering", Phys. Rev. Lett. **104**, 240501 (2010).

[119] M. Paternostro, G. Adesso, and S. Campbell, "Passing quantum correlations to qubits using any two-mode state", Phys. Rev. A **80**, 062318 (2009).

[120] S. J. Jones and H. M. Wiseman, "Nonlocality of a single photon: paths to an einstein-podolsky-rosen-steering experiment", Phys. Rev. A. **84**, 012110 (2011).

[121] R. Tatham, L. Mišta, Jr., G. Adesso, and N. Korolkova, "Nonclassical correlations in continuous-variable non-gaussian werner states", Phys. Rev. A **85**, 022326 (2012).

[122] D Cavalcanti, P Skrzypczyk, G. Aguilar, R. Nery, P. S. Ribeiro, and S. Walborn, "Detection of entanglement in asymmetric quantum networks and multipartite quantum steering", Nat. Commun. **6**, 7941 (2015).

[123] M. D. Reid, "Monogamy inequalities for the einstein-podolsky-rosen paradox and quantum steering", Phys. Rev. A **88**, 062108 (2013).

[124] V. V. Dodonov, V. I. Man'ko, and V. V. Semjonov, Nuovo Cimento B **83**, 145 (1984).

[125] V. V. Dodonov, O. V. Man'ko, and V. I. Man'ko, Phys. Rev. A **50**, 813 (1994).

[126] J. Fiurášek and J. Peřina, "Quantum statistics of light propagating in nonlinear optical couplers", in *Coherence and statistics of photons and atoms*, edited by J. Peřina (J. Wiley, New York, 2001) Chap. 2, pp. 65–110.

[127] A. Erdélyi, ed., *BATEMAN MANUSCRIPT PROJECT: higher transcendental functions* (McGraw-Hill, New York, 1953).

[128] A. Garg, J. N. Onuchic, and V. Ambegaokar, "Effect of friction on electron transfer in biomolecules", J. Chem. Phys. **83**, 4491 (1985).

[129] L. Hartmann, I. Goychuk, and P. Hänggi, "Controlling electron transfer in strong time-dependent fields: theory beyond the golden rule approximation", J. Chem. Phys. **113**, 11159 (2000).

[130] J. Roden, W. T. Strunz, K. B. Whaley, and A. Eisfeld, "Accounting for intramolecular vibrational modes in open quantum system description of molecular systems", J. Chem. Phys. **137**, 204110 (2012).

[131] F. Binder, L. A. Correa, C. Gogolin, J. Anders, and G. Adesso, eds., *Thermodynamics in the quantum regime*, Fundamental Theories of Physics (Springer, 2018).

[132] R. Alicki, M. Horodecki, P. Horodecki, R. Horodecki, L. Jacak, and P. Machnikowski, "Optimal strategy for a single-qubit gate and the trade-off between opposite types of decoherence", Phys. Rev. A **70**, 010501 (2004).

[133] D. P. McCutcheon and A. Nazir, "Quantum dot rabi rotations beyond the weak exciton–phonon coupling regime", New J. Phys. **12**, 113042 (2010).

[134] K. D. B. Higgins, B. W. Lovett, and E. M. Gauger, "Quantum thermometry using the ac stark shift within the rabi model", Phys. Rev. B **88**, 155409 (2013).

[135] I. de Vega and D. Alonso, "Dynamics of non-markovian open quantum systems", Rev. Mod. Phys. **89**, 015001 (2017).

[136] R. P. Feynman and F. Vernon Jr, "The theory of a general quantum system interacting with a linear dissipative system", Ann. Phys. (N. Y.) **281**, 547 (2000).

[137] B. L. Hu, J. P. Paz, and Y. Zhang, "Quantum Brownian motion in a general environment: Exact master equation with nonlocal dissipation and colored noise", Phys. Rev. D **45**, 2843 (1992).

[138] Y. Tanimura, "Nonperturbative expansion method for a quantum system coupled to a harmonic-oscillator bath", Phys. Rev. A **41**, 6676 (1990).

[139] J. T. Stockburger and H. Grabert, "Exact *c*-number representation of non-markovian quantum dissipation", Phys. Rev. Lett. **88**, 170407 (2002).

[140] D. Alonso and I. de Vega, "Multiple-time correlation functions for non-markovian interaction: beyond the quantum regression theorem", Phys. Rev. Lett. **94**, 200403 (2005).

[141] M. Wagner, *Unitary transformations in solid state physics*, Vol. 15, Modern Problems in Condensed Matter Sciences (North-Holland, 1986).

[142] A. Würger, "Strong-coupling theory for the spin-phonon model", Phys. Rev. B **57**, 347 (1998).

[143] B. M. Garraway, "Decay of an atom coupled strongly to a reservoir", Phys. Rev. A **55**, 4636 (1997).

[144] R Martinazzo, B Vacchini, K. Hughes, and I Burghardt, "Universal markovian reduction of brownian particle dynamics: communication", J. Chem. Phys. **134**, 011101 (2011).

[145] M. Woods, R Groux, A. Chin, S. Huelga, and M. B. Plenio, "Mappings of open quantum systems onto chain representations and markovian embeddings", J. Math. Phys. **55**, 032101 (2014).

[146] J. Iles-Smith, N. Lambert, and A. Nazir, "Environmental dynamics, correlations, and the emergence of noncanonical equilibrium states in open quantum systems", Phys. Rev. A **90**, 032114 (2014).

[147] A. Nazir and G. Schaller, "Thermodynamics in the quantum regime", in, edited by F. Binder, L. A. Correa, C. Gogolin, J. Anders, and G. Adesso, Fundamental Theories of Physics (Springer, 2018) Chap. 23, p. 551.

[148] K. H. Hughes, C. D. Christ, and I. Burghardt, "Effective-mode representation of non-markovian dynamics: a hierarchical approximation of the spectral density. i. application to single surface dynamics", J. Chem. Phys. **131**, 024109 (2009).

[149] J. Iles-Smith, A. G. Dijkstra, N. Lambert, and A. Nazir, "Energy transfer in structured and unstructured environments: master equations beyond the born-markov approximations", J. Chem. Phys. **144**, 044110 (2016).

[150] P. Strasberg, G. Schaller, N. Lambert, and T. Brandes, "Nonequilibrium thermodynamics in the strong coupling and non-markovian regime based on a reaction coordinate mapping", New J. Phys. **18**, 073007 (2016).

[151] S. Restrepo, J. Cerrillo, P. Strasberg, and G. Schaller, "From quantum heat engines to laser cooling: floquet theory beyond the born–markov approximation", New J. Phys. **20**, 053063 (2018).

[152] M. Wertnik, A. Chin, F. Nori, and N. Lambert, "Optimizing co-operative multi-environment dynamics in a dark-state-enhanced photosynthetic heat engine", J. Chem. Phys. **149**, 084112 (2018).

[153] H. Maguire, J. Iles-Smith, and A. Nazir, "Environmental non-additivity and franck-condon physics in non-equilibrium quantum systems", arXiv preprint arXiv:1812.04502 (2018).

[154] R. Puebla, G. Zicari, I. Arrazola, E. Solano, M. Paternostro, and J. Casanova, "Spin-boson model as a simulator of non-markovian multiphoton jaynes-cummings models", Symmetry **11**, 695 (2019).

[155] N. Martensen and G. Schaller, "Transmission from reverse reaction coordinate mappings", Eur. Phys. J. B **92**, 30 (2019).

[156] C. McConnell and A. Nazir, "Electron counting statistics for non-additive environments", arXiv preprint arXiv:1903.05264 (2019).

[157] N. Lambert, S. Ahmed, M. Cirio, and F. Nori, "Virtual excitations in the ultra-strongly-coupled spin-boson model: physical results from unphysical modes", arXiv preprint arXiv:1903.05892 (2019).

[158] P. Strasberg, G. Schaller, T. L. Schmidt, and M. Esposito, "Fermionic reaction coordinates and their application to an autonomous maxwell demon in the strong-coupling regime", Phys. Rev. B **97**, 205405 (2018).

[159] G. Schaller, J. Cerrillo, G. Engelhardt, and P. Strasberg, "Electronic maxwell demon in the coherent strong-coupling regime", Phys. Rev. B **97**, 195104 (2018).

[160] S. Restrepo, S. Böhling, J. Cerrillo, and G. Schaller, "Electron pumping in the strong coupling and non-markovian regime: a reaction coordinate mapping approach", arXiv preprint arXiv:1905.00581 (2019).

[161] J. O. González, L. A. Correa, G. Nocerino, J. P. Palao, D. Alonso, and G. Adesso, "Testing the validity of the 'local' and 'global' gkls master equations on an exactly solvable model", Open Syst. Inf. Dyn. **24**, 1740010 (2017).

[162] A. Asadian, D. Manzano, M. Tiersch, and H. J. Briegel, "Heat transport through lattices of quantum harmonic oscillators in arbitrary dimensions", Phys. Rev. E **87**, 012109 (2013).

[163] A. O. Caldeira and A. J. Leggett, "Path integral approach to quantum Brownian motion", Physica A **121**, 587 (1983).

[164] G. W. Ford, J. T. Lewis, and R. F. O'Connell, "Quantum langevin equation", Phys. Rev. A **37**, 4419 (1988).

[165] U. Weiss, *Quantum dissipative systems*, Vol. 13 (World Scientific Pub Co Inc, 2008).

[166] H. Breuer and F. Petruccione, *The Theory of Open Quantum Systems* (Oxford University Press, USA, 2002).

[167] Y. Subaşi, C. H. Fleming, J. M. Taylor, and B. L. Hu, "Equilibrium states of open quantum systems in the strong coupling regime", Phys. Rev. E **86**, 061132 (2012).

[168] V. Gorini, A. Kossakowski, and E. Sudarshan, "Completely positive dynamical semigroups of n-level systems", J. Math. Phys. **17**, 821 (1976).

[169] G. Lindblad, "On the generators of quantum dynamical semigroups", Comm. Math. Phys. **48**, 119 (1976).

[170] C. Joshi, P. Öhberg, J. D. Cresser, and E. Andersson, "Markovian evolution of strongly coupled harmonic oscillators", Phys. Rev. A **90**, 063815 (2014).

[171] A. Levy and R. Kosloff, "The local approach to quantum transport may violate the second law of thermodynamics", Europhys. Lett. **107**, 20004 (2014).

[172] J. T. Stockburger and T. Motz, "Thermodynamic deficiencies of some simple Lindblad operators", Fortschr. Phys. **65**, 6 (2016).

[173] J. Kołodyński, J. B. Brask, M. Perarnau-Llobet, and B. Bylicka, "Adding dynamical generators in quantum master equations", Phys. Rev. A **97**, 062124 (2018).

[174] H. Wichterich, M. J. Henrich, H.-P. Breuer, J. Gemmer, and M. Michel, "Modeling heat transport through completely positive maps", Phys. Rev. E **76**, 031115 (2007).

[175] A. Trushechkin and I. Volovich, "Perturbative treatment of inter-site couplings in the local description of open quantum networks", Europhys. Lett. **113**, 30005 (2016).

[176] F. Barra, "The thermodynamic cost of driving quantum systems by their boundaries", Sci. Rep. **5**, 14873 (2015).

[177] F. Barra and C. Lledó, "The smallest absorption refrigerator: the thermodynamics of a system with quantum local detailed balance", Eur. Phys. J. Spec. Top. **227**, 231 (2018).

[178] G. De Chiara, G. Landi, A. Hewgill, B. Reid, A. Ferraro, A. J. Roncaglia, and M. Antezza, "Reconciliation of quantum local master equations with thermodynamics", New J. Phys. **20**, 113024 (2018).

[179] A. Suárez, R. Silbey, and I. Oppenheim, "Memory effects in the relaxation of quantum open systems", J. Chem. Phys. **97**, 5101 (1992).

[180] P. Gaspard and M. Nagaoka, "Slippage of initial conditions for the Redfield master equation", J. Chem. Phys. **111**, 5668 (1999).

[181] H. Spohn, "An algebraic condition for the approach to equilibrium of an open N-level system", Lett. Maths. Phys. **2**, 33 (1977).

[182] H. Spohn, "Entropy production for quantum dynamical semigroups", J. Math. Phys. **19**, 1227 (1978).

[183] A. Ferraro, S. Olivares, and M. Paris, *Gaussian states in continuous variable quantum information*, edited by I. 88-7088-483-X (Bibliopolis, Napoli, 2005).

[184] R. Alicki, "The quantum open system as a model of the heat engine", J. Phys. A **12**, L103 (1979).

[185] R. Kosloff and A. Levy, "Quantum Heat Engines and Refrigerators: Continuous Devices", Anual Rev. Phys. Chem. **65**, 365 (2014).

[186] P. Riseborough, P. Hanggi, and U. Weiss, "Exact results for a damped quantum-mechanical harmonic oscillator", Phys. Rev. A **31**, 471 (1985).

[187] M. Ludwig, K. Hammerer, and F. Marquardt, "Creation and destruction of entanglement by a nonequilibrium environment", Phys. Rev. A **82**, 012333 (2010).

[188] C. Fleming, A. Roura, and B. Hu, "Exact analytical solutions to the master equation of quantum brownian motion for a general environment", Ann. Phys. (N. Y.) **326**, 1207 (2011).

[189] L. A. Correa, A. A. Valido, and D. Alonso, "Asymptotic discord and entanglement of nonresonant harmonic oscillators under weak and strong dissipation", Phys. Rev. A **86**, 012110 (2012).

[190] E. A. Martinez and J. P. Paz, "Dynamics and Thermodynamics of Linear Quantum Open Systems", Phys. Rev. Lett. **110**, 130406 (2013).

[191] A. A. Valido, A. Ruiz, and D. Alonso, "Quantum correlations and energy currents across three dissipative oscillators", Phys. Rev. E **91**, 062123 (2015).

[192] N. Freitas and J. P. Paz, "Analytic solution for heat flow through a general harmonic network", Phys. Rev. E **90**, 042128 (2014).

[193] G. Ford, M Kac, and P Mazur, "Statistical mechanics of assemblies of coupled oscillators", J. Math. Phys. **6**, 504 (1965).

[194] L. A. Correa, M. Perarnau-Llobet, K. V. Hovhannisyan, S. Hernández-Santana, M. Mehboudi, and A. Sanpera, "Enhancement of low-temperature thermometry by strong coupling", Phys. Rev. A **96**, 062103 (2017).

[195] A. A. Valido, L. A. Correa, and D. Alonso, "Gaussian tripartite entanglement out of equilibrium", Phys. Rev. A **88**, 012309 (2013).

[196] N. Freitas and J. P. Paz, "Fundamental limits for cooling of linear quantum refrigerators", Phys. Rev. E **95**, 012146 (2017).

[197] T. Motz, J. Ankerhold, and J. T. Stockburger, "Currents and fluctuations of quantum heat transport in harmonic chains", New J. Phys. **19**, 053013 (2017).

[198] T. Motz, M. Wiedmann, J. T. Stockburger, and J. Ankerhold, "Rectification of heat currents across nonlinear quantum chains: a versatile approach beyond weak thermal contact", New J. Phys. **20**, 113020 (2018).

[199] A. Uhlmann, "The "transition probability" in the state space of a $*$-algebra", Rep. Math. Phys. **9**, 273 (1976).

[200] L. Banchi, S. L. Braunstein, and S. Pirandola, "Quantum fidelity for arbitrary gaussian states", Phys. Rev. Lett. **115**, 260501 (2015).

[201] A. Ferraro, A. García-Saez, and A. Acín, "Intensive temperature and quantum correlations for refined quantum measurements", EPL (Europhysics Letters) **98**, 10009 (2012).

[202] A. García-Saez, A. Ferraro, and A. Acín, "Local temperature in quantum thermal states", Phys. Rev. A **79**, 052340 (2009).

[203] M. Kliesch, C. Gogolin, M. J. Kastoryano, A. Riera, and J. Eisert, "Locality of temperature", Phys. Rev. X **4**, 031019 (2014).

[204] S. Hernández-Santana, A. Riera, K. V. Hovhannisyan, M. Perarnau-Llobet, L. Tagliacozzo, and A. Acín, "Locality of temperature in spin chains", New J. Phys. **17**, 085007 (2015).

[205] P. Strasberg and M. Esposito, "Stochastic thermodynamics in the strong coupling regime: an unambiguous approach based on coarse graining", Phys. Rev. E **95**, 062101 (2017).

[206] D. Newman, F. Mintert, and A. Nazir, "Performance of a quantum heat engine at strong reservoir coupling", Phys. Rev. E **95**, 032139 (2017).

[207] D. Tamascelli, A. Smirne, S. F. Huelga, and M. B. Plenio, "Nonperturbative treatment of non-markovian dynamics of open quantum systems", Phys. Rev. Lett. **120**, 030402 (2018).

[208] P. A. M. Dirac, "The quantum theory of the emission and absorption of radiation", Proc. Roy. Soc. Lond, A **114**, 243 (1927).

[209] L. Susskind and J. Glogower, "Quantum mechanical phase and time operator", Physics **1**, 49 (1964).

[210] S. M. Barnett and D. T. Pegg, "Phase in quantum optics", J. Phys. A: Math. Gen. **19**, 3849 (1986).